NUMERICAL AND EXPERIMENTAL INVESTIGATION ON LASER DAMAGE THRESHOLD OF HIGHLY REFLECTIVE MULTILAYER THIN FILMS

A THESIS SUBMITTED TO
THE GRADUATE SCHOOL OF NATURAL AND APPLIED SCIENCES
OF
MIDDLE EAST TECHNICAL UNIVERSITY

BY

MUSTAFA OCAK

IN PARTIAL FULFILLMENT OF THE REQUIREMENTS
FOR
THE DEGREE OF DOCTOR OF PHILOSOPHY
IN
MECHANICAL ENGINEERING

JANUARY 2016

Approval of the thesis:

NUMERICAL AND EXPERIMENTAL INVESTIGATION ON LASER DAMAGE THRESHOLD OF HIGHLY REFLECTIVE MULTILAYER THIN FILMS

submitted by **MUSTAFA OCAK** in partial fulfillment of the requirements for the degree of **Doctor of Philosophy in Mechanical Engineering Department, Middle East Technical University** by**,**

Prof. Dr. Gülbin Dural Ünver ____________________
Dean, Graduate School of **Natural and Applied Sciences**

Prof. Dr. R. Tuna Balkan ____________________
Head of Department, **Mechanical Engineering**

Assist. Prof. Dr. Cüneyt Sert ____________________
Supervisor, **Mechanical Engineering Dept., METU**

Assoc. Prof. Dr. Tuba Okutucu Özyurt ____________________
Co-supervisor, **Mechanical Engineering Dept., METU**

Examining Committee Members:

Assoc. Prof. Dr. İlker Tarı ____________________
Mechanical Engineering Dept., METU

Assist. Prof. Dr. Cüneyt Sert ____________________
Mechanical Engineering Dept., METU

Prof. Dr. Caner Durucan ____________________
Metallurgical and Materials Engineering Dept., METU

Assoc. Prof. Dr. Barbaros Çetin ____________________
Mechanical Engineering Dept., Bilkent University

Assist. Prof. Dr. Özlem Duyar Coşkun ____________________
Physics Engineering Dept., Hacettepe University

Date : 26.01.2016

I hereby declare that all information in this document has been obtained and presented in accordance with academic rules and ethical conduct. I also declare that, as required by these rules and conduct, I have fully cited and referenced all material and results that are not original to this work.

Name, Last name : Mustafa Ocak

Signature :

ABSTRACT

NUMERICAL AND EXPERIMENTAL INVESTIGATION ON LASER DAMAGE THRESHOLD OF HIGHLY REFLECTIVE MULTILAYER THIN FILMS

Ocak, Mustafa
Ph.D, Department of Mechanical Engineering
Supervisor : Assist. Prof. Dr. Cüneyt Sert
Co-supervisor : Assoc. Prof. Dr. Tuba Okutucu Özyurt
January 2016, 148 pages

The laser induced temperature distributions on the optical thin films are investigated in this study. Effects of optical design modifications on thermal performance of highly reflective (HR) multilayer thin films are analyzed. Firstly, a conventional 19 layer HR coating is selected as a reference and the laser induced temperature distribution is evaluated on it. Then, alternative HR designs are developed by employing non-quarter wave layers, over coat (OC) layers and two high index materials in the coating stacks. Temperature distributions for the design alternatives are then computed and compared with the conventional design. Herein, usage of non-quarter wave layers decreases the maximum temperature (at most 24.6%) and the highest interface temperature (at most 21.6%) at the top layer pairs of the alternative designs; however it causes higher absorption through inner layer pairs. Therefore, a new design method is proposed for which layer thicknesses are calculated using the developed MATLAB code to avoid high laser absorption. Results confirm that proposed design shows higher thermal performance by decreasing the internal and interface temperatures (at most 15.4%) compared to prior alternative designs.

In the meantime, the conventional and alternative designs are fabricated for the laser induced damage threshold (LIDT) tests and damage morphology investigations. Herein damage types are identified and changes on damage characteristics are scrutinized. Results show that usage of modified layer thicknesses increased the LIDT by changing the damage characteristics and damage profiles due to decreased temperature rise by the low refractive index layers in accordance with the numerical simulations.

Keywords: Optical thin films, Temperature field theory, Non-quarter wave design, Three material coatings, Damage morphology

ÖZ

ÇOK KATMANLI YÜKSEK YANSITICI ÖZELLİKLİ İNCE FİLMLERİN LAZER HASAR EŞİĞİNİN SAYISAL VE DENEYSEL OLARAK İNCELENMESİ

Ocak, Mustafa

Doktora, Makina Mühendisliği Bölümü

Tez Yöneticisi : Yrd. Doç. Dr. Cüneyt Sert

Ortak Tez Yöneticisi : Doç. Dr. Tuba Okutucu Özyurt

Ocak 2016, 148 sayfa

Bu çalışmada, ince film kaplamalı optik elemanlar üzerindeki sıcaklık dağılımı, incelenmiştir. Optik tasarım değişikliklerinin yüksek yansıtıcı özellikli, çok katmanlı ince film kaplamalarının ısıl performansına olan etkisi çalışılmıştır. Öncelikler, 19 katmanlı yüksek yansıtıcı özellikli alışılagelmiş bir kaplama referans olarak seçilmiştir. Bu referans kaplama üzerinde, lazer ışınımı sebebiyle oluşan lazer enerji emilimi ve sıcaklık dağılımı hesaplatılmıştır. Sonrasında referans kaplamaya alternatif olacak tasarımlarlar geliştirilmiştir. Alternatif tasarımların yapısında değiştirilmiş dalga çeyreği katmanları, üst yüzey kaplama katmanları ve iki farklı yüksek kırılma indisli malzemeler denenmiştir. Alternatif tasarımların üzerindeki sıcaklık dağılımları da hesaplatılmış ve referans kaplama ile karşılaştırılmıştır. Karşılaştırmalar, değiştirilmiş dalga çeyreği katmanlarının, üst kaplama katmanlarındaki en yüksek sıcaklık değerini (en çok % 24.6) ve en yüksek ara yüzey sıcaklık değerini (en çok % 21.6) düşürdüğünü göstermiştir. Diğer yandan iç katmanlardaki lazer emiliminin ise arttığı gözlenmiştir. Bu noktada iç katmanlardaki emilimi azaltan yeni bir tasarım yöntemi önerilmiştir. Yeni yöntem için katman kalınlıkları, geliştirilen MATLAB kodunca hesaplanmaktadır. Sonuçlar, yeni yöntem

ile yapılan tasarımdaki sıcaklık değerlerinin önceki alternatif tasarımlara göre iç ve ara yüzey sıcaklıklarında (en çok %15.4) düşüş sağladığını ortaya çıkarmıştır.

Sayısal çalışmalarla birlikte, imal edilen referans kaplama ve alternatif tasarımlara sahip kaplamalar üzerinde lazer hasar eşiği (LHE) testleri ve hasar morfolojisi incelemeleri yapılmıştır. Bu doğrultuda hasar tipleri tanımlanmış ve hasar karakteristiklerindeki değişiklikler incelenmiştir. İnceleme sonuçları, değiştirilen katman kalınlıkları ile sayısal çalışmalarda da hesaplatıldığı gibi, sıcaklık değerlerinin düşük kırılma indisli katmanlar yardımıyla indirgendiğini ve LHE değerini iyileştirildiğini göstermiştir.

Anahtar Kelimeler: Optik ince film kaplamalar, Sıcaklık alan teorisi, Değiştirilmiş dalga çeyreği tasarımı, Üç malzemeli kaplamalar, Hasar morfolojisi

To my family

ACKNOWLEDGMENTS

The author wishes to express his sincere appreciation to his supervisor Assist. Prof. Dr. Cüneyt SERT and Co-supervisor Assoc. Prof. Dr. Tuba OKUTUCU ÖZYURT for the endless support, encouragement and patience during his research activities.

The author would like to thank ASELSAN, Inc. and his project leader Alp Eren Sinan ÖZHAN, for his support and guidance in his study and let to use experimental facilities of optical design department.

The author is thankful to his superior Dr. Ali M. ÇOLAKOĞLU for the encouragement and guidance. Without his unconditional support in guiding the author to study on thin film optics, this dissertation would never have come into existence.

The author owes special thanks to his colleagues Hacı BATMAN, Gülgün H. A. KURU and M. Burak COŞAR for their assistance and contributions to experimental parts of the dissertation.

The authors would like to express his appreciation to his colleagues Dr. Arif C. GÖZÜKARA, Dr. A. Berkan ERDOĞMUŞ, Dr. Güvenç CANBALOĞLU and Argün KATIRCI for their valuable support and understanding.

Lastly the author would like to express his endless gratitude to his wife and parents for their love, support and faith in him.

TABLE OF CONTENTS

LIST OF TABLES

TABLES

LIST OF FIGURES

FIGURES

LIST OF SYMBOLS AND LIST OF ABBREVIATIONS

Symbols

a_o	: Beam radius [m]
C	: Specific heat capacity [j/kg·K]
d	: Physical layer thickness [m]
$\vec{E}$	: Electric field vector
E	: Total electric field at some position
E_n^2	: Square of the normalized electric field intensity
E_a	: Free admittance
E_0^+	: Electric field in the incident wave
g	: Temporal shape of laser pulse
H	: Total height of the stack
$\vec{H}$	: Magnetic field vector
I_o	: Peak power intensity [MW/cm^2]
k	: Thermal conductivity [W/m·K]
m	: Number of layer pairs
M	: Characteristic matrix of each layer
M	: Characteristic matrix of the stack
M'	: Inverse of M

M'' : Resultant matrix product of M and M'

n : Refractive index

$\tilde{n}$: Complex refractive index

N : Number of total layer

R' : Reflectivity

R : Radius of the lens [m]

R : Second high refractive index layer

S' : Poynting vector

S : Substrate

t : Time [s]

T : Temperature [K]

T_o : Initial temperature

q : Heat source term [W/m^3]

Q_{abs} : Local laser energy absorption

Q_{las} : Incident laser intensity

Z : Arbitrary distance [m]

Greek Symbols

α	: Absorption coefficient [m^{-1}]
β	: Optical phase thickness
κ	: Extinction coefficient
λ	: Wavelength [m^{-1}]
ρ	: Density [kg/m^3]
ϱ	: Effective refractive index
θ	: Indicator of the absorbed laser energy

Subscripts

$_H$	: High refractive index
i	: Layer number
$_L$	: Low refractive index

Abbreviations

APS	: Advanced Plasma Source
CVD	: Chemical Vapor Deposition
DIC	: Differential Interference Contrast
EB	: Electron Beam
EFI	: Electric Field Intensity
FEM	: Finite Element Method
H	: High refractive index layer
HR	: Highly reflective
IP	: Ion Plating
IBS	: Ion Beam Sputtering
L	: Low refractive index layer
LIDT	: Laser Induced Damage Threshold
LP	: Low Pressure
NQWD	: Non-Quarter Wave Design
OC	: Over Coat
PE	: Plasma Enhanced
PIAD	: Plasma Ion-Assisted Deposition
RF	: Radio Frequency
RFS	: Radio Frequency Diode Sputtering
TE	: Transverse Electric
TM	: Transverse Magnetic

TMC	: Three Material Coating
UDF	: User Defined Function
QWD	: Quarter Wave Design
WLI	: White Light Interferometry

CHAPTER 1

INTRODUCTION

1.1 Motivation

Laser technology is one of the most promising technologies in engineering world since its great potential has been accepted by the engineers. Scientific advancements enabled engineers to build up more powerful (high intensity) laser devices in a variety of wavelength regimes. Output power intensities of contemporary lasers can reach kilowatt level for continuous wave operations [1] and petawatt level for pulsed systems [2]. Such kind of ultimate lasers are employed in applications including, but not limited to, military grade solid state laser weapons [3-4] and laser range finders [5]. One major problem with high intensity laser irradiation is that it conversely affects optical components (e.g. mirrors, prisms and lenses) of the laser assembly. Therefore optical parts of laser systems are designed as durable as possible against to destructive effects of the high power lasers. Herein the weakest parts of optical lenses and mirrors, are thin films, which are delicate to high intensity laser fluences. Therefore the endurance limit of these thin films become a limiting agent for the laser systems output intensity [6-8].

As expected, when the low intensity laser beam passes through an optical lens or reflected from an optical mirror, no destructive effect might be seen. However if the output of the irradiation is reached to a very high level it may cause irreversible modifications (damages) on multilayer thin film coatings such as delamination, smashing, melting, pitting and cracking. For this reason it is important to reveal interaction between laser irradiation and multilayer coatings to predict and avoid potential damages. The critical laser fluence level or value that results a non-reversible change (or in other words damage) is named as LIDT.

Researchers sorted damage mechanisms into three category [6]. The primary and significant damage mechanism is observed as the thermal laser damage. The thermal laser damage is resultant from the absorbed laser energy which is converted into heat actually. In detail, the energy absorption causes sudden and local temperature rise and this starts the local deformation. The second damage mechanism is the dielectric breakdown and the third one is the multiphoton ionization. The second and third damage mechanisms are effective when the Electric Field Intensity (EFI) is extremely great to pick off electrons from the lattice structure at the picoseconds pulse width levels.

As pointed out above durability of thin films became a limiting factor for the laser system output intensity. For this reason numerous studies have been performed on laser damage for optical materials with analytical, numerical and experimental methods over the last forty years [9-11]. In these studies, durability of optical coatings have been tried to be increased by studying the effects of production methods and laser parameters on LIDT. Moreover optical design modifications have also been proposed to increase laser resistance of conventional optical designs. In most of the studies, standing wave electric field distributions have been modified by employing overcoat layers, non-quarter wave layers or secondary high refractive index materials. Effects of these optical design modifications have been studied from a heat transfer point of view by only few researchers. In those studies, laser irradiation induced temperature distributions inside optical coatings are obtained by solving the unsteady heat diffusion equation. However, only positive effects of the modifications on thermal performance of the coatings have been stated without giving any details. Disadvantages of these modifications have not been clarified.

In the present study effects of optical design modifications on thermal performance of HR multilayer thin films are studied. It is believed that both benefits and drawbacks of these optical design modifications on thermal performance can be revealed by performing versatile numerical simulations on the modified optical designs. Then, the observed drawbacks can be scrutinized with in details and solutions can be proposed. Moreover, modified optical designs can be fabricated to perform experimental LIDT tests. LIDT measurement tests and complementary damage morphology investigations can support numerical studies.

By performing the mentioned numerical and experimental studies, the effects of optical design modifications on thermal performance can be revealed and further enhancements on the modified optical coatings can be achieved.

1.2 Literature Survey

As pointed out in the previous subsection, one of the main goals of this dissertation is to study the effects of optical design modifications on thin films' thermal performance. In order to achieve this, firstly the laser irradiation induced temperature distribution in multilayer thin films needs to be calculated. Considering this requirement, in this subsection, literature studies are investigated to understand how laser irradiation causes temperature rise in the multilayer coatings. In the light of literature, the interaction between laser irradiation and multilayer optical coatings is clarified as follows.

When a laser ray is pointed upon an optical lens or mirror, some part of energy is absorbed in the form of heat. The amount of absorbed energy depends on intensity of the laser beam, wavelength of laser, optical, mechanical and thermal characteristic of the irradiated optical component. The absorbed laser energy which is in the form of heat causes temperature rise on the component surface as expected. The max temperature variation behavior of on an optical component can be seen in Figure 1.1 for different laser pulse temporal shapes [6].

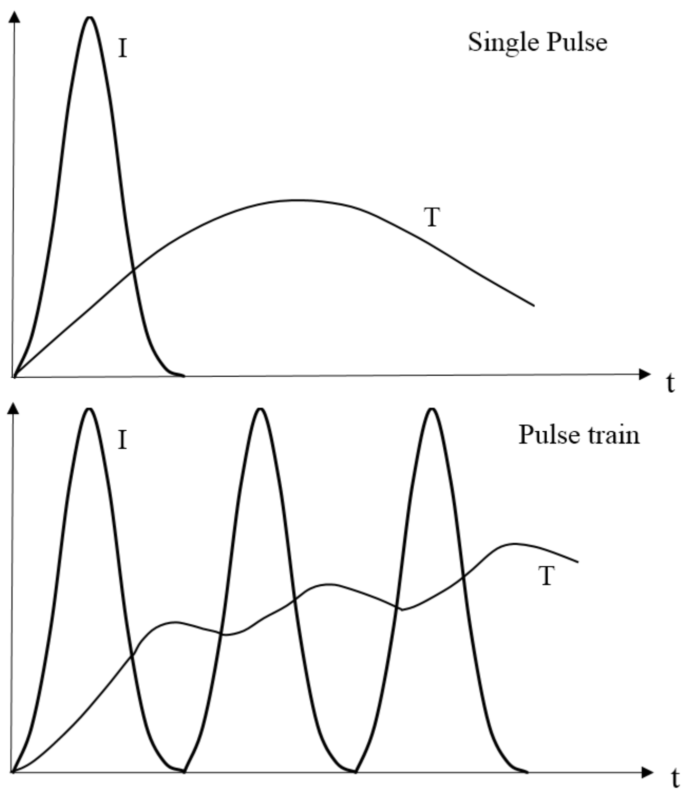

Figure 1.1 The max temperature variation behavior for different laser pulse temporal shapes, *T*: Surface temperature, *I*: Laser beam intensity, *t*: time [6].

The temperature rise on the surface or bulk of the material is undesired for most of the case. Because the temperature rise may causes thermal expansion, strain, distortion, movement of internal defects, cracking, melting or catastrophic shattering on material. Moreover if the laser peak power intensity is increased enormously, phenomenological events may occur such as self focusing, nonlinear absorption-transmittence, electoro-optic effects, 2nd harmonic creation, optical oscillation and etc. [6]. The mentioned phenomenological events may cause amplification on the amount of energy absorbed.

The absorbed laser energy in a cylindrical volume on the axis of the laser beam when passing through a transmitting medium can be calculated using mathematical relations and laser parameters. In literature [12-16] absorbed laser energy computations are combined with the heat diffusion equation. Numerical and analytical studies are performed to determine temperature rise on the surfaces of laser radiation exposed optical components in most of the cases. Studies related with laser induced heating of optical parts can be separated in two groups as laser induced heating on bulk materials (such as on substrates) and laser induced heating of multilayer optical coatings.

1.2.1 Laser Induced Heating On Bulk Materials

Laser induced heating or in other words laser thermal effect as described in previous parts is the dominant damage mechanism. Because it causes melting, ablation, surface morphology changes and etc.. Therefore it is important to predict laser induced temperature rise and its distribution on a bulk material (such as an uncoated lens or a silicon detector) at the design stages. In literature numerical studies were performed to obtain temperature distribution for such cases. The heat diffusion equation had been used and the heat source was computed according to laser parameters, optical properties and material properties of the heated bulk objects.

Cheng *et al.* [12] used the heat diffusion equation in their study to numerically investigate the axisymmetric excitation of the thermoelastic waves in plates by a pulsed laser. The time scale of the laser pulse was 1 μs for that study. Lu *et al.* [13] studied the problem of transient thermal conduction and temperature distribution generated by laser pulses in a planar sample. In order to simulate heating effect of pulsed laser, the heat diffusion equation was solved numerically. The pulse duration of the laser was 4 ns. Mi *et al.* [14] used 2D Finite Element Method (FEM) based numerical model in cylindrical coordinates for film-substrate system. The heat diffusion equation was used as governing equation. The used pulse duration was 4 ns in that study. Shuja *et al.* [15] studied on pulsed laser heating of solid surface to compute melting and mushy zones due to temperature rise.

One of the important studies on laser induced heating for a bulk material (silicon crystal) was performed by Wang *et al.* [16] in 2010. In this study, thresholds of laser induced damage were computed using theoretical and mathematical models. The mathematical model that is a two dimensional FEM numerical scheme was used to compute temperature increase on silicon in cylindrical coordinates numerically, Figure 1.2.

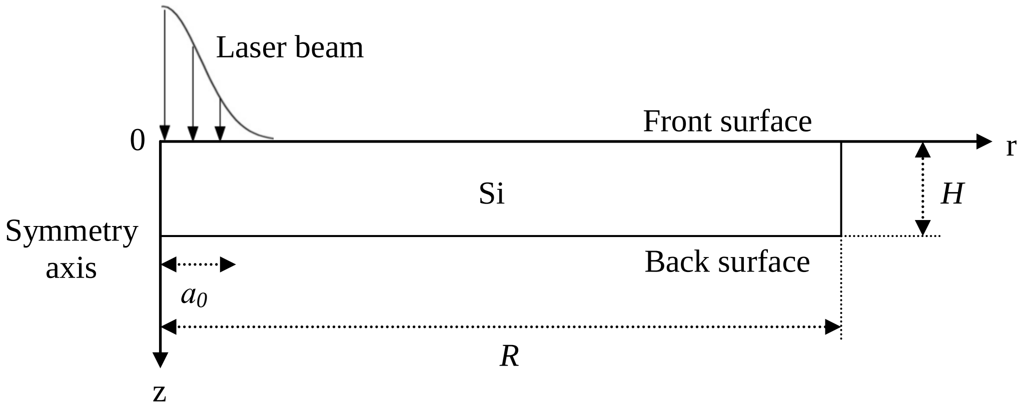

Figure 1.2 Schematic of the axisymmetric FEM model [16]. Reprinted from “Laser-induced damage threshold of silicon in millisecond, nanosecond, and picosecond regimes,” by X., Wang, Z. H., Lu, J., Shen, and X. W. Ni, 2010, *Journal of Applied Physics, 108*(3), p. 033103. Copyright 2015 by the Copyright Clearance Center.

One of the remarkable outcomes about that study was the timescale. It was pointed in the study “multiphoton avalanche ionization gradually become dominant at pulse lengths shorter than 10^{-13} s” and that was also adjoined “it is feasible to simulate the heating process of silicon on thermal conduction theory for 10 ps pulse width”. Considering these observations, the governing equation was determined as the heat diffusion equation. The axisymmetric form of the heat diffusion equation was given in the study as follows;

$$\rho C\frac{\partial T(r,z,t)}{\partial t}=\frac{1}{r}\frac{\partial}{\partial r}\left(rk_i\frac{\partial T(r,z,t)}{\partial r}\right)+\frac{\partial}{\partial z}\left(k_i\frac{\partial T(r,z,t)}{\partial z}\right)+q_i(r,z,t) \tag{1.1}$$

In Eqn. (1.1), ρ, k and C are the density, the thermal conductivity and the specific heat capacity, respectively. T is the unknown temperature distribution and the $q_i(r,z,t)$ is the key parameter heat source term. The heat source was computed with using the following equation.

$$q_i(r,z,t)=I_o(1-R')\left(\frac{4\pi\kappa}{\lambda}\right)e^{\left(-2r^2/a_0^2\right)}g(t)e^{\left(-4\pi\kappa z/\lambda\right)} \tag{1.2}$$

In Eqn. (1.2), I_0 is the peak power intensity of the laser, R' is the reflectivity, κ is the extinction coefficient, λ is the wavelength, $g(t)$ is the temporal shape of the laser pulse, a_0 is the beam radius ($1/e^2$). For the solution of Eqn. (1.1) following boundary conditions were used.

$$\left.\frac{\partial T(r,t)}{\partial z}\right|_{z=H}=0 \tag{1.3}$$

$$\left.\frac{\partial T(z,t)}{\partial r}\right|_{r=R}=0 \tag{1.4}$$

No heat flux transfers along the radial direction on the z-axis, therefore in the axisymmetric model it was assumed that;

$$\left.\frac{\partial T(z,t)}{\partial r}\right|_{r=0}=0 \tag{1.5}$$

The initial condition was given in Eqn. (1.6).

$$T_0=300\text{ K} \tag{1.6}$$

In the study some assumptions were also noted to solve problem. These assumptions are (1) silicon material was assumed as homogeneous and isotropic, (2) the model was large enough that heat will not transfer to the boundary through laser radiation, (3) the back surface of the model was adiabatic, (4) convection and radiation at the front surface were disregarded.

1.2.2 Laser Induced Heating On Multilayer Optical Coatings

Due to current trends in optical industry, an optical element (lens or a mirror) can not be considered without its thin film. Unfortunately (as described in previous chapters) optical coatings are the weakest structures in the optical systems. Since the thicknesses of the multilayer optical coatings are on the order of 10-100 nanometers, material properties are different than bulk forms. The order of thickness and weak material properties (according to bulk forms) made optical coatings more likely to damage. Consequently prediction of temperature increase on optical coatings has been drawn more interest in optical systems where high power lasers are used.

In literature, various numerical studies were performed to compute temperature rise and spatial distribution on optical lenses together with their multilayer optical coatings. As described in previous chapters, the computation of the amount of energy that is absorbed by optical element is important. The amount of absorbed energy in the form of heat can be computed as given in Eqn. (1.2) for a bulk material such as an optical substrate. Unfortunately Eqn. (1.2) can not be used for optical coatings due to reflections from film/film and film/substrate interfaces. In literature Maxwell's equations has been used to compute the amount of absorbed laser energy in multilayer structures [17-18]. The computation procedure was given by Grigoropoulos in his "Transport in Laser Microfabrication" book, explicitly. The explanation of Grigorpoulos gives the amount of absorbed laser energy in terms of poyinting vector as seen in Eqn. (2.7) for a laser heated conventional N layer stratified coating stack.

$$Q_{abs}(x,y,z,t)=Q_{las}(x,y,t)\ \frac{dS'(z)}{dz} \tag{1.7}$$

In Eqn. (2.7), Q_{las} is the incident laser intensity distribution and $S'(z)$ represents poyinting vector. Explicit form of poyinting vector is also given in Eqn. (1.8).

$$S'(z)=\frac{1}{2}\mathrm{Re}\left[\vec{E}(z)\times\vec{H}(z)\right] \tag{1.8}$$

In Eqn. (2.8), $\vec{E}(z)$ and $\vec{H}(z)$ represents the variation of electric and magnetic fields through the stratified coating stack. Interested readers may find more specific solution corresponding to electric and magnetic fields in the Grigoropoulos' study.

Even though Grigoropoulos gave the solution of the Maxvwell's equation using characteristic transmission matrix method for the poynting vector variation through z direction, the explicit form of the $Q_{las}(x,y,t)$ term was not provided.

Wang *et al.* provided the explicit form of the spatial and temporal distribution of laser absorption through a laser heated multilayer optical stack (Figure 1.3) in their study, [19]. In that study, the axisymmetric form of the heat diffusion equation (Eqn. (1.1)) was used in cylindrical coordinates.

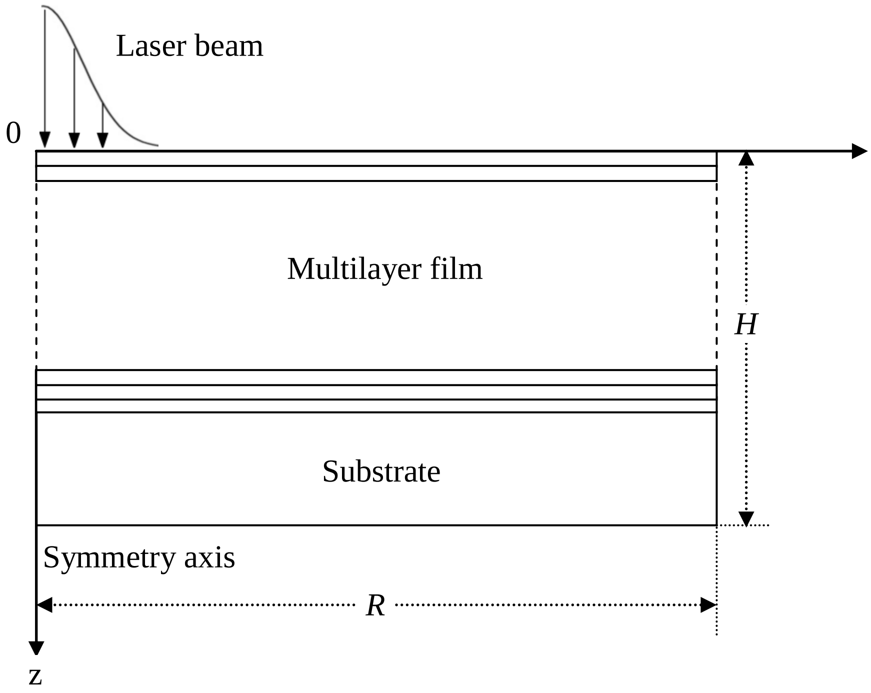

Figure 1.3 Schematic of the axisymmetric model given for multilayer optical stack [19]. Reprinted from "Effect of defects on long-pulse laser-induced damage of two kinds of optical thin films," by B., Wang, Y., Qin, X., Ni, Z., Shen, and J., Lu, 2010, *Applied Optics*, *49*(29), p. 5537. Copyright 2015 by the Copyright Clearance Center.

Then the explicit form of $q_i(r,z,t)$ (which is the heat source term in Eqn. (1.1)) and boundary conditions were given explicitly (Eqn. (1.9) and Eqn. (1.10)).

$$q_i(r,z,t) = \left\{\frac{4\pi\kappa_i}{\lambda} E_n(z)^2\, n_i\right\}\, I_0\, exp\left(-\frac{2r^2}{a_0^2}\right)\, g(t) \tag{1.9}$$

$$\left.\frac{\partial T(r,t)}{\partial z}\right|_{z=H} = \left.\frac{\partial T(z,t)}{\partial r}\right|_{r=L} = \left.\frac{\partial T(z,t)}{\partial r}\right|_{r=0} = 0 \tag{1.10}$$

In Eqn. (1.9), $E_n(z)^2$ is the square of the normalized EFI, n is the refractive index and $4\pi\kappa_i/\lambda$ is also called as absorption coefficient, α.

1.3 Objective Of The Dissertation

In the literature, laser resistance improvements of thin films have been studied for HR multilayer thin films. LIDT of the multilayer coatings is attempted to be increased using the modified conventional optical designs. Positive effects of these modified optical designs on thermal performance of the coatings are also studied by few researchers. However, none of these studies perform a systematical assessment study on the benefits and drawbacks of these modifications on thermal performance. Considering this lack in the literature, a versatile investigation study that corresponds to optical design modifications on thermal performance is aimed. Both numerical and experimental studies are performed for this purpose. Firstly studies which involve numerical computation of the laser irradiation induced temperature distribution calculations are reviewed in the literature. In these studies numerical techniques, governing equations, boundary conditions, material properties and laser parameters are explored. Then, numerical studies are performed to find out the effects of optical design modifications on thermal performance. To this end, a conventional 19 layer HR thin film is selected as a reference design. Firstly, laser induced temperature distribution is obtained for this design. Then, alternative HR designs are developed by modifying the optical layer thicknesses. Optical layer modifications are done by employing non-quarter wave layers, upper surface OC layers and two high index materials in the coating stacks.

The effects of usage of non-quarter wave layers on thermal performance are examined by numerical simulations. In the numerical simulations both single shot and multiple shot laser irradiations are used. For the single shot laser irradiation, it is observed that temperatures inside the high index layers and the interfaces can be decreased by using the non-quarter wave layers. Unfortunately the non-quarter wave layers cause penetration of more laser energy inside the inner layers because the penetration of laser energy increases the laser absorption and hence, results higher temperatures. It is also realized that the laser absorption drawback plays a more important role for the multiple shot laser irradiation case. In order to decrease the laser absorption, a new NQWD is proposed. Layer thicknesses of the new design are calculated using the in-house developed MATLAB code. The newly proposed design shows better thermal performance by decreasing the internal and interface temperatures compared to other alternative designs.

The effects of OC layers and three material coatings (TMC) (in which two high index materials used in the same coating stack) on temperature distributions are also studied numerically. Herein no positive effects has been observed when the OC layers are used. On the other hand, for the TMC designs, it is seen that temperatures can be decreased at the top laser resistant layer pairs by modifying a few top layer pair thicknesses; however it causes temperature increase at HR inner layer pairs. Moreover, the modification of top layer pairs also yields lower maximum temperature value in the stack compared to conventional quarter wave layers.

In addition to the numerical studies, base design and alternative designs are also fabricated for the experimental LIDT testes. The purpose of the LIDT measurements is to support numerical investigations and to find out optical design improvements on LIDT value and laser induced damage morphologies. LIDT measurements show that better LIDT performance can be obtained by using the modified optical designs. After the LIDT measurement tests, damage morphologies on these HR coatings are also investigated. According to best of writer’s knowledge, effects of optical design modifications on damage morphologies are firstly studied in this dissertation, systematically. These investigations enable the identification of damage types and damage profile characteristics. Results of the experimental studies indicated that LIDT measurements should be evaluated along with the damage morphology investigations as only the morphology investigations can reveal the exact influence of optical design modifications on LIDT performance. This way, damage types which are resultant from other reasons (coating process resultant imperfections, contaminations etc.) can be eliminated.

1.4 Outline Of The Dissertation

In the present study, the effects of optical design modifications on thermal performance of HR multilayer thin films are investigated through numerical and experimental studies. Numerical studies are employed to find out advantages and drawbacks of the electric field modification methods on the laser induced temperature distribution inside the coating layers. Observed drawbacks are scrutinized and a new non-quarter wave design (NQWD) alternative is proposed to obtain reduced temperatures inside the coating stack. In addition to numerical efforts, fabrication and experimental LIDT measurement processes are also performed. The outline of the dissertation is given below:

In the second chapter material properties, thermal conductivity and refractive index are discussed for the thin film forms. Effects of production methods, film thickness orders and measurement methods on the material properties are presented. Significant studies which report the measured thermal conductivity and refractive index values of commonly used thin film materials are summarized.

In the third chapter, numerical model is presented. Based on the numerical model, the effect of different parameters are discussed. Firstly, a literature review about the numerical calculation of the laser induced temperature distribution on multilayer stacks is presented. Then, the performed validation study is elucidated which involves the details of the followed numerical procedure. In the third subsection, numerical simulations which are performed with alternative NQWDs are reported in terms of temperature distributions and laser absorption amounts. Investigation of temperature distribution results has continued with the multiple shot laser irradiation simulations. At the end of this part, a newly proposed alternative design is introduced. Effects of OC layers on temperature distribution are also reported in the third chapter. In the last part of the chapter, TMC designs are investigated. Modified layer thicknesses are used in the design and their effects has been discussed.

In the fourth chapter, experimental studies are presented under three subsections. In the first subsection, thin film deposition technique and the fabricated HR coatings are introduced in detail. In the second subsection, the LIDT measurement setup which is settled down in ASELSAN Inc. is demonstrated. In the third subsection, the statistical LIDT measurement results are reported for the fabricated HR coatings. In addition, damage morphology investigations on the tested HR coatings are presented. Both damage type identifications and the damage profiles are discussed for each of the fabricated design. Important aspects about the damage morphology investigations are stated.

In the last chapter, summary of the dissertation, conclusions and the future recommendations are presented.

CHAPTER 2

EFFECTIVE THIN FILM MATERIAL PROPERTIES FOR LASER INDUCED HEATING

Material properties of thin films show discrepancies compared to those of their bulk forms because of microstructure and stoichiometry in thin films and interface effects [20] .Thin film microstructure (size and shape of grains, vacancies and dislocations, anisotropy, phase composition, presence of cracks and etc.) is relevant with the production method [21]. Particularly, optical thin films are fabricated in vacuum chambers and various techniques have been used to produce these films in these chambers such as physical vapor deposition, chemical vapor deposition, sputtering, ion plating and etc. [22]. All these methods produce thin films atom by atom and resultant thin films have thicknesses on the order of nanometers. Such small thickness values and non-traditional production processes lead to differences in microstructure and corresponding material properties compared to bulk counterparts.

In the current study three of the key thin film material properties are investigated in the literature for their thin film forms. They are the thermal conductivity k, the refractive index n and the extinction coefficient κ. Actually the last two term can be combined under a single parameter which is complex refractive index $\tilde{n} = n - j\kappa$. The heat diffusion equation and corresponding heat source terms are given in Eqn. (1.1) and Eqn. (1.9) in pervious chapter. As seen in Eqn. (1.1) and Eqn. (1.9), these thin film material properties are important for the solution of the heat diffusion equation on multilayer stacks [13, 16-18].

2.1 Thermal Conductivity Of Thin Films

The thermal conductivity of thin films has become an important parameter since its size dependent variation was firstly reported by Amudsen and Olsen [23] in 1965. Attentions to thermal conductivity of thin films have increased since 1980, due to demands of solutions to thermal management problems in microelectronics and optoelectronics applications.

The increasing attention to thermal conductivity of thin films steers researchers to study on thermal conductivity measurements for thin films. But measurement and evaluation of thin film thermal conductivity are not easy. Conventional measurement techniques cannot be applied to thin films due to the order of the thickness of films (≈100 nm).

One of the earliest studies about thermal conductivity of thin films was published by Ristau and Ebert [24] in 1986. In that study a thermographic laser calorimeter was used to measure absorption and thermal conductivity of SiO_2, TiO_2, HfO_2, Al_2O_3 and Ta_2O_5 thin films. Measurements were performed for 4, 8 and 12 quarter wave optical thicknesses and results are given in a tabular form for each coating material as seen in Table 2.1

Table 2.1 Thermal conductivities of the films reported by Ristau and Ebert [24].

Material	**Absorption coefficient (cm^{-1})**	**Thermal conductivity (W/cm·°C)**
HfO_2	6.7	7.7×10^{-6}
Al_2O_3	16.3	3.3×10^{-1}
Ta_2O_5	6.8	2.6×10^{-4}
TiO_2	37.2	1.8×10^{-4}
SiO_2	0.8	1.0×10^{-3}

Ristau and Ebert pointed out that the thermal conductivities of thin films are much smaller than those of the bulk materials except Al_2O_3. Extremely low thermal conductivity of HfO_2 was conducted to “cracking of some layers causing disconnections of the heat flow across the surface”.

Another pioneering study about thin film thermal conductivity was published by Lambropoulos *et al.* [25] in 1989. They used an improved thermal comparator device to measure thermal conductivity.

In that study, both thin film thermal conductivities and film/substrate interface resistances were reported. The film/substrate interface resistance was introduced as the indicator of the deposition technique effect. Measured thermal conductivities and interface resistances were summarized in a table for various thin film materials as shown in Table 2.2. As seen in the table, thin films were deposited on substrates with using two different techniques. One of them is Electron Beam (EB) evaporation and the other one is Ion Beam Sputtering (IBS).

Table 2.2 Thermal conductivity and interfacial resistance table reported by Lambropoulos *et al.* [25]

Material / Deposition method	**Thermal conductivity (W/m·K)**	**Interface resistance (mm^2·K/W)**
SiO_2 / EB	0.61	1.1
SiO_2 / IBS	1.05	1.8
TiO_2 / EB	0.59	2.7
TiO_2 / IBS	0.48	0.54
HfO_2 / EB	0.052	N.A.
Al_2O_3/EB	0.72	1.0

At the end of that study, it was pointed out “thermal conductivity of oxide and fluoride films is as much as two orders of magnitude lower than the thermal conductivity of the corresponding bulk solids”. Another important conclusion was drawn as silica films show serious thickness dependence in the range from 0 to 4 micron.

Decker [26] presented a summary for thin film thermal conductivity measurement techniques in his paper in 1990. Different experimental procedures were explained and thin film thermal conductivities for various materials were given. Measurement techniques were sorted as direct measurement (using dc potentiometric), comparator methods and photothermal techniques. At the end of that work thermal conductivity values were summarized for a few thin film materials which are commonly used in high power laser applications. Results also indicate variation of thermal conductivity values for different deposition techniques such as IBS and EB evaporation.

Henager and Pawlewicz [27] studied on thermal conductivity values of sputtered thin films in 1992. They both measured thermal conductivities of single layers of Al(SiO_2/Si_3N_4), Al(Al_2O_3/AIN) thin films and conventional coating materials SiO_2, Al2O_3, Ta2O_5, Ti and Si. A thermal comparator based apparatus was constructed and employed to measure thermal conductivities. Hanegar and Pawlewicz noted that thermal conductivity values of thin films are 10-100 times lower than that of bulk materials on normal to plane. The main reason of this reduction was conducted to irregularities in the amorphous (glassy) crystalline structure which means that the thin film lattice structure contains imperfections due to manufacturing type (Note: Thin films are growth atom by atom in sputtering process and it causes structural disorder in the film). The second reason of the lower thermal conductivity of optical thin films was pointed out as the interface between the thin film and the substrate. This interface behaves like a resistance against to heat transfer between film and the substrate. And that was also concluded, the interface between film and substrate has more significant effect on dielectric films according to metal films.

An important review study on photothermal characterization of thin films was published by Wu *et al.* [28] in 1997. Various photothermal characterization techniques such as photothermal deformation, mirage effect, thermal lensing and photothermal reflectance were explained extensively. These photothermal methods were declared as not only capable for thermal conductivity measurements but also for weak absorption measurements, local defects analysis and in situ laser-film interactions. In the study, measurement results of mirage effect, photothermal reflectance, photothermal deformation, and transient thermal grating methods values were compared for different thin film materials. Wu *et al.* observed, the results of the mirage effect method agree well with those from the transient thermal grating technique and disagree with those from photothermal reflectance and deformation methods. The discrepancy between the results of mirage effect method and other photothermal techniques was mainly associated to the existence of thermal anisotropy in the thin films. Wu *et al.* concluded that “Precise measurement of thermal conductivity can provide information about finite size effects, structural anisotropies, defects and impurities, as well as the effects of interfaces and grain boundaries. It can also give insight into understanding the roles of thermal effects in the failure of optical thin film coatings due to high power laser irradiation.”

One of the important researches on thermal conductivity value of SiO_2 (which is a commonly used material in optical coatings) was studied by Burzo *et al.* [29] in 2002. In this study, variation of SiO_2 thermal conductivity in the range of 10-100 nm was extensively investigated. In addition to that interface resistance value between SiO_2 and gold layers were investigated. In addition, thin film thermal conductivities declared in the past studies were criticized because of the uncertainties. And that was concluded “investigating the literature one can reach only a qualitative conclusion; namely, that dielectric thin films are characterized by a thermal conductivity considerably lower than that of bulk samples, but no quantitative conclusions can be drawn”. Burzo *et al.* used a complicated measurement set up to find thin film thermal conductivity and interface resistances. The setup was called as transient thermo-reflectance. Burzo *et al.* focused their study on four sets of film/substrate samples for measurements of thin film thermal conductivity of SiO_2. For the first set, silicon oxide deposited on substrate by a thermal process (so called thermally grown). In the second set, sample was coated with additional chromium layer. In the third set silicon oxide deposited by IBS technique and in the fourth set additional chromium layer was coated. After then all sample sets were coated with Au layer. The purpose of Au layer coating was to minimize uncertainty of transient thermo-reflectance system. The purpose of chromium layer was to decrease interface resistance between silicon oxide and gold layer. Results of the measurements showed the reduction in the thermal conductivity of the film with the decrease in the thickness of the SiO_2 layer. Moreover, the results illustrate that the decrease in the conductivity is less than one order of magnitude, as compared with the bulk value. The origin of the decrease in thermal conductivity was conducted to two reasons by the writers. The first reason is the boundary scattering of the thermal carriers. Since the mobility of the phonon (thermal carrier in dielectrics) is affected by the scattering process due to defects and internal or external boundaries, which can be more important in thin films than in bulk materials. The second cause is the microstructure and stoichiometry of the SiO_2 layers. Microstructures of the thin films are highly porous near the layer interfaces. Thus, “a series of anisotropic microvoids oriented parallel with the plane of the films located at the interface can produce a significant density deficit”, which explicitly reduce the heat transport through the interfaces.

Another study about thin film thermal conductivity of SiO_2 was performed by Yamane *et al.* [30] in 2002. In this study an electrical non-destructive measurement technique (so called 3ω method) was used. Measurements were performed for various deposition methods such as thermal oxidation, Plasma Enhanced (PE) Chemical Vapor Deposition (CVD), Low Pressure (LP) CVD, sputtering and EB evaporation. Results of the study showed that the SiO_2 thin films above ~500 nm thickness growth by thermal oxidation agrees with the reported values of the bulk SiO_2. But for the films which are prepared by plasma CVD, sputtering, and evaporation are different. For SiO_2 thin films where the film thickness is below the 250 nm (prepared by thermal oxidation, plasma CVD, and sputtering) the observed thermal conductivity systematically decreases as a function of thin film thickness regardless of deposition technique. Another conclusion was drawn for the discrepancy of the thermal conductivity value for different deposition techniques. Films have different microstructure (porosity) for different deposition techniques and it greatly affects thermal conductivity of the film. The porosity in the microstructure causes decrease of thermal conductivity of the film.

Kim *et al.* [31] performed a study on measurement of thermal conductivity of TiO_2 thin films using 3ω method in 2003. Writers pointed out that, thermal conductivity measurements have errors due to thermal radiation and heat loss in the temperature measurement but 3ω method can overcome these difficulties because it uses thin metal strip as both heater and thermometer. In that study film samples were prepared with two thicknesses of 150 and 80 nm by a dc magnetron sputtering machine. TiO_2 films were deposited on substrates at different temperatures (80K-350K) to evaluate the deposition temperature on coating quality. Reported results revealed that thermal conductivity of TiO_2 was increased with the increasing deposition temperature and also it was pointed out in the study the thermal conductivity is dependent to film thickness strictly.

Chien *et al.* [32] proposed an easy to use technique to measure thin film thermal conductivity. The excellence of that method was noted as simplicity. The setup just involves commonly used instruments and also it doesn't involve any signal processing circuit. The method was defined as an electrical heating/sensing technique by authors. Measurements were performed on SiO_2 thin films. To evaluate the effect of film thickness on thermal conductivity, measurements were repeated for different coating thicknesses. In addition to that coatings were also deposited with three different techniques to appraise the effect of deposition technique. E-beam results were presented with in Figure 2.1.

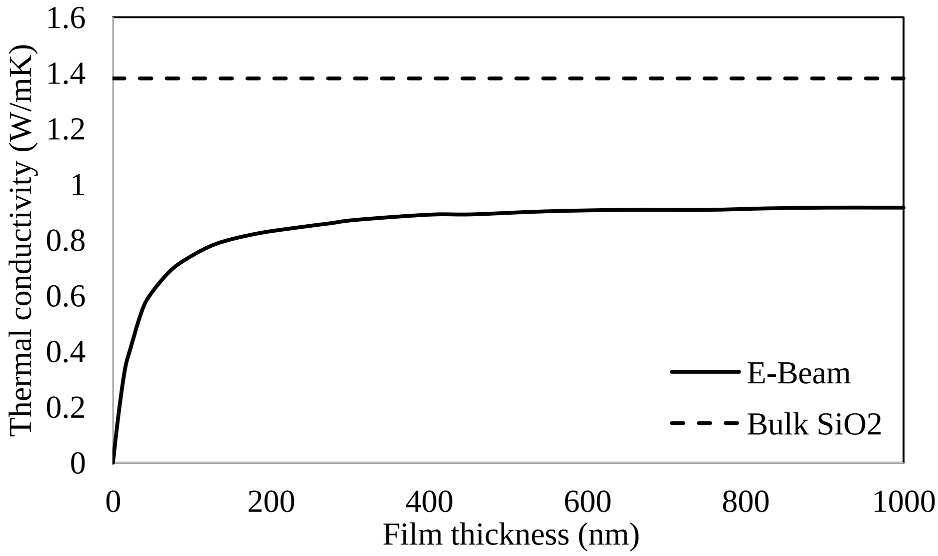

Figure 2.1 Thermal conductivity of SiO_2 thin film reported by Chien *et al.* [32]. 32. Reprinted from "Thermal conductivity measurement and interface thermal resistance estimation using SiO2 thin film," by H. C., Chien, D. J., Yao, M. J., Huang, and T. Y., Chang, 2008, *Review of Scientific Instruments*, *79*(5), p. 054902. Copyright 2015 by the Copyright Clearance Center.

The uncertainty of the measurement was reported as approximately "11% for 50 nm thickness and 3.4% for 500 nm thickness" by authors.

As explained in the current chapter, thermal conductivity is much smaller (10-100 times) than bulk value for thin films. Considering reference studies, the reduction of thermal conductivity value can be conducted to two main reasons.

The first reason of the reduction is the microstructural factors. Any microstructural or stoichimetric irregularity leads to decrease of thermal conductivity of thin films. For example, amorphous (non-crystalline) structure of thin films is the one of the microstructural factors that decreases the thermal conductivity. Porosity (especially near the boundaries of the thin films) is another microstructural irregularity example. Porosity causes a series of anisotropic microvoids oriented parallel with the plane of the films located at the interface produce density shortage. The second reason of the reduction of thermal conductivity is the interface resistance. Both film/substrate and film/film (for multilayer stacks) interfaces affects energy transfer through the film stack considerably. The interfaces behave like barriers against to heat flow because the mobility of the (thermal) energy carriers (phonons and electrons) are affected by the scattering process due to internal or external boundaries [22].

However there is an agreement about the lower thermal conductivity values for thin films, the order of decrease is not exact. Thin film thermal conductivities are usually 10-100 times lower than conductivities for the same materials in bulk form. The reason of the variation (10 to 100 times) of order of reduction can be conducted to deposition (production) techniques [21]. Different deposition techniques cause different thin film thermal conductivities. Old deposition techniques such as CVD cause much smaller thermal conductivities than relatively new deposition techniques such as IBS. The reason of this discrepancy is the energy transferred to material atoms during the deposition process. As expected more energy transferred to atoms in new deposition techniques and denser thin films can be obtained.

The size dependent behavior of the thin film thermal conductivity is well investigated in the past as summarized above, however the temperature dependence of thermal conductivity for optical coatings is not studied in literature, according to best of author’s knowledge. The possible reason of this literature gap may be the dielectric property of the optical coating materials. Conventional optical coating materials such as TiO_2, HfO_2 and SiO_2 are all dielectric. For dielectric materials, it is known that, temperature dependence for thermal conductivity is very poor [33].

2.2 Refractive Index Of Thin Films

The refractive index which is a well known optical property can be defined as a radiometric quantity. It is basically a ratio of how hard it is for light to travel through a media. Complex refractive index contains both the real and the imaginary parts as given in Eqn. (3.1),

$$\tilde{n} = n - j\kappa \tag{3.1}$$

Where the first term of the right hand side, n, indicates the refractive index and the second term, κ, indicates the extinction coefficient.

The refractive index values of optical thin films can be found in literature. Typically these values are obtained through optical measurements with the help of spectrometers. The refractive index values of thin films are greatly affected by deposition methods. For this reason researchers usually specifies the deposition technique together with the reported refractive index values. A few literature works are summarized below that contains the refractive index values for commonly used thin film materials.

Torchio *et al.* [34] measured transmittance and reflectance of SiO_2 and HfO_2 thin films. These thin films were deposited both with Ion Plating (IP) and Plasma Ion-Assisted Deposition (PIAD) methods. In that study, the refractive index values were calculated with “numerical fitting of calculated spectral curves to the experimental curves by use of a single-layer model”. Refractive index results of that study were summarized in a graphical form as seen in Figure 2.1 and Figure 2.2 for SiO_2 and HfO_2 materials.

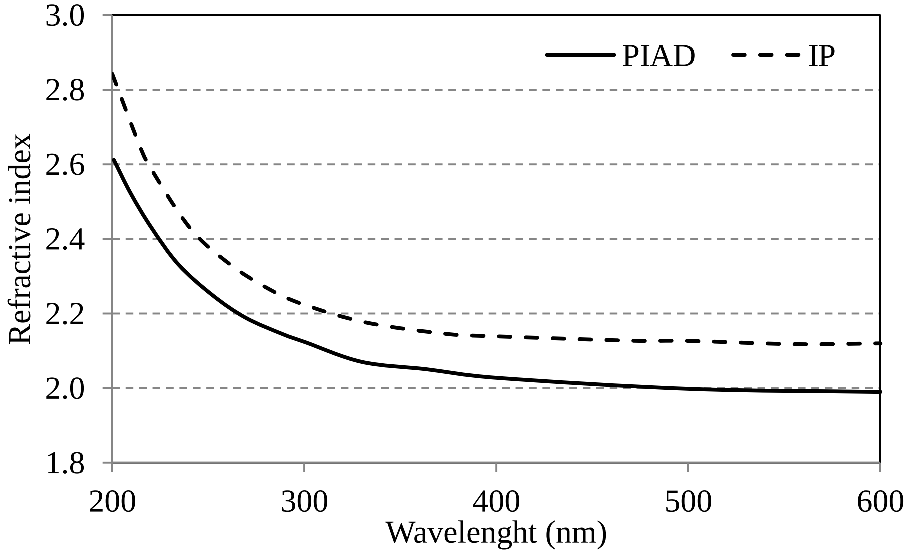

Figure 2.2 Refractive indices of HfO_2 films deposited by IP and PIAD [34]. Reprinted from "High-reflectivity HfO_2-SiO_2 ultraviolet mirrors,"by P., Torchio, A., Gatto, M., Alvisi, G., Albrand, N., Kaiser, and C., Amra, 2002, *Applied Optics*, *41*(16), p. 3256. Copyright 2015 by the Copyright Clearance Center.

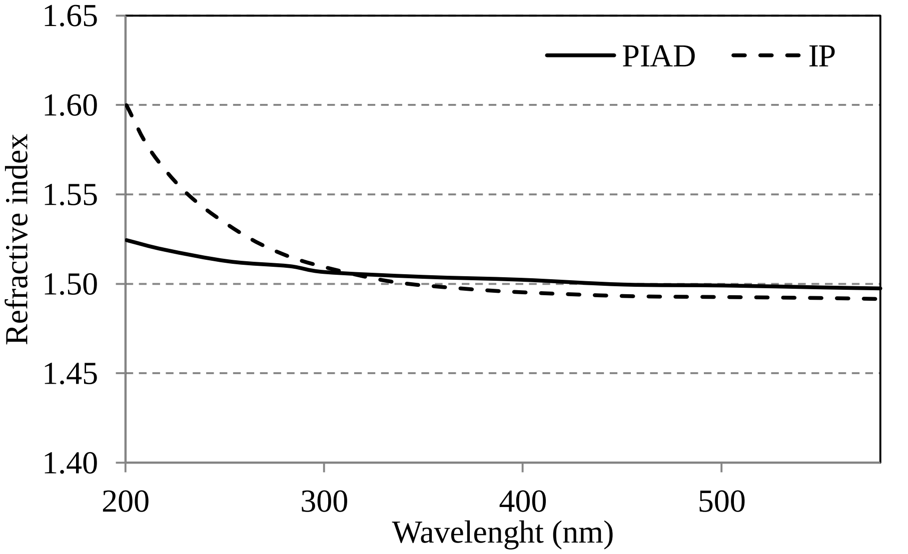

Figure 2.3 Refractive indices of SiO_2 films deposited by IP and PIAD [34]. Reprinted from "High-reflectivity HfO_2-SiO_2 ultraviolet mirrors,"by P., Torchio, A., Gatto, M., Alvisi, G., Albrand, N., Kaiser, and C., Amra, 2002, *Applied Optics*, *41*(16), p. 3256. Copyright 2015 by the Copyright Clearance Center

Another study was published by Commandre and Pelletier [35]. They measured the extinction coefficient of TiO_2 films with using sensitive collinear photothermal deflection method. Measurements were repeated on nineteen samples which were fabricated by different manufacturers and deposition techniques. Extinction coefficient results were reported in a tabular form in that study, Table 2.3. As seen in the table, both extinction coefficient mean values and corresponding standard deviations were given for different deposition methods. The lowest extinction coefficient mean value was obtained when IP method was employed for deposition. EB and IAD methods gave similar results for the mean value. It was noted in that study, comparatively high standard deviation values, observed at IBS and IAD methods, are conducted to the manufacturers. Authors also pointed out that number of tested samples have to be increased for more accurate calculation of extinction coefficient values.

Table 2.3 Extinction coefficient values reported by Commandre and Pelletier [35]

Deposition method	**Extinction coefficient**	
	Mean value	**Standard deviation**
EB	$1.1x10^{-4}$	$6.1x10^{-5}$
IAD	$1.3x10^{-4}$	$1.1x10^{-4}$
IBS	$2.1x10^{-4}$	$1.4x10^{-4}$
IP	$4.5x10^{-5}$	$7.0x10^{-6}$

Khoshman and Kordesch [36] investigated the refractive index value of amorphous HfO_2 thin films in their study. A set of single layer amorphous HfO_2 films were growth on quartz substrates using Radio Frequency (RF) reactive magnetron sputtering method. Then refractive index values were measured using spectrometric methods. Measurement results were reported for variation of refractive index in the 200-1400nm wavelength interval as seen in Figure 2.4.

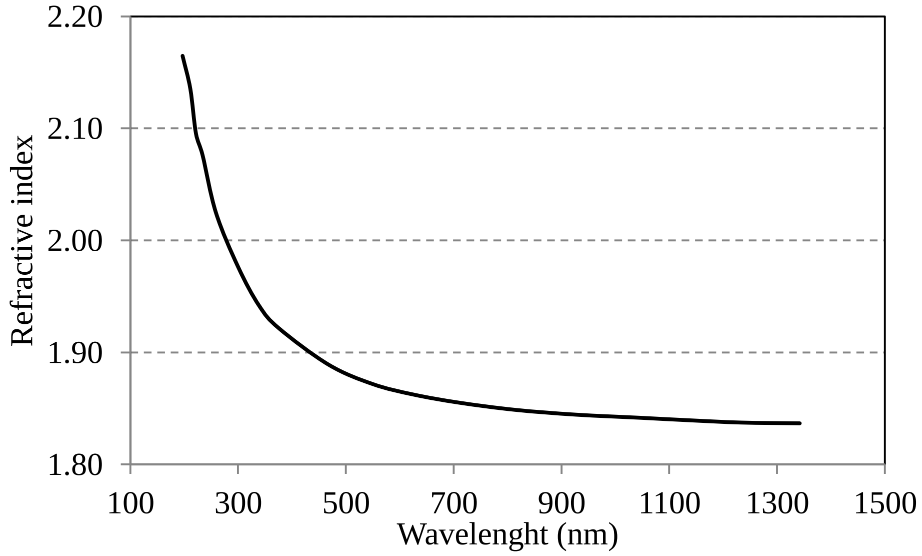

Figure 2.4 Refractive index and the extinction coefficients of amorphous HfO_2 films deposited by RF reactive magnetron sputtering method [36]. Reprinted from "Optical properties of a-HfO_2 thin films," by J. M., Khoshman, and M. E., Kordesch, (2006). *Surface and Coatings Technology*, *201*(6), p. 3530. Copyright 2015 by the Copyright Clearance Center.

Similar studies in which the refractive index values are reported for HfO_2, SiO_2, TiO_2, Ta_2O_5 thin films were also published by other researchers such as Stenzel *et al.* [37], Cevro and Carter [38], Ghodsi *et al.* [39], Thielsch *et al.* [40], Ai and Xiong [41].

CHAPTER 3

NUMERICAL STUDIES

Computation of temperature rise due to absorption of laser energy by layers of optical coatings has been investigated in literature [18, 42-55]. In most of them numerical approaches had been preferred instead of analytical solutions to compute temperature rise on multilayer coating stacks. In addition to that, commercial programs (which are developed for heat transfer analyses) were also used for computations.

According to best of author's knowledge, the first numerical study about the laser induced heating of multilayer optical coating was performed by Mansuripur *et al.* [18] in 1982. In that study, absorption of laser energy by the layers of optical coating and resultant temperature rise were studied extensively. A numerical technique which was called as "alternating direction – implicit" was used in numerical part of the study. The heat diffusion equation, Eqn. (1.1) was solved and the heat source term was computed with using electric and magnetic field components. The study was exemplified with a case numerical study in which temperature variation is computed for substrate (PMMA), aluminum, glass, magnetic film (MnBi), overcoat quadlayer stack. Thicknesses of layers are 32, 72, 12 and 100 nm respectively and the pulse length of the laser is 40 ns. Positive conclusions were drawn about the stability of the used numerical technique.

Another study in which temperature increase was computed with using heat diffusion equation was presented by Fan *et al.* [42] in 1992. The multilayer structure which was a high reflection stack has ZrO_2 and SiO_2 layers. The coating total thickness was on the order of 2000 nm and layer number was more than 13. The heat source term was computed with respect to poynting vector as described in the first chapter. Similar studies (in which the heat diffusion equation is used and the heat source is computed with respect to pointing vector) were published by other researchers such as Zhao and Fan [43], Papernov and Schmid [44], Zhao *et al.* [45], Hu *et al.* [46], Liu *et al.* [47], Wang *et al.* [48], Gallias and Commandre [49], Li *et al.* [50], Shan *et al.* [51], Chiang *et al.* [52], Liang et al. [53].

Wang *et al.* [19] presented a notable study about numerical computation of laser heating on multilayer coatings as mentioned in subchapter 1.2. Heat diffusion equation was used as the governing equation as used in the other studies [18, 42-55]. However in that study the heat source term was computed with using equations to electric and magnetic field components, it was presented in a more compact form as given in Eqn. (1.9). Indeed the Eqn. (1.9) is exactly the same equation with the Eqn. (1.7) but expressed in more explicit mode. If the square of the normalized EFI term of Eqn. (1.9) is computed with the help of commercial optical coating design software such as MacLeod® or TFCalc™, one can find the heat source term without solving characteristic transmission matrices separately.

In the following subsections, laser induced temperature distributions are calculated on HR optical coatings. In the first subsection an example problem is studied to examine the capability of finite volume solver ANSYS Fluent and its mesher GAMBIT about the calculation of laser induced temperature distribution on the multilayer thin films. The multilayer thin film configuration is selected from literature and used as a reference in the validation study. The conventional quarter wave design (QWD) method and its effects on laser absorption distribution are discussed in the second subsection. In the third, fourth and fifth subsections optical design modifications and their effects on laser absorption distribution and corresponding temperature distributions are investigated. In those subsections usage of non-quarter wave layers, upper surface OC layers, two high refractive index materials in the optical design of the HR thin films are studied systematically. All these investigations are done through numerical simulations, both advantages and drawbacks of the optically modified designs are scrutinized. Moreover, sources of the observed drawbacks are inspected to find out possible solutions.

3.1 Validation Study

The validation study is used to assess performance (applicability) of finite volume solver (ANSYS Fluent) and its mesher (GAMBIT) on laser induced heating of a multilayer thin film problem. Therefore a study, which contains an example thin film configuration, is selected from literature as a reference study, [55]. In the reference study, a laser induced heating problem was solved and temperature values were computed numerically for a typical HR coating stack. The out-of-scale schematic view of the HR multilayer coating stack is given in Figure 3.1.

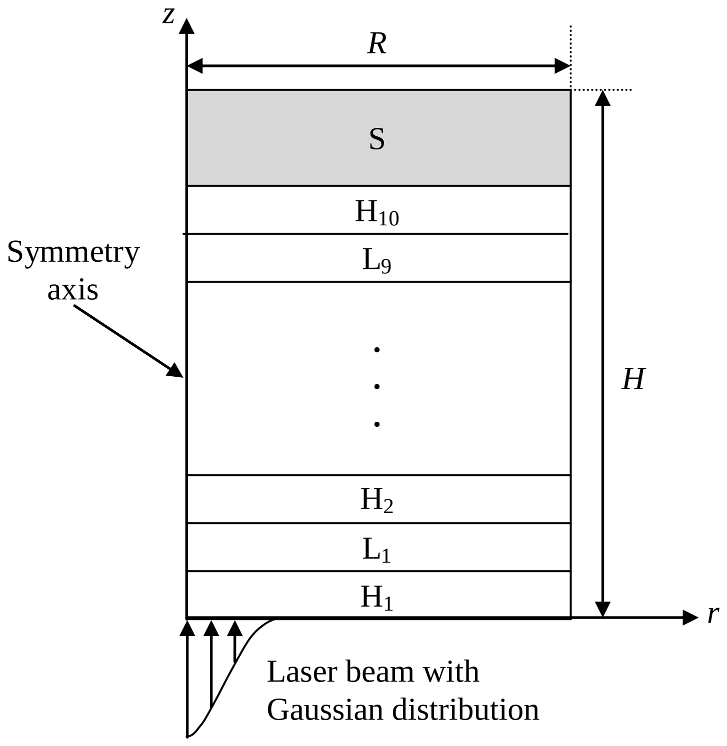

Figure 3.1 Schematic representation of a 19 layer coating stack with a substrate (out of scale).

As seen in figure, the multilayer stack involves 19 layers indicating a HR mirror in the form of {Air/$(HL)^9$H/S} configuration. TiO_2 and SiO_2 materials are given as high refractive and low refractive index materials, respectively. In high, low refractive index layers and substrate are marked as "H", "L" and "S", respectively. The H and L subscripts indicate the pair numbering of the layers. Laser beam irradiates in the z direction and hits the H_1 layer firstly.

In order to solve reference problem, axisymmetric numerical model is drawn in GAMBIT software using geometrical dimensions that are calculated in accordance with QWD method. The quarter wave layer thicknesses are given in Table 1.

Table 3.1 Geometrical dimensions of the multilayer coating.

	Thickness	**Width**
High refractive index (H) layers	120 nm	1.25 μm
Low refractive index (L) layers	185 nm	1.25 μm
Substrate (S)	1.25 μm	1.25 μm

Two-dimensional domain with 19 layers are meshed using the GAMBIT software, Figure 3.2. Each layer of the stack contains 30 cells along the *z* direction. As seen in Figure 3.2, structured quadrilateral cells are employed in the layers and unstructured triangular cells are used for the substrate.

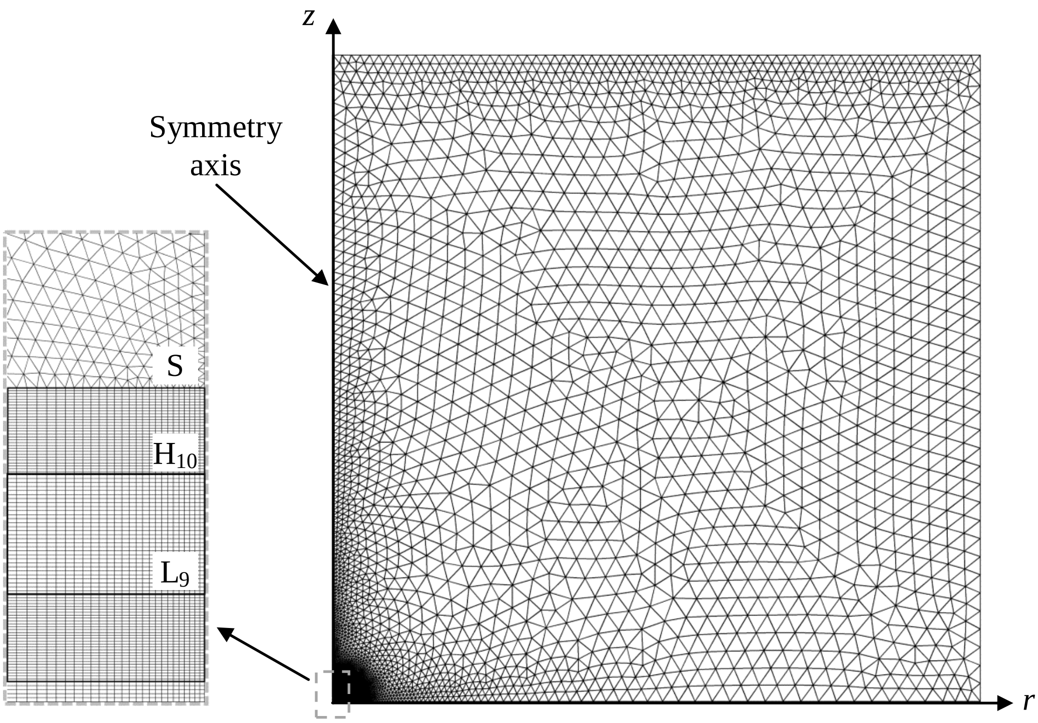

Figure 3.2 Two-dimensional grid of the axisymmetric problem domain. Zoomed in view of the center region (left) and the entire domain (right).

The prepared numerical model together with the calculated mesh structure are inserted in to finite volume solver ANSYS Fluent. After than the heat source term Eqn. (1.9), which is a time and space dependent function, is computed using the square of the normalized EFI variation, material properties (refractive index) and laser parameters.

The important term of the heat source term is the square of the normalized EFI variation. As known, square of the normalized EFI term gives the variation of energy flow through z direction. In order to compute this parabolic variation, firstly EFI variation is computed via MacLeod for the reference coating stack as given in the Figure 3.3

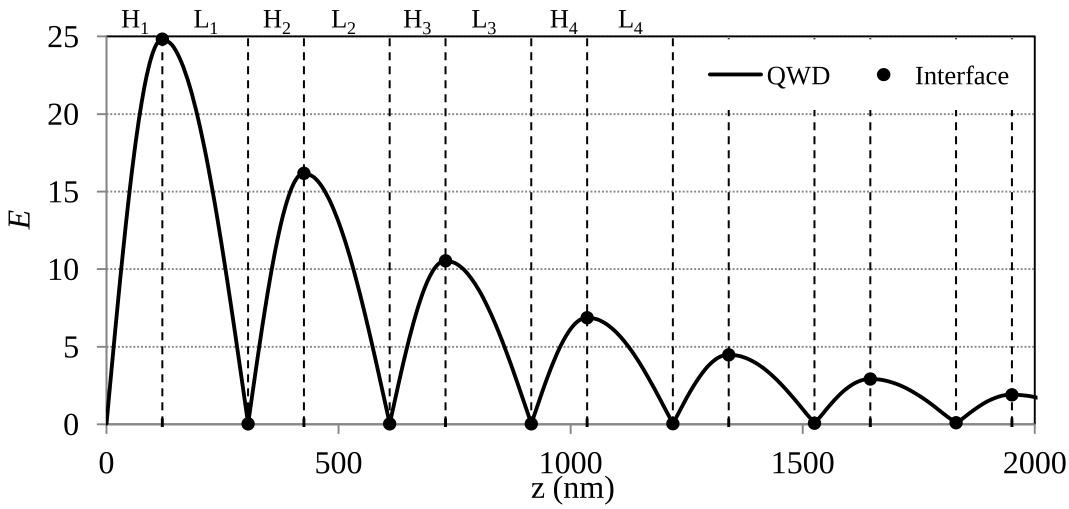

Figure 3.3 EFI graph.

After then the EFI curve is converted to square of the normalized form using Eqn. (3.1).

$$E_n^2(z) = \frac{EFI^2(z)}{E_a^2(z)} \tag{3.1}$$

In Eqn. (4.1), $E_a^2(z)$ is the square of the free admittance. Resultant square of the normalized EFI variation is plotted in Figure 3.4.

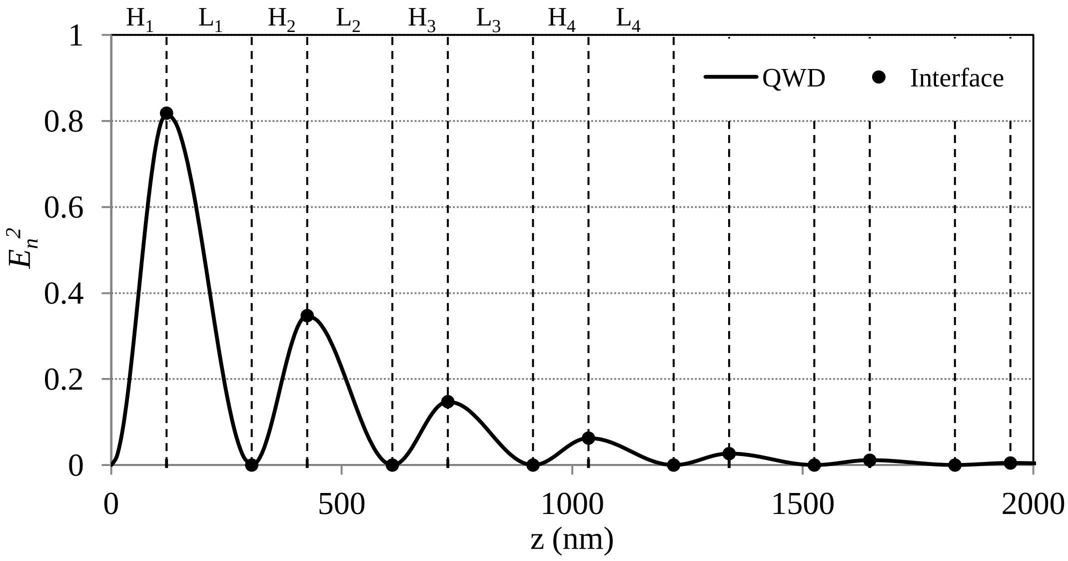

Figure 3.4 Square of the normalized EFI graph.

Thin film material properties and laser parameters are also used for computation of the heat source term. Thin film material properties are given in Table 3.2, laser parameters are given in Table 3.3 and Figure 3.5.

Table 3.2 Thin film material properties [55].

Material	**Refractive Index**	**Specific Heat (J/kg·K)**	**Thermal Conductivity (W/m·K)**
TiO_2 (H)	2.21 - j 0.0005	700	0.018
SiO_2 (L)	1.44 – j 0.0002	841	0.17
Substrate	1.46	1428	0.2

Table 3.3 Laser parameters [55].

Peak Power	**Beam Radius**	**Pulse Length**	**Wave length**
100 kW	$1x10^{-4}$ m	50 ns	1064 nm

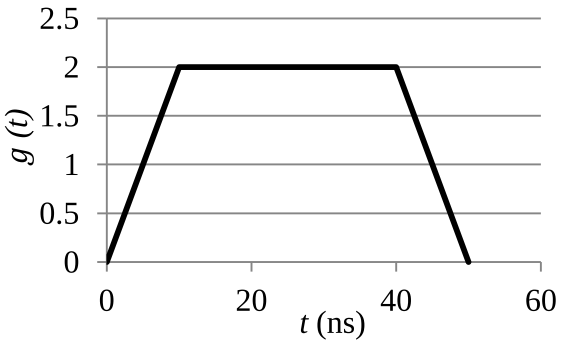

Figure 3.5 Temporal shape of the laser pulse [55].

As the heat source term is a complicated polynomial function of time and space (Eqn. (3.1)), it can only be inserted to ANSYS Fluent with using a User Defined Function (UDF). "A user-defined function is a function that you program that can be dynamically loaded with the ANSYS Fluent solver to enhance the standard features of the code" [56]. In this study, UDFs are written in C++ coding language and inserted into ANSYS Fluent as the heat source term.

<u>UDF for the heat source term computation</u>

```
#include "udf.h"
#include "math.h"

DEFINE_SOURCE(h_s_2D_19L_h1,cell,thread,dS,eqn)
{
  real x[ND_ND];
  real source;
  real a;
  real b;
  real t=CURRENT_TIME;
  C_CENTROID(x,cell,thread);
  a=x[0];
  b=x[1];
  if (t <= 0.00000001){
  source =((4.1541357964048952824E16)*(0.00000000003177*pow((b*10E8),5)
  if (t > 0.00000001 && t <= 0.00000004){
  source =((4.1541357964048952824E16)*(0.00000000003177*pow((b*10E8),5)
  if (t > 0.00000004 && t <= 0.00000005){
  source =((4.1541357964048952824E16)*(0.00000000003177*pow((b*10E8),5)
  dS[eqn] =0.0;
  return source;
}
```

Boundary conditions are also defined in ANSYS Fluent. The top and side boundaries of the two dimensional computational domain is assumed as adiabatic. Natural convection boundary condition, in which heat transfer coefficient is assumed as 20 $W/m^2 \cdot K$, is applied to the bottom surface.

At the final step of the validation study, the solution is obtained by marching numerical model in time for single pulse duration. In the meantime, energy residuals are also monitored as the convergence parameter during the numerical simulations. The ANSYS Fluent uses, 10^{-6} value, as the convergence criteria for the energy equation residuals and this criteria is achieved (on the order of 10^{-11}) during the simulation. Therefore no convergence problem is occurred for the ANSYS Fluent solution. After the solution, temperature results are obtained. One-dimensional temperature distribution along the *z*-axis (*r* = 0) is given in Figure 3.6.

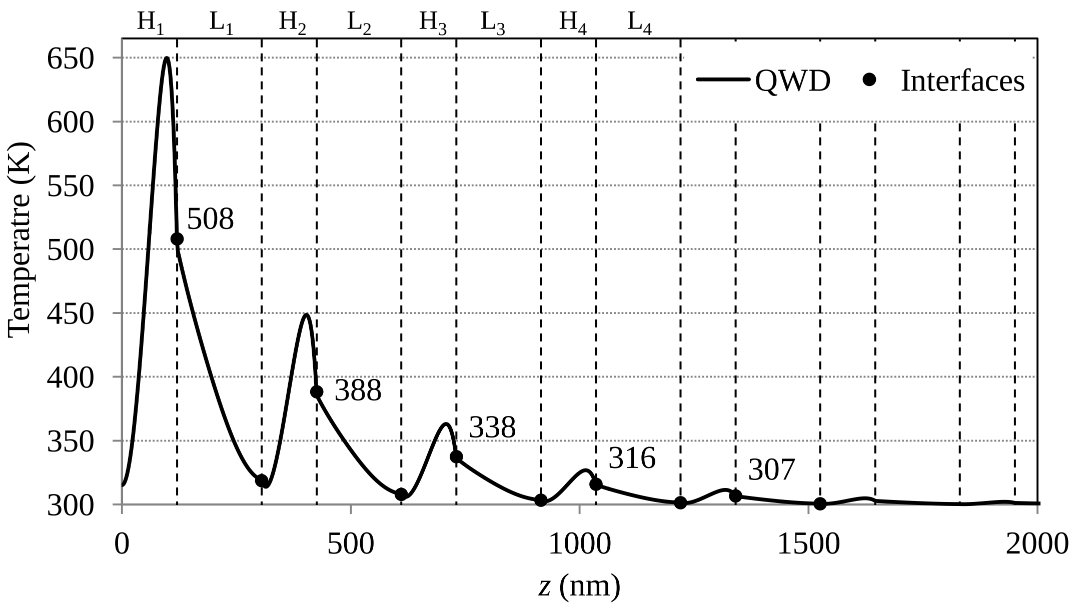

Figure 3.6 Temperature distribution along the *z*-axis.

Results of the present and reference studies are also compared in Figure 3.7 as planned before. As seen in the figure, results obtained in our study are in well agreement with the reference study, with small deviations. Thus it is validated, the finite volume solver is capable to calculate laser induced temperature distributions on multilayer thin films as desired.

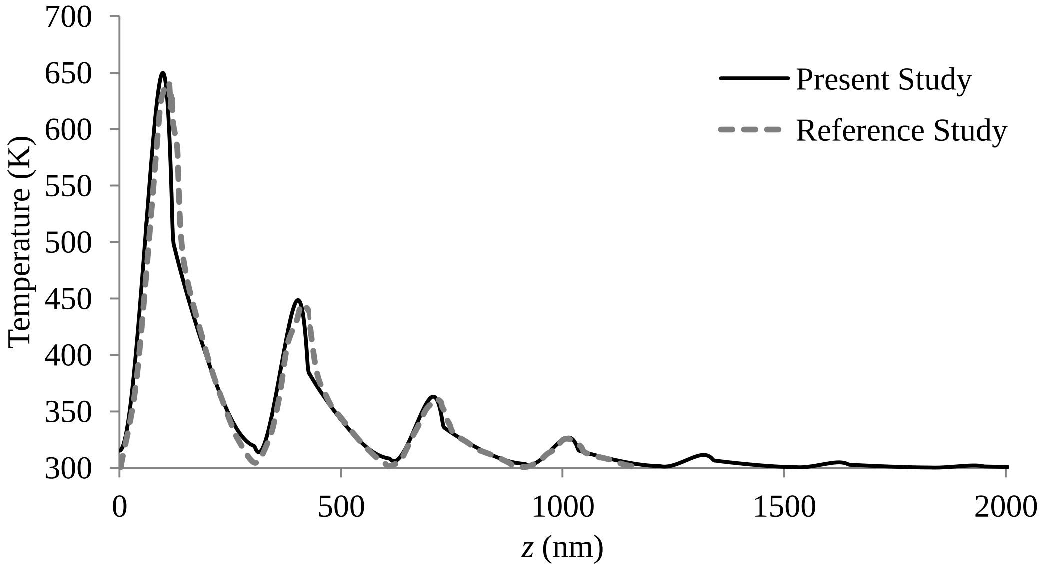

Figure 3.7 Comparison of temperature distributions along the z-axis, (K).

3.2 QWD Method And Its Effects On Laser Energy Absorption Distribution

As mentioned in previous subsection, coating layer thicknesses of the HR mirror were calculated using the conventional QWD method. In this conventional method, coating stack consists of consecutive high and low index layers to achieve desired reflectance. Eqn. (3.2) presents that how physical thicknesses are calculated in QWD method.

$$d = \lambda/_{4n} \tag{3.2}$$

where, d represents the coating layer physical thickness.

Temperature results of QWD method are given in Figure 3.6. As seen in that figure, highest temperature is found to be inside the H_1 layer. Moreover, there are temperature peaks inside all other H layers. Thermal and optical material properties such as thermal conductivity, refractive index, extinction coefficient are different at each side of the interfaces. That explains why temperature peaks occurs inside H layers rather than at the interfaces. But, still these peak points are close to interfaces, causing high interface temperatures, which are indicated in the figure as filled circles.

The temperature distribution can also be scrutinized in terms of the absorbed laser energy by reviewing the components of Eqn. (1.9). One of the important terms of the Eqn. (1.9) is the square of the normalized EFI variation, its plot is given in Figure 3.4. As seen in that plot, square of the normalized EFI variation peaks are occurred at the interfaces. In addition to that the refractive index and absorption coefficient plots are also given in Figure 3.8 to emphasize the wide differences between optical material properties.

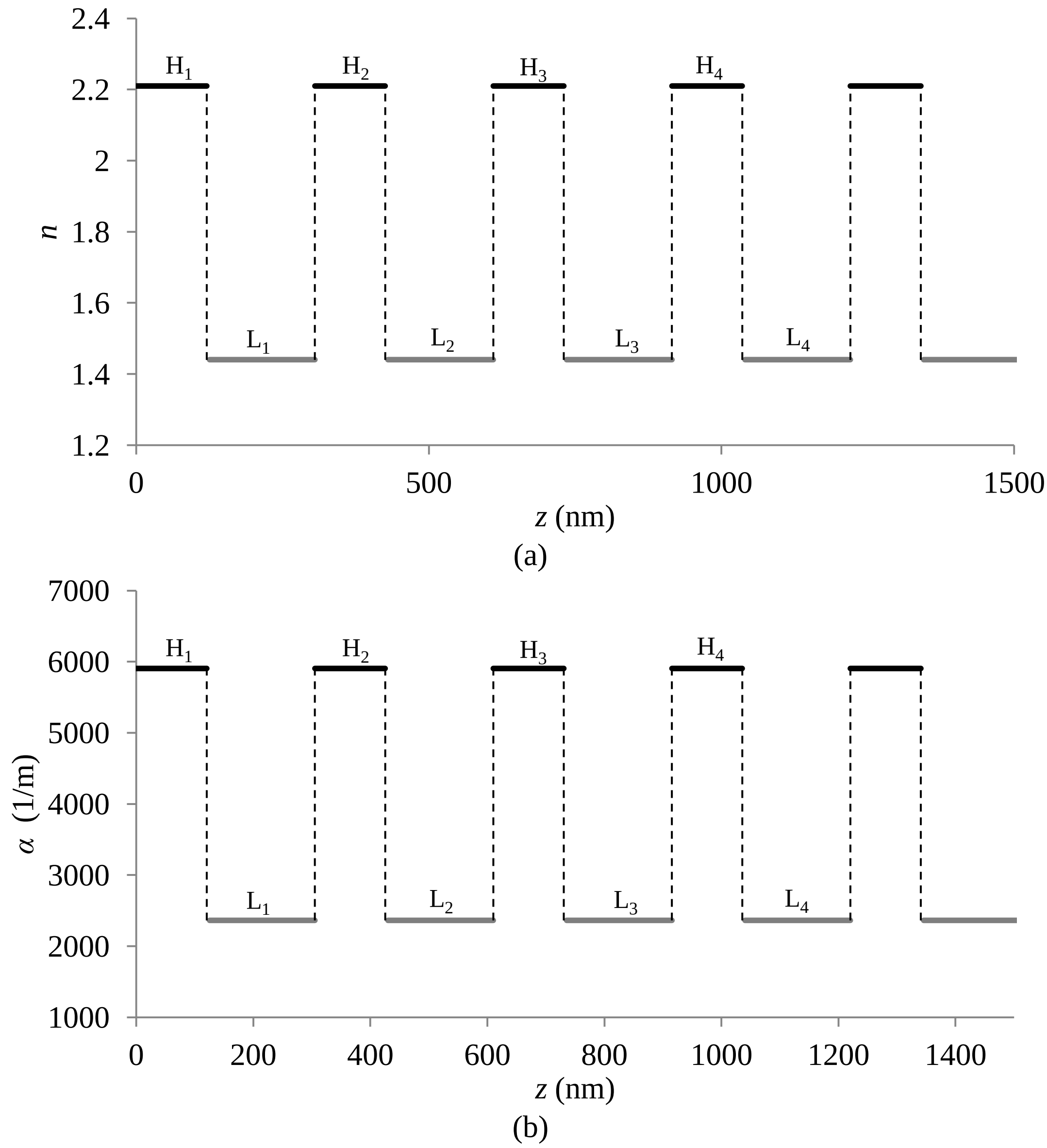

Figure 3.8 Variation of optical material properties along z-axis; (a) refractive index and (b) absorption coefficient.

In order to visualize the distribution of absorption of laser through z direction easily, the terms within the curly brackets of Eqn. (1.9) can be used. Actually it is nothing but the multiplication of the Figure 3.4, Figure 3.8 and this multiplication gives us the relative distribution for absorption of laser along the z direction, Figure 3.9. Moreover, the amount of the laser energy, absorbed in coating layers, can also be calculated by integrating the terms within the curly brackets of Eqn. (1.9) along the z direction. In Eqn. (3.3), θ_i is an indicator of the absorbed energy for the i^{th} coating layer. Other terms of Eqn. (1.9) are not included in the integral because they will be the same for all layers of the coating. The resulting θ_i values are plotted in Figure 3.10.

$$\theta_i = \int_{z_i}^{z_{i+1}} \left(\frac{4\pi\kappa_i}{\lambda}\right) \left(E_n^2(z)\right) (n_i)\, dz \tag{3.3}$$

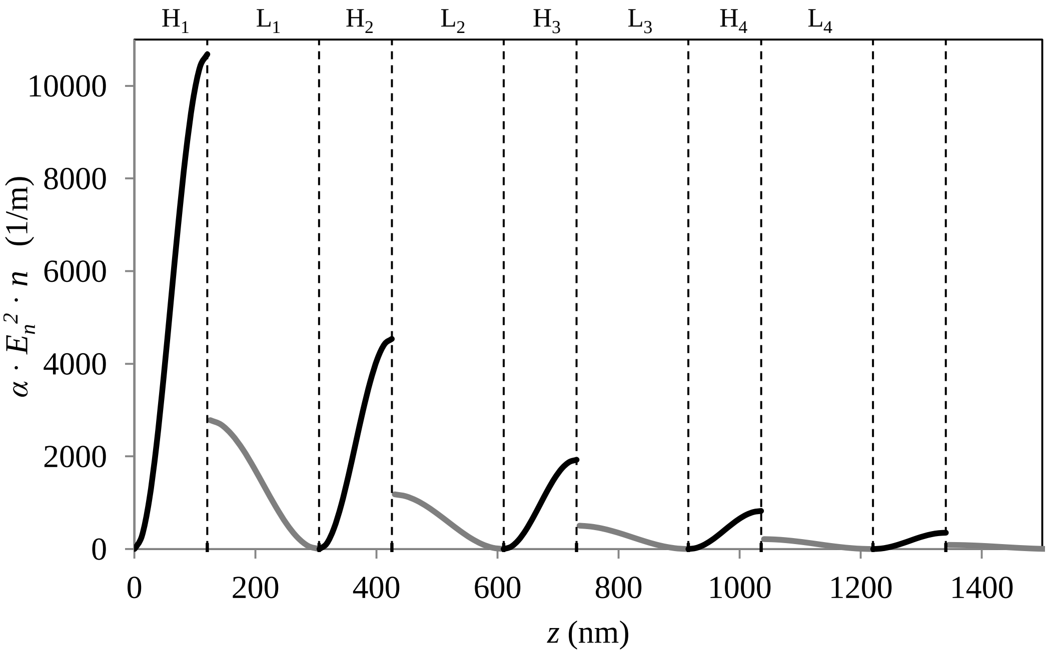

Figure 3.9 Distribution of absorption of laser through z-axis.

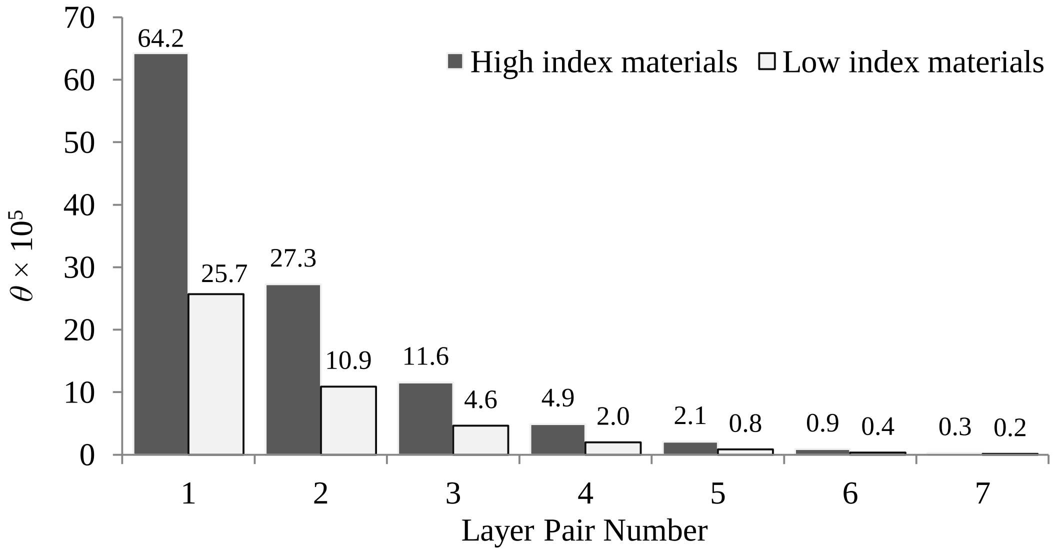

Figure 3.10 Absorption of laser by the coating layers.

As seen in Figure 3.10 the amount of laser absorption by H layers is larger than that by L layers for QWD. In addition to that (TiO_2) H layers have lower thermal conductivity according to (SiO_2) L layers which reduces heat transfer. As a result of these reasons, temperature peaks are observed in high index layers and correspondingly high temperature values are seen at the interfaces.

3.3 NQWD Method And Its Effects on Laser Absorption Induced Temperature Distribution

In the previous subsection, coating layer thicknesses have been determined according to conventional QWD method. This caused high temperatures in high index layers and high temperatures at H/L layer interfaces, as seen in Figure 3.6. Such a temperature distribution is not desired because interfaces are weaker regions of multilayer coatings and high index layers have low thermal conductivity and high extinction coefficient, hence tend to absorb the heat more.

In literature it is pointed out, the laser damage resistance of HR coatings can be improved by manipulating coating layer thicknesses which eventuates electric field distribution alternation [57-60]. By doing so electric field peaks can be shifted from interfaces and can be suppressed inside the low index layers. If the quarter wave thicknesses of high and low index layers are changed to non-quarter wave ones for few top layer pairs, EFI distribution can be modified as desired. But computation of non-quarter wave thicknesses (without reducing the desired optical performance) is not an easy task.

Gill *et al.* [58] published a remarkable study that propose the usage of non-quarter wave layers to increase the damage resistance of the reflectors. Gill *et al.* claimed that their NQWDs are much durable to laser irradiation according to quarter wave counterparts. Formulations, which were used by Gill *et al.* for the computation of non-quarter wave layer thicknesses, are given in Eqn. (3.4) and Eqn. (3.5).

Low index layer: $$\sin\beta_{2i-1} = \frac{1}{\sqrt{i(n_H/n_L)^2 - (i-1)}}$$

$$0 < i \leq m \quad and \quad \varphi_{2i-1} > {}^{\pi}\!/_{2} \qquad (3.4)$$

High index layer: $$\tan\beta_{2i} = \frac{(n_H/n_L)}{\sqrt{i((n_H/n_L)^2 - 1)}}$$

$$0 < i \leq m \quad and \quad \varphi_{2i-1} > {}^{\pi}\!/_{2} \qquad (3.5)$$

In Eqn. (3.4) and Eqn. (3.5), $\beta_i = 2\pi n_i d_i \cos(\emptyset_i)/\lambda$ and m being the number of pairs of non-quarter wave layers. β represents the optical phase thickness.

In order to better emphasize the difference between NQWD and QWD, following square of the normalized EFI distributions are plotted in Figure 3.11. As seen in this figure, the H_1 and L_1 layer thicknesses are changed. The high index layer thickness is decreased and low index layer thickness is increased. By doing so the square of the normalized EFI value is decreased from 0.818 to 0.517 at the first interface. In addition to that the first peak of square of the normalized EFI distribution is shifted from interface towards to the first low index layer (L_1). But unfortunately the magnitude of the first peak of the square of the normalized EFI distribution is increased from 0.818 to 1.214.

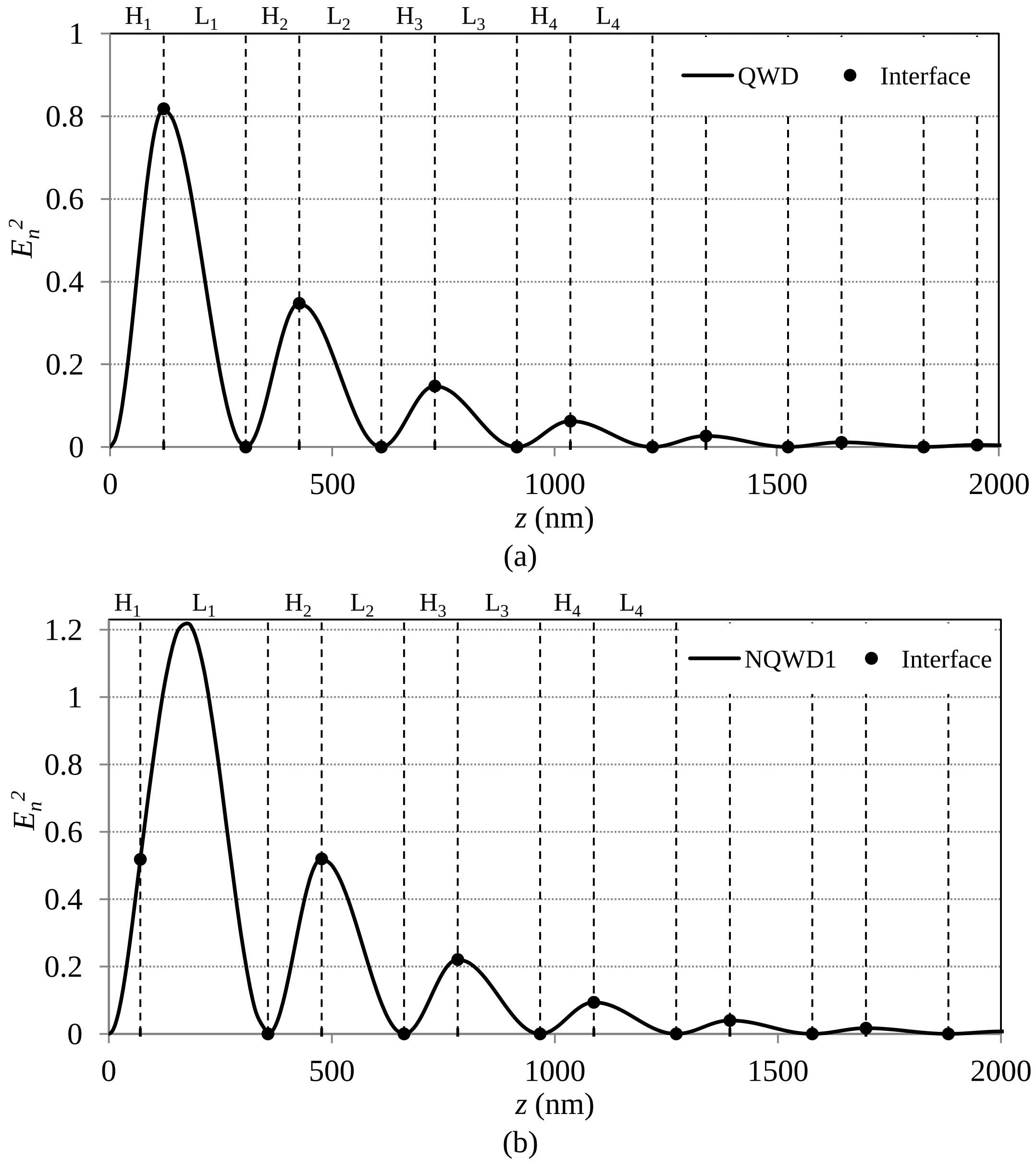

Figure 3.11 Square of the normalized EFI distribution plot; (a) QWD and (b) NQWD.

Moreover the relative distribution and the relative amount of absorption of laser are also changed for modified layers due to changing layer thicknesses as given in Figure 3.12 and Figure 3.13.

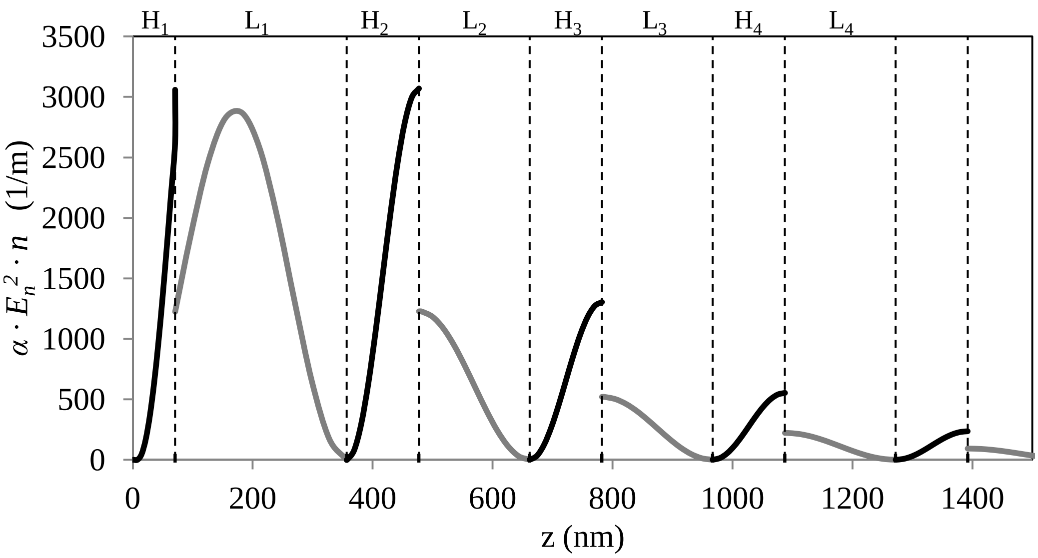

Figure 3.12 The relative distribution plot of absorption of laser through *z*-axis for NQWD.

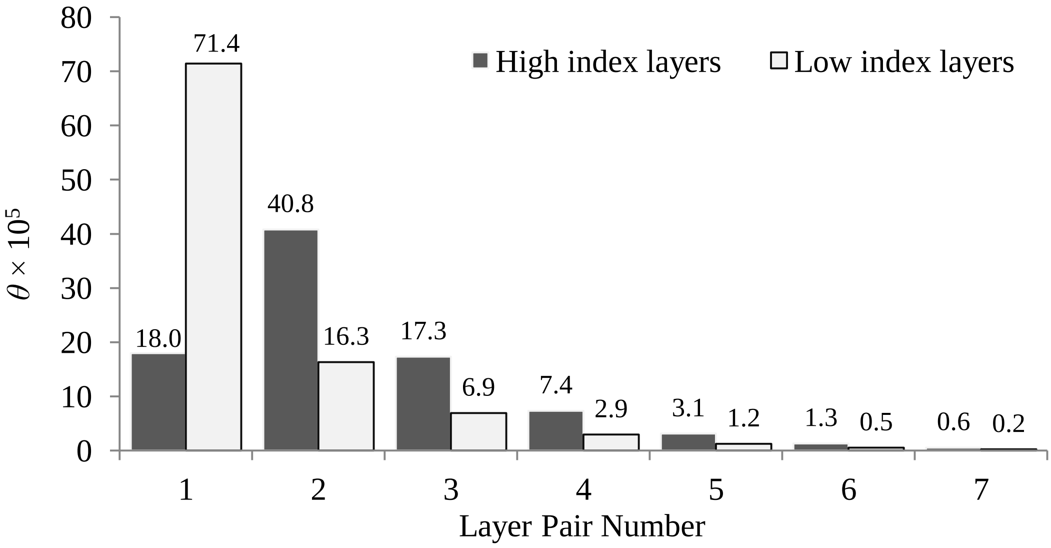

Figure 3.13 Absorption of laser by the coating layers for NQWD.

As seen in Figure 3.11-Figure 3.13 usage of NQWD method enable us to change EFI variation in the coating stack as desired. But the effect of NQWD method on temperature distribution is not seen yet. Hence it will be investigated with in details in the following subsection by performing a versatile systematical study.

3.3.1 Investigation Of Effects Of NQWD Method On Temperature Distribution For The Single Shot Laser Irradiation

In this subsection, five NQWD alternatives are developed by changing the layer thicknesses of the basic QWD. Layer thicknesses are changed as given in Table 3.4 using Eqn. (3.4) and Eqn. (3.5). As shown in Table 3.4, thicknesses of the first layer pair (H_1 and L_1) are changed only in NQWD1. In NQWD2, thicknesses of both the first and the second layer pairs (H_1, L_1, H_2 and L_2) are changed. Similar logic is used to create the other three NQWDs.

Table 3.4 Modified TiO_2/SiO_2 layer thicknesses (nm) for NQWDs together with the reference QWD values

Layer	QWD	NQWD1	NQWD2	NQWD3	NQWD4	NQWD5
H_1	120	71	58	50	45	41
L_1	185	286	305	315	322	326
H_2	120	120	71	58	50	45
L_2	185	185	286	305	315	322
H_3	120	120	120	71	58	50
L_3	185	185	185	286	305	315
H_4	120	120	120	120	71	58
L_4	185	185	185	185	286	305
H_5	120	120	120	120	120	71
L_5	185	185	185	185	185	286

*Shaded cells indicates that these layer thicknesses are modified

This subsection is mainly based on the proceeding “Ocak, M., Sert, C., & Okutucu-Özyurt, T. (2013, November). Investigation of non-quarter wave design on multilayer optical thin film coatings from a heat transfer point of view. In *SPIE Laser Damage* (pp. 888506-888506).

Numerical computations are repeated for each NQWD alternative by following the steps which are explained in chapter 3.1 to calculate temperature distributions. Temperature distributions are given in Figure 3.14 for NQWDs at the end of one pulse duration.

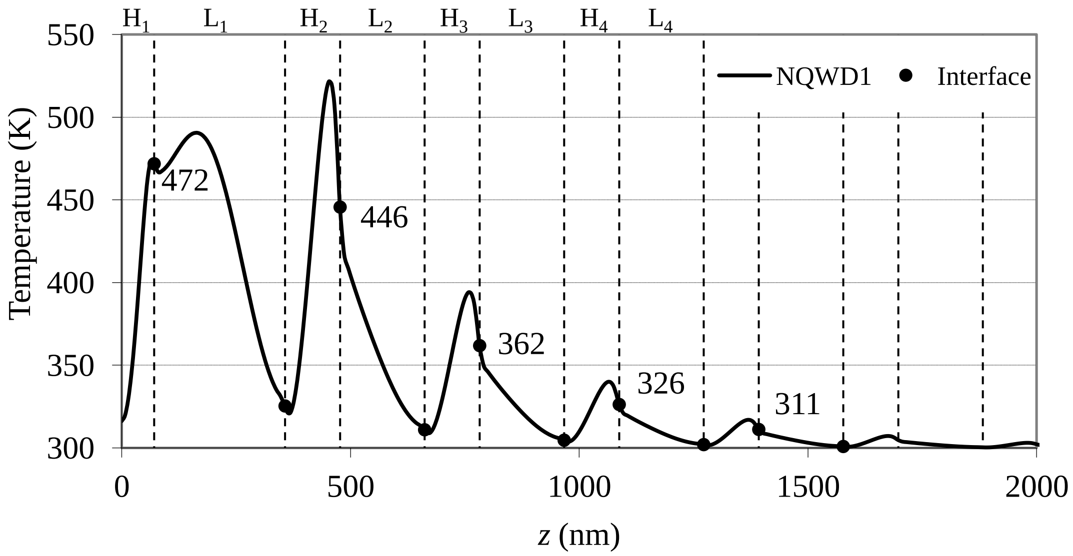

(a)

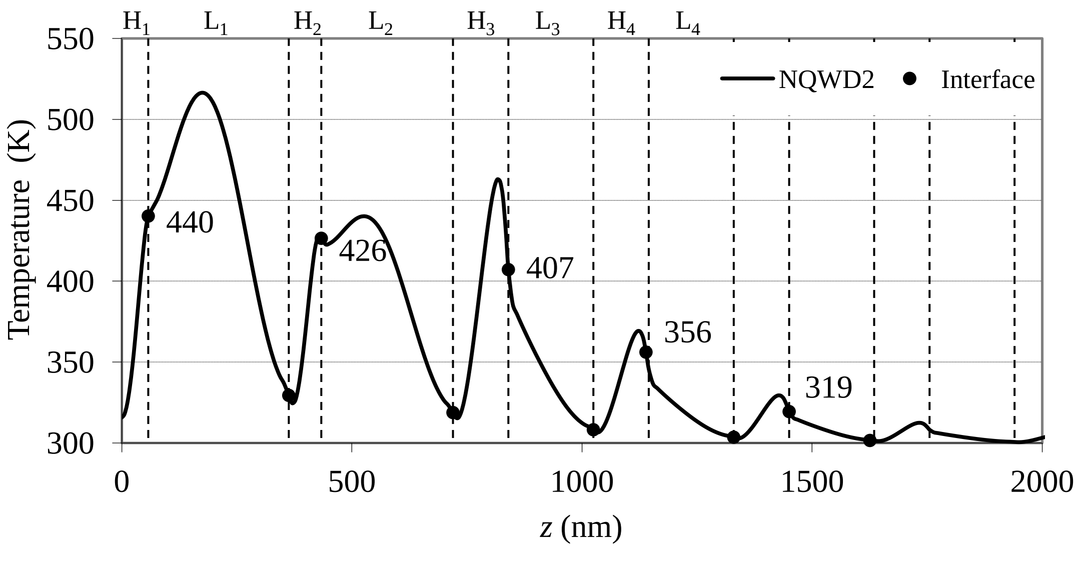

(b)

Figure 3.14 Temperature distributions along the *z*-axis; (a) NQWD1, (b) NQWD2, (c) NQWD3, (d) NQWD4 and (e) NQWD5.

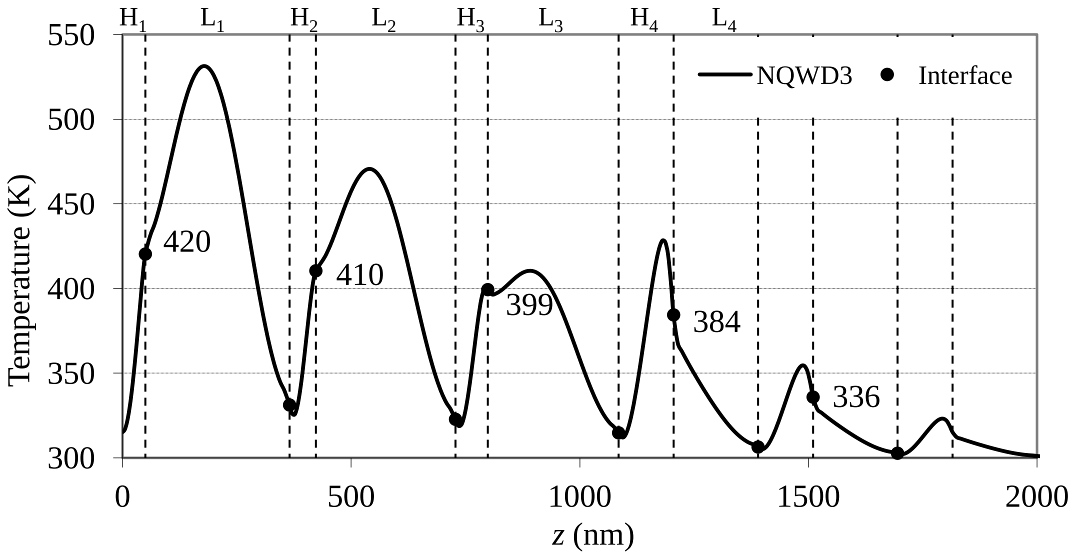

(c)

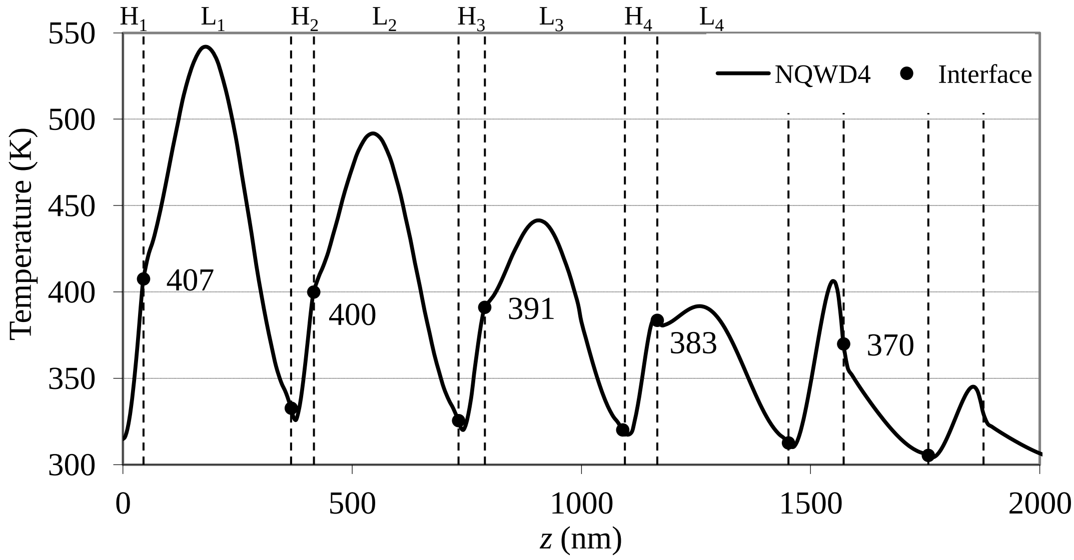

(d)

Figure 3.14 (continued) Temperature distributions along the *z*-axis; (a) NQWD1, (b) NQWD2, (c) NQWD3, (d) NQWD4 and (e) NQWD5.

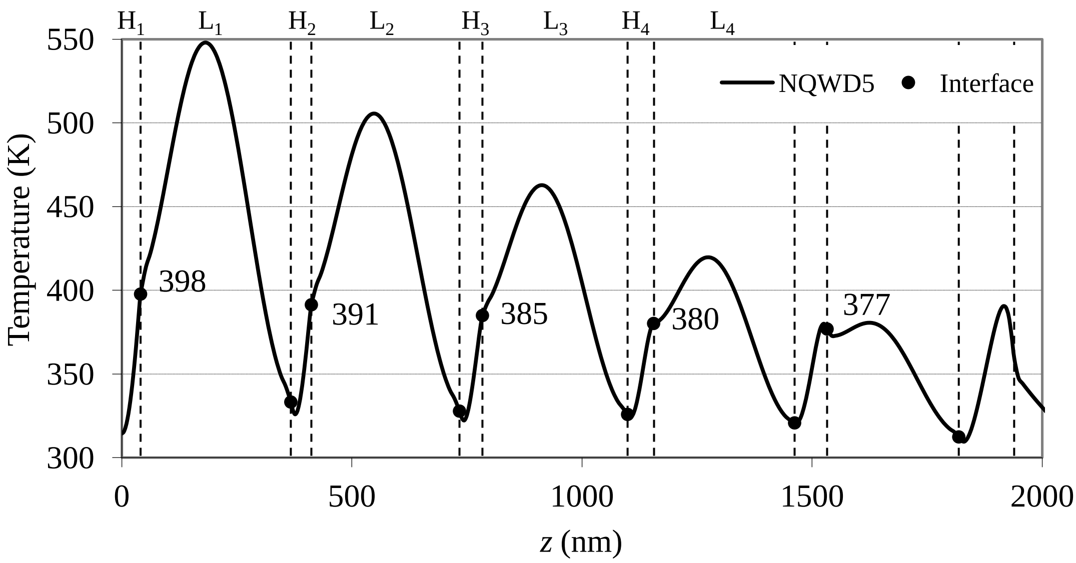

(e)

Figure 3.14 (continued) Temperature distributions along the *z*-axis; (a) NQWD1, (b) NQWD2, (c) NQWD3, (d) NQWD4 and (e) NQWD5.

As seen in Figure 3.14.a, modified H_1 and L_1 thicknesses result in the drop of the peak temperature in the H_1 layer, as well as the temperature at the H_1/L_1 interface for NQWD1. The maximum temperature in the H_1 layer is 491 K, which was 650 K (Figure 3.6) for QWD. As a quick positive conclusion one can say that the maximum temperature is decreased by about 160 K. Also the first interface temperature is decreased to 472 K, which was 508 K for QWD. However, similar temperature drops cannot be observed for the 2nd and the following H/L interfaces. For example the temperature value is 446 K at the 2nd H/L interface for NQWD1, which was 394 K for QWD. Similar trends are observed in all other NQWDs, as shown in Figure 3.14. For example in Figure 3.14.b; 1st, 3rd and 5th H/L interface temperatures are 440 K, 426 K and 407 K, respectively. These temperatures were 508 K, 394 K and 340 K for QWD.

In addition to temperature distribution plots, layer based laser absorption graphs are also plotted in Figure 3.14 for NQWDs. As explained in previous sections, these bar type plots presents the amount of laser absorption for coating layers individually.

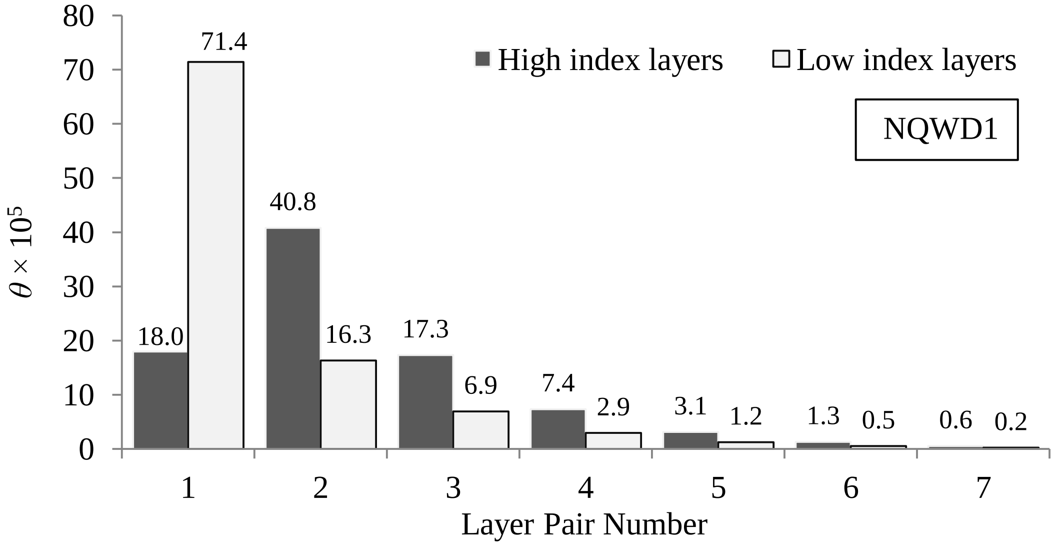

(a)

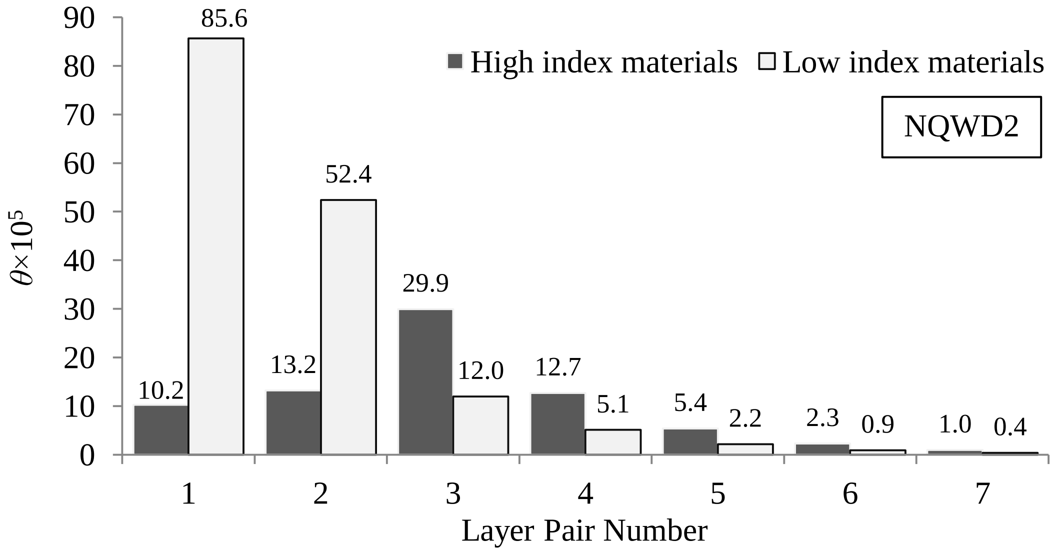

(b)

Figure 3.15 Absorption of laser by the coating layers; (a) NQWD1, (b) NQWD2, (c) NQWD5.

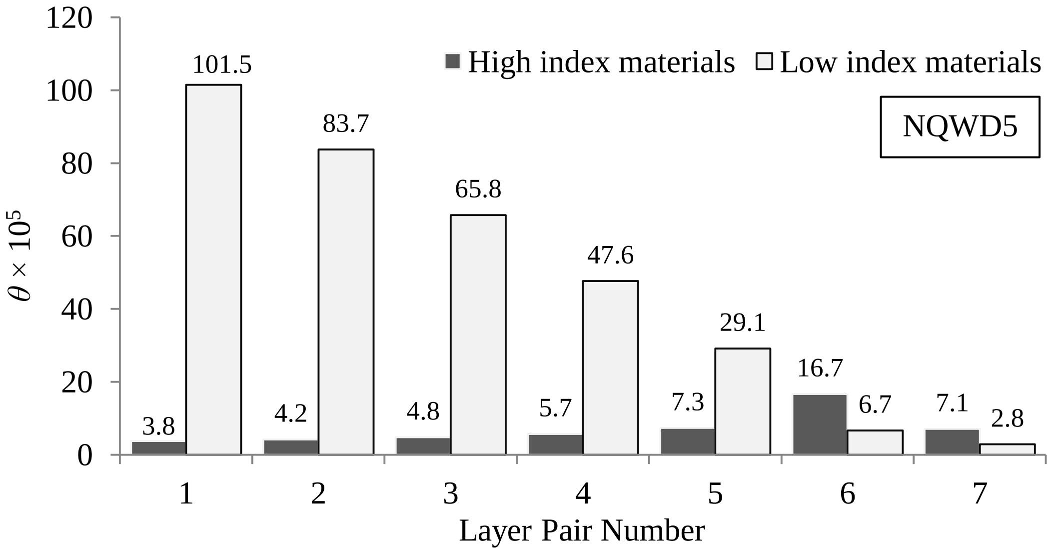

(c)

Figure 3.15 (continued) Absorption of laser by the coating layers; (a) NQWD1, (b) NQWD2, (c) NQWD5.

As given in Figure 3.10 for QWD, the amount of laser absorption by high index layers are greater than that absorption by low index layers. This result leads temperature peaks inside high index layers and high temperature values at H/L interfaces. But the laser absorption by the first low index layer (L_1) is greater than that of the first high index layer (H_1) for NQWD1 (Figure 3.15) due to modified 1st layer pair (H_1/L_1 pair) thicknesses and corresponding square of the normalized EFI distribution. This result is expected on the point of thermal performance because low index layers have higher thermal conductivity and lower refractive index according to high index layers.

On the other hand NQWD method has side effects, for example the laser absorption in the 2nd layer pair (H_2/L_2 pair) of the NQWD1 is greater than that of QWD. However, the 2nd layer pair thicknesses are not modified for NQWD1 as presented in Table 3.4. Unfortunately, this increment causes higher temperature value at the 2nd H/L interface as noted above. Similar increments can also be seen in Figure 3.15 for the 3rd layer pair of NQWD2 and 6th layer pair of NQWD5. The reason of the increased absorption at the non-modified layers is conducted to the local reflectivity decrease at the modified layer pairs, definitely. Because, the total reflectivity of the NQWDs are not decreased considerably as presented in Table 3.5 compared to

QWD. Besides, the reflectivity decrease of the entire stack can easily be defeated by adding extra HL layer pairs to configuration. However, the local reflectivity decrease at the modified layers is more important and can not be avoided with the addition of extra layers. Herein, the local reflectivity decrease at the modified layers of NQWDs causes the entrée of more laser energy through the remaining part of the stack and it corresponds to higher amount of absorption.

Table 3.5 Percentage reflectivity values for NQWDs together with the QWD

	Reflectivity (%)
QWD	99.79
NQWD1	99.73
NQWD2	99.63
NQWD3	99.46
NQWD4	99.17
NQWD5	98.61

Considering temperature (Figure 3.14) and laser absorption (Figure 3.15) distributions, one can conclude that; although NQWD decreases the temperatures at the modified layer pair interfaces, it causes the increase of laser absorption and temperature peaks at non-modified layer pairs. Increase in the amount of laser absorption also increases the probability of the thermal laser damage. Considering these numerical outcomes NQWD1 and/or NQWD2 are assessed as appropriate alternative designs instead of the conventional QWD. Herein, the modification of the first and the second layer pairs enables the suppression of EFI and temperature peaks in the durable low refractive index layers. The other alternative designs, for example NQWD5, includes more non-quarter wave layers which causes the more laser absorption through the coating stack and increase of the damage probability ratio at the layers of the stack.

3.3.1.1 Investigation Of Possible Effects Of Interface Resistance Values On Temperature Distribution

Physical material properties of thin films show differences compared to those of their bulk forms, as stated in chapter two. Particularly, the thin film thermal conductivity is size dependent property. Thus, thin film thermal conductivity values are reviewed in literature and reported in chapter 2.1. It is noted at that chapter, thermal conductivity of thin films can be one order of magnitude lower compared to their bulk forms. Hence, thin film thermal conductivity values are employed in the numerical simulations instead of bulk material values. Further, a particular study is performed in the present subsection to investigate effect of film/film interface resistances on laser induced temperature distribution on multilayer thin films. Herein, two typical resistance values are attended on film/film interfaces. The typical resistance values are determined with respect to literature studies [30, 61-62,75]. In literaure, it is pointed out the interface thermal resistance magnitude is one order of magnitude lower than the thin films resistance. Accordingly $1x10^{-6}$ m^2K/W and $1x10^{-7}$ m^2K/W resistance values are attended to QWD thin film interfaces. However, no remarkable effect is observed on the temperature distribution of QWD for the $1x10^{-7}$ m^2K/W value as presented in Figure 3.16.a. Therefore, only $1x10^{-6}$ m^2K/W value is examined for NQWD1 and NQWD5, Figure 3.17.

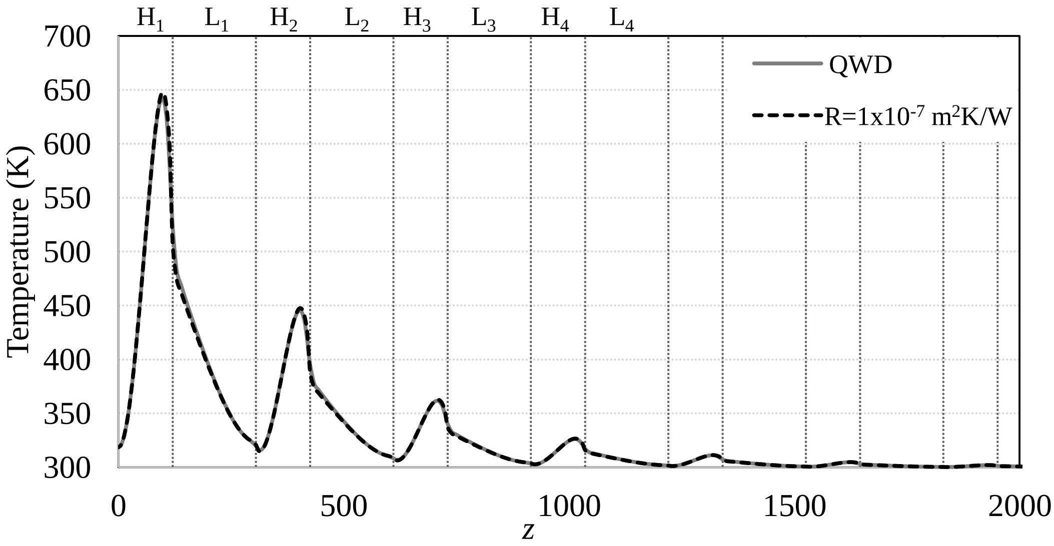

(a)

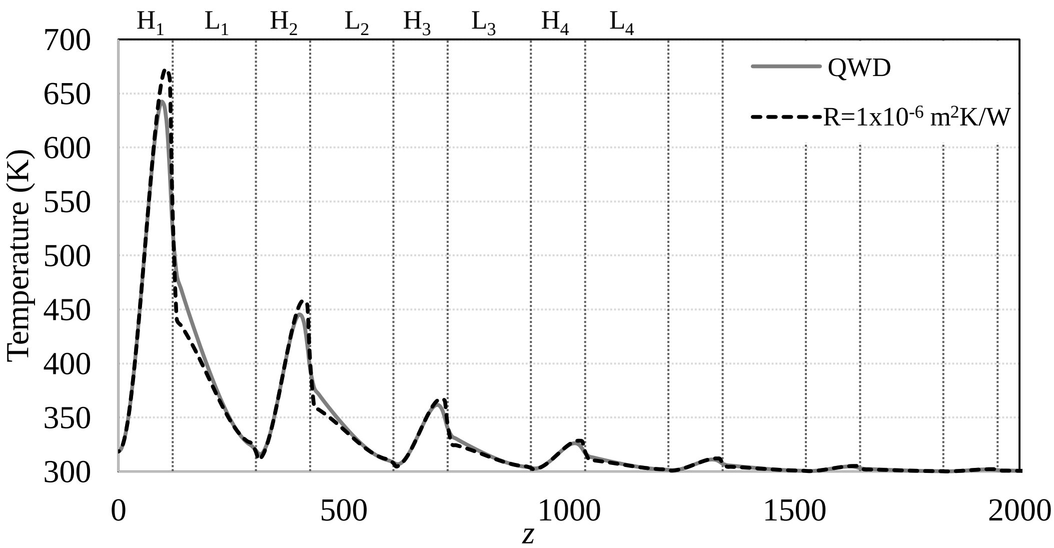

(b)

Figure 3.16 Effects of interface resistance values on QWD temperature distribution through z-axis; (a) R=1x10^{-7} m^{2}K/W, (b) R=1x10^{-6} m^{2}K/W.

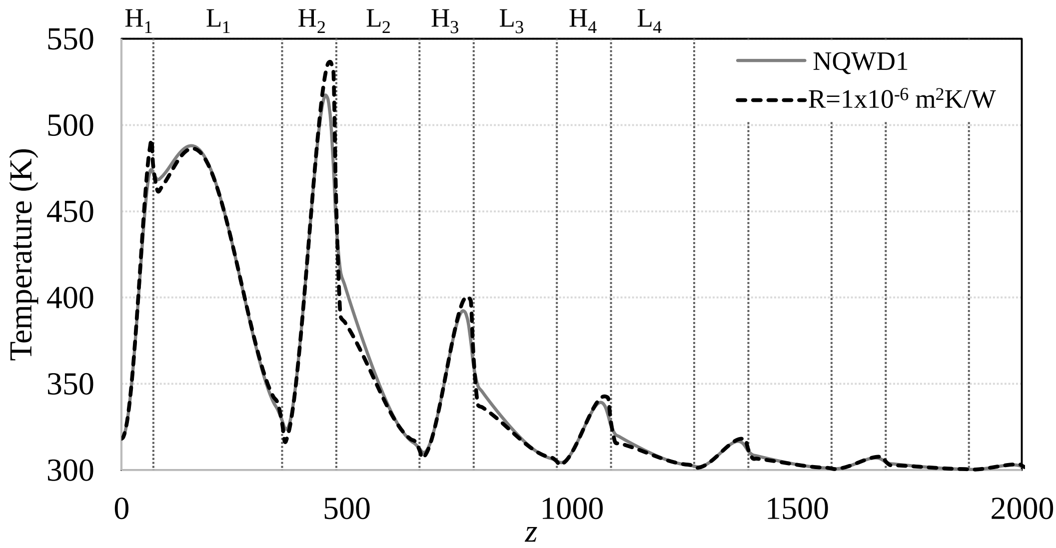

(a)

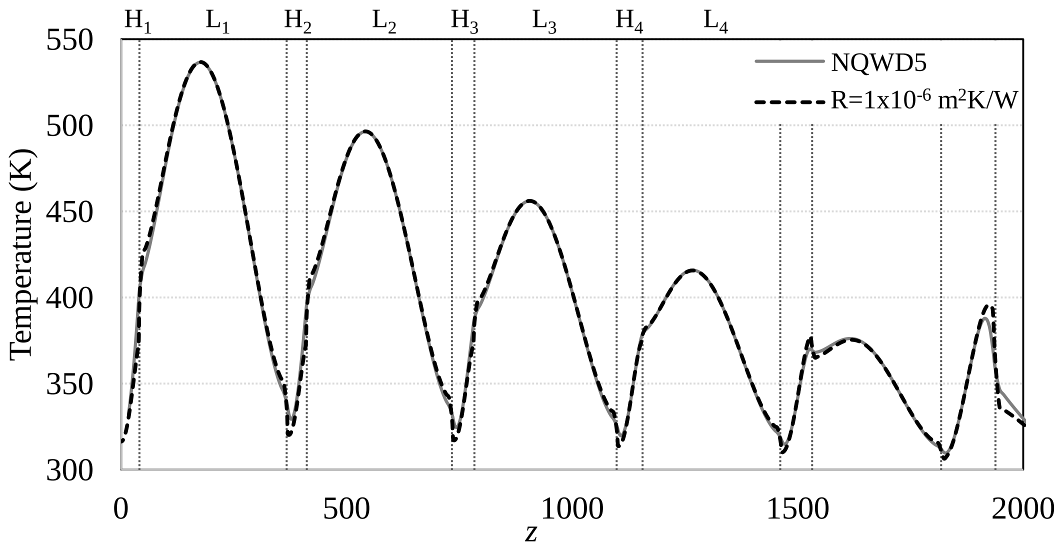

(b)

Figure 3.17 Effects of interface resistance value (R=1x10^{-6} m^{2}K/W) on temperature distribution through *z*-axis; (a) NQWD1, (b) NQWD5.

Temperature distribution results show that the interface resistance value, R=1x10^{-6} m^{2}K/W, causes the interruption of heat transfer between layers. Due to this interruption temperature peak magnitudes are increased inside the non-modified high index layers. Accordingly the temperature peaks will be higher, if an advanced resistance value is selected compared to current one in the numerical simulations. Consequently, it is comprehended; temperatures are increased inside the layers when the resistance values are attended to interfaces; however the general temperature distribution is not significantly changed. In accordance with that, temperatures inside the modified layers are decreased (Figure 3.17) when the EFI peaks are suppressed in low refractive index layers as shown in previous sections.

3.3.2 Investigation Of Effects Of NQWD Method On Temperature Distribution For The Multiple Shot Laser Irradiation

In chapter 3.3.1, the authors performed, for the first time in the literature, a systematical assessment study for the NQWD method, based on the temperature distributions inside the coating stacks [63]. In that chapter, numerical simulations have been performed to calculate the temperature distribution induced by a single shot laser irradiation over the coating layers. Besides in optics industry, the multilayer thin films (e.g. HR mirrors) are also tested under multiple shot laser irradiation. For this reason, apart from the chapter 3.3.1, multiple shot laser irradiation is exposed to NQWD alternatives in the current subsection. Moreover, a new high index material, hafnium dioxide (HfO_2), is used instead of titanium dioxide (TiO_2) as well. In the chapter 3.3.2 firstly the advantages and characteristics of hafnium dioxide are summarized in the first subsection (3.3.2.1). Then, numerical studies that are performed for multiple shot laser irradiation case, are presented in the second subsection (3.3.3.2)

3.3.2.1 Advantages And Characteristics Of Hafnium Dioxide As A High Refractive Index Material

Hafnium dioxide (HfO_2) material is one of the most commonly used high index thin film materials for laser damage resistant multilayer mirrors. As known high refractive index and low extinction coefficient are primary concerns for high index layers. Amorphous structure, low mechanical stress and high density are also desired too [64]. HfO_2 meets these demands by its low extinction coefficient, amorphous structure, high density and low mechanical stress (on its crystalline structure). In addition to that high melting point, chemical and thermal stability are other advantages of the HfO_2 [65]. High density of the HfO_2 is also a benefit which prevents impurity diffusion during thin film processes [36].

Further improvements have also been performed to increase endurance limit of the HfO_2 against the laser irradiance. Adjustment of the oxygen partial pressure and deposition temperature during the coating process are well known methods which increase the laser resistance of the HfO_2 layers. Fadel *et al.* [66] reported that the stability and the hardness of HfO_2 thin film layers are increased when the substrate temperature is heated to 573 K without effecting transmissivity and reflectivity spectral distributions. Haque *et al.* [67] stated that high band gap, high refractive index and low void content HfO_2 layers can be fabricated with keeping the oxygen partial pressure 15-30% during the coating process, as well.

HfO_2 particulate reduction during the deposition process is another research area for the production of HfO_2 layers with higher quality. Miller *et al.*'s [68] study showed that number of HfO_2 particulates can be reduced on the order of 50% by manipulating electrostatic fields and deposition rate. Similarly, reduction of the deposition rate can also increase the laser resistance by preventing hafnium metal (Hf) and/or HfO_2 nanoclusters inside coated layers. Oliver *et al.* [69] found that usage of production rates lower than 0.6 $\dot{A}$/s can increase laser resistance of the HfO_2 layers by preventing crystalline inclusions of HfO_2 within the desired amorphous structure.

Usage of hafnium metal as a coating material instead of HfO_2 may also increase the laser resistance by providing cleaner deposition ambient in the coating chamber. Stolz *et al.* [70] pointed out, the quality, in other words laser resistance, of HfO_2/SiO_2 multilayers can be increased by evaporating Hf metal instead of HfO_2 in an e-beam coating process. By doing so, the defect density and plume instability may be decreased 3-10 times and 3 times, respectively. In contrary to this, Zhang *et al.* [71] noted that usage of Hf metal as starting material may cause non-oxidizes Hf particles in HfO_2 layers which is one of the main factors that decreases the LIDT value.

Selection of appropriate coating method also enables production of high quality HfO_2 layers. It is stated in Ai *et al.*'s [41] study, increase in refractive index and density can be achieved by selecting ion assistant deposition and ion beam sputtering methods instead of conventional electron beam deposition method. Selection of xenon as the working gas in the plasma ion assisted deposition process is also another functional way for the increment of packing density of HfO_2 layers. Stenzel *et al.* [72] proved that higher refractive indices, lower band gaps and smoother film surfaces can be produced using xenon as a working gas instead of argon.

Annealing (as a post process) of HfO_2 layers after deposition process increases the laser resistance as well. Mei-Qiong *et al.* asserted that annealing of hafnium oxide coatings at 473 K yields removing of water, hydro carbon and carbon contaminations from the HfO_2 layers. Removed contaminations increase laser resistance by decreasing absorption. On the other hand annealing of HfO_2 layers within higher ambient temperature (>450ºC) cause corruption of amorphous structure. Blanchin *et al.* [73] reported that crystalline structure formation starts when the annealing temperature exceeds 450ºC which is not desired for high quality HfO_2 layers.

Although hafnium dioxide is the most preferred thin film material for the high power applications, it has some disadvantages which are low refractive index and scattering drawbacks. The other popular high index materials such as Ta_2O_5 and ZrO_2 have higher refractive indices. Also Ta_2O_5 tends to make lower scattering than HfO_2.

3.3.2.2 Numerical Studies For The Multiple Shot Laser Irradiation

In this subsection NQWD method is investigated numerically for the multiple shot laser irradiation case. Again layer thicknesses are modified according to Eqn. (3.4) and Eqn. (3.5) as done in chapter 3.3.1. As seen in Eqn. (3.4) and Eqn. (3.5) refractive index is the required optical material property for the modification of layer thickness. Optical and thermal material properties for HfO_2 and SiO_2 are given in Table 3.6.

Table 3.6 Optical and thermal material properties of HfO_2 and SiO_2 [75-77]

Material	**Refractive Index**	**Specific Heat (J/kg·K)**	**Thermal Conductivity (W/m·K)**
HfO_2 (H)	2.033 - *j* 0.00003	320	0.68
SiO_2 (L)	1.464 – *j* 0.00001	2000	1.1
Substrate	1.46	1428	0.2

Modified layer thicknesses are given in Table 3.7 for five NQWDs. As shown in

This subsection is mainly based on the manuscript (in preparation) "Ocak, M., Sert, C., & Okutucu-Özyurt, T." (2015, December). A novel highly reflective multilayer optical coating design with modified layer thicknesses.

table, thicknesses of the H_1 and L_1 layers (first layer pair) are changed only for NQWD1 as done in chapter 3.3.1. In NQWD2 thicknesses of both the first and the second layer pairs (H_1, L_1, H_2 and L_2) are changed. Similar logic is used to create the other three NQWDs.

Laser parameters have also been changed to simulate multiple shot laser irradiation. Laser parameters and the laser temporal shape are given in Table 3.8 and Figure 3.18. The laser parameters which are used in this subsection is determined regarding the study of Stolz and Runkel [78] in which multilayer HfO_2/SiO_2 HR mirrors are tested under multiple shot laser irradiation.

Table 3.7 Modified HfO_2/SiO_2 layer thicknesses (nm) of NQWDs together with the reference QWD thicknesses

Layer	**QWD**	**NQWD1**	**NQWD2**	**NQWD3**	**NQWD4**	**NQWD5**
H_1	131	80	66	58	52	48
L_1	182	270	290	301	308	313
H_2	131	131	80	66	58	52
L_2	182	182	270	290	301	308
H_3	131	131	131	80	66	58
L_3	182	182	182	270	290	301
H_4	131	131	131	131	80	66
L_4	182	182	182	182	270	290
H_5	131	131	131	131	131	80
L_5	182	182	182	182	182	270

Table 3.8 Laser parameters for multiple shot laser irradiation case

Peak power intensity	**Beam radius (a)**	**Pulse length**	**Wave length**	**# of shot**
1500 MW/cm^2	$2.5x10^{-4}$ m	20 ns	1064 nm	200

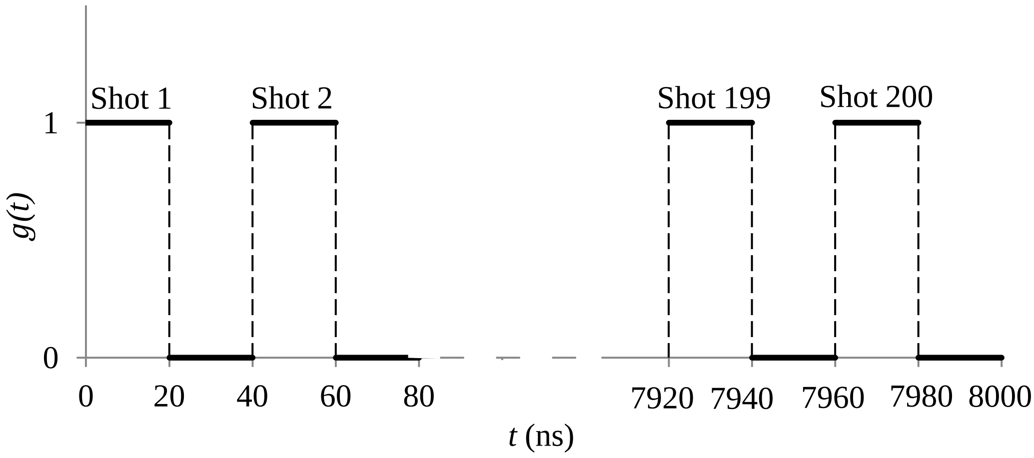

Figure 3.18 Temporal pulse shape of the laser (multiple shot laser irradiation).

As seen in Figure 3.18, more than one shot (totally two hundred) is sent to coating stack in the current case in order to simulate multiple shot laser irradiation. Then numerical computations are repeated for QWD and NQWD alternatives by following steps which are explained in chapter 3.1 to calculate temperature distributions. Calculated temperature distributions are given in Figure 3.20 at the end of 200 shot (t=8000ns).

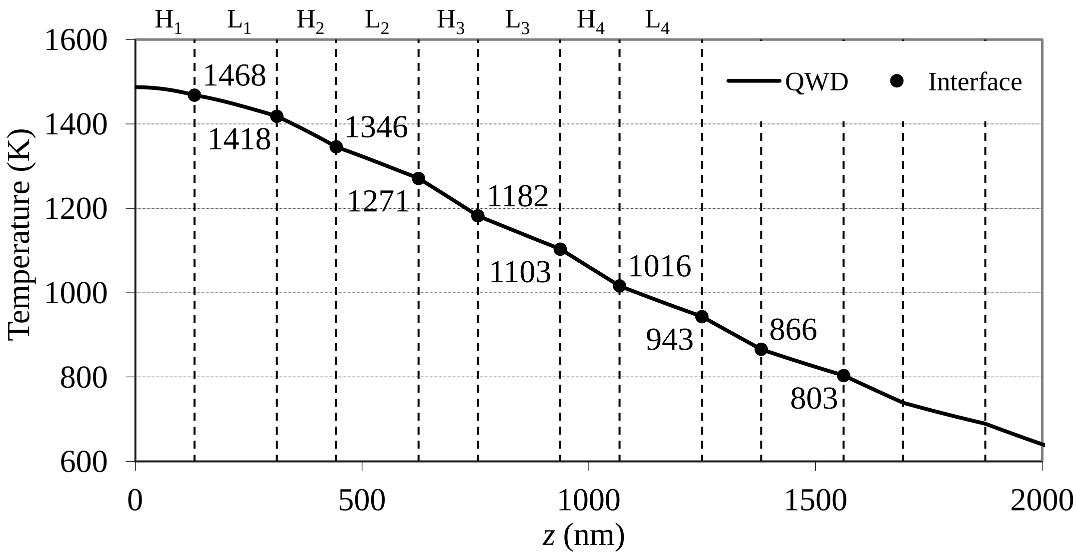

(a)

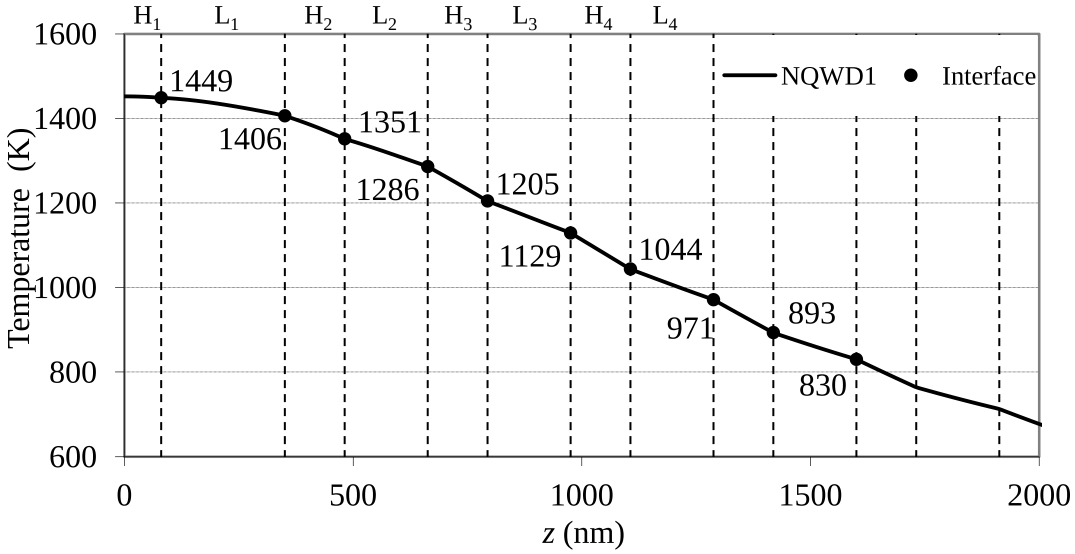

(b)

Figure 3.19 Temperature distributions along the *z*-axis resultant from multiple shot laser irradiation; (a) QWD, (b) NQWD1, (c) NQWD2, (d) NQWD3, (e) NQWD4 and (f) NQWD5.

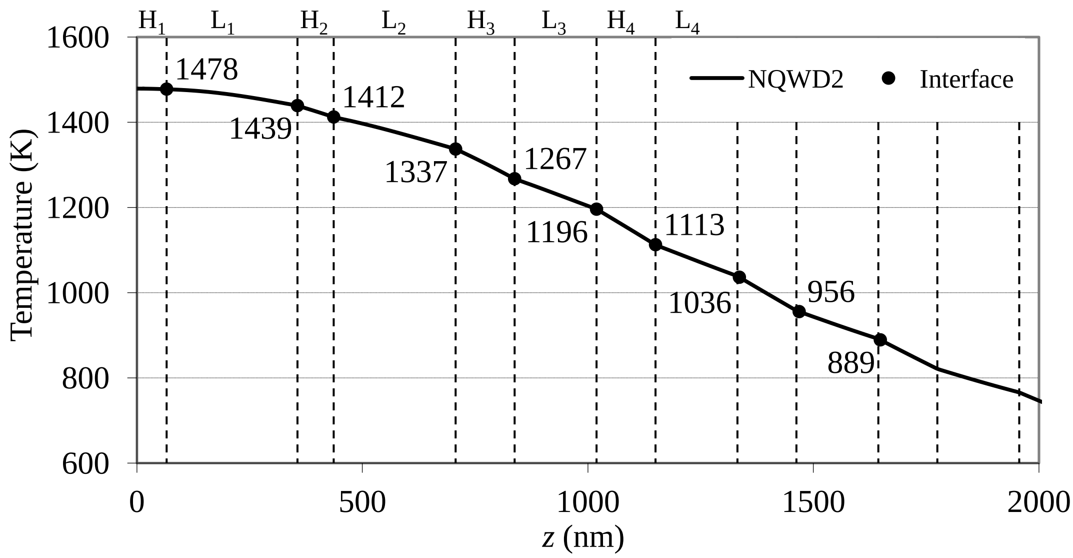

(c)

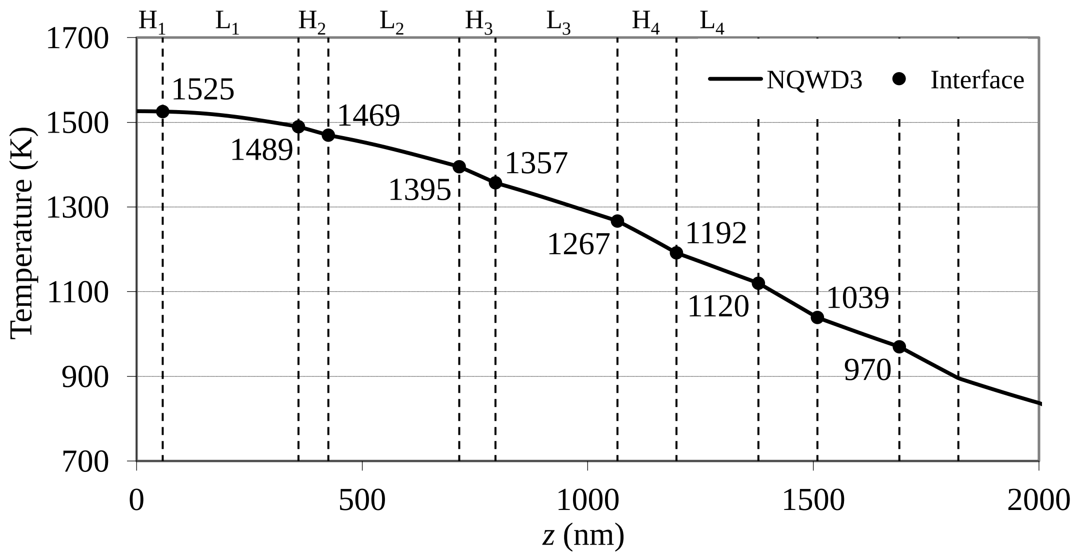

(d)

Figure 3.19 (continued) Temperature distributions along the *z*-axis resultant from multiple shot laser irradiation; (a) QWD, (b) NQWD1, (c) NQWD2, (d) NQWD3, (e) NQWD4 and (f) NQWD5.

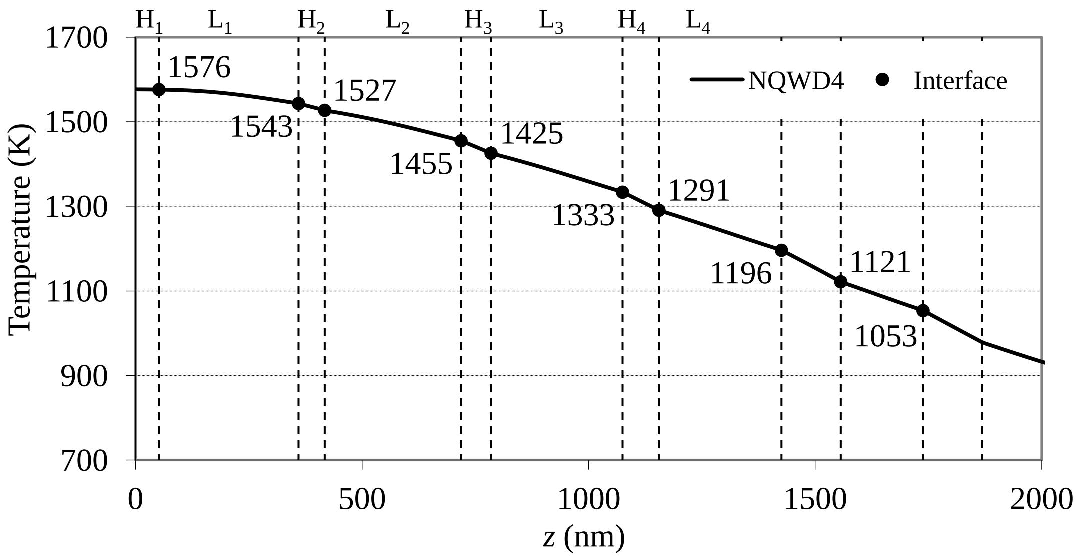

(e)

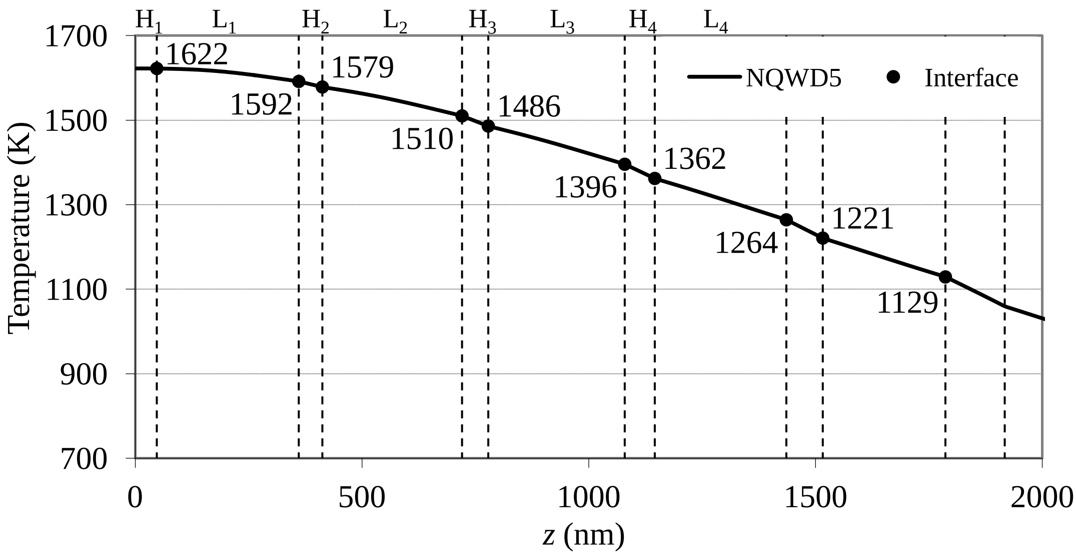

(f)

Figure 3.19 (continued) Temperature distributions along the *z*-axis resultant from multiple shot laser irradiation; (a) QWD, (b) NQWD1, (c) NQWD2, (d) NQWD3, (e) NQWD4 and (f) NQWD5.

As seen in Figure 3.19, temperature distributions are quite different when compared with the temperature distributions that are given in Figure 3.14 for single shot laser irradiation case. In the current case temperatures are increased both in QWD and NQWDs due to multiple shot laser irradiation as expected. Moreover sharp peaks are vanished in temperature distributions because laser irradiation duration is increased due to multiple laser shots and that provides much more time for the thermal equilibrium. In addition, thermal conductivity of high refractive index material HfO_2 is higher than TiO_2 of single shot case.

Effects of NQWD method on temperature distributions are obvious as seen in Figure 3.19. It is observed that the highest temperature, 1487 K, is inside the H_1 layer and the highest interface temperature is 1468 K which is at the 1st H_1/L_1 interface for the temperature distribution of basic QWD. Herein the employment of 1st NQWD alternative induce temperature distribution change. The highest temperature is (1452 K) inside the H_1 layer and the highest interface temperature is (1449 K) at 1st H_1/L_1 interface are decreased. In addition temperatures at the following L_1, H_2 layers and 2nd, 3rd interfaces are also decreased when NQWD1 is used. Temperature distribution for NQWD2 (Figure 3.19.c) is also reveals that only the highest temperature (1479 K) is decreased compared to QWD. In NQWD3, NQWD4 and NQWD5 both highest temperature value and interface temperatures are higher than the temperatures of the basic QWD, Figure 3.19.

In order to scrutinize effects of NQWD on temperature distribution, laser absorption amounts are calculated using θ_i values of Eqn. (3.3) and given in Figure 3.20.

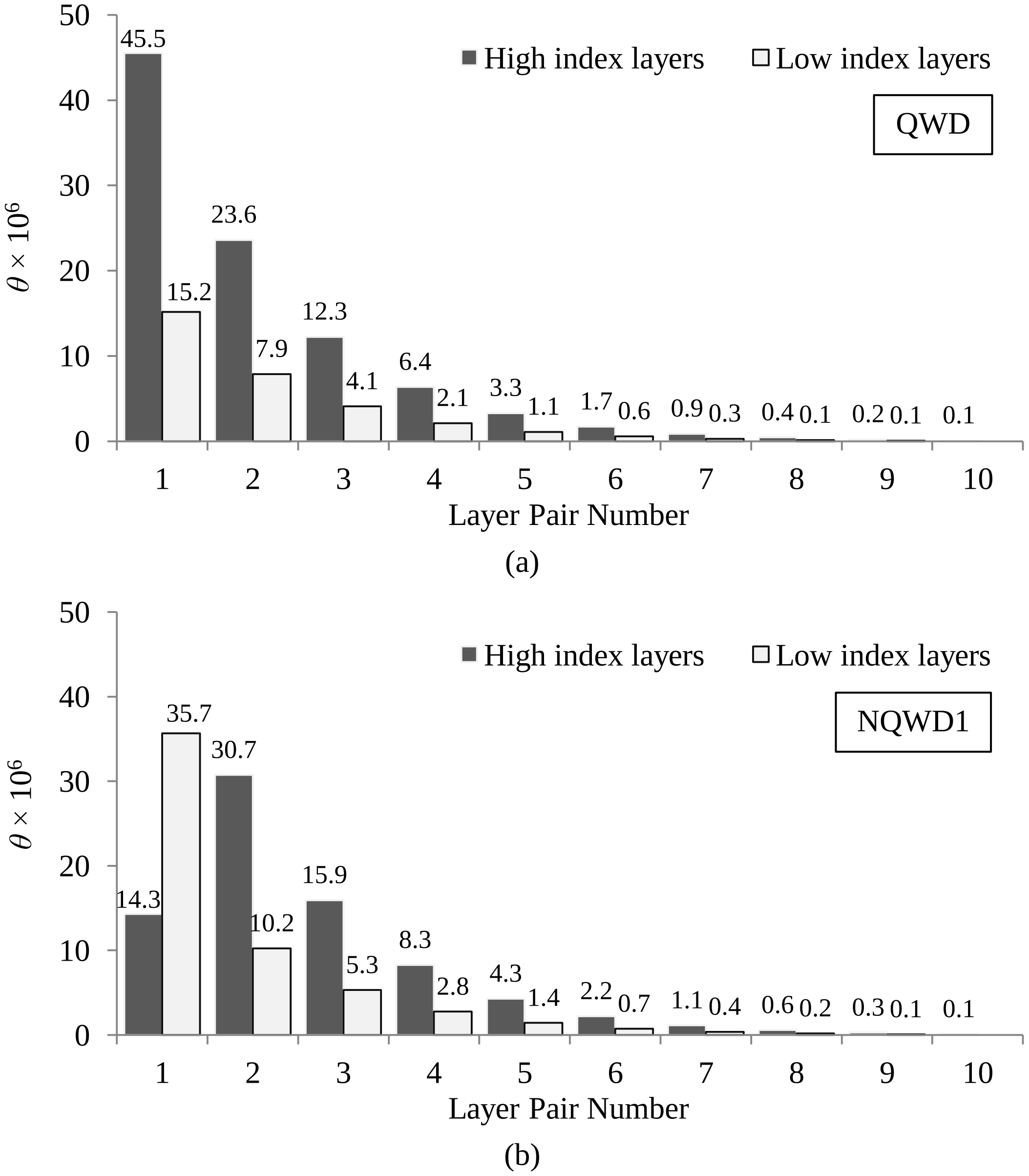

Figure 3.20 Absorption of laser by the coating layers for the multiple shot case; (a) QWD, (b) NQWD1, (c) NQWD2, (d) NQWD3, (e) NQWD4 and (f) NQWD5.

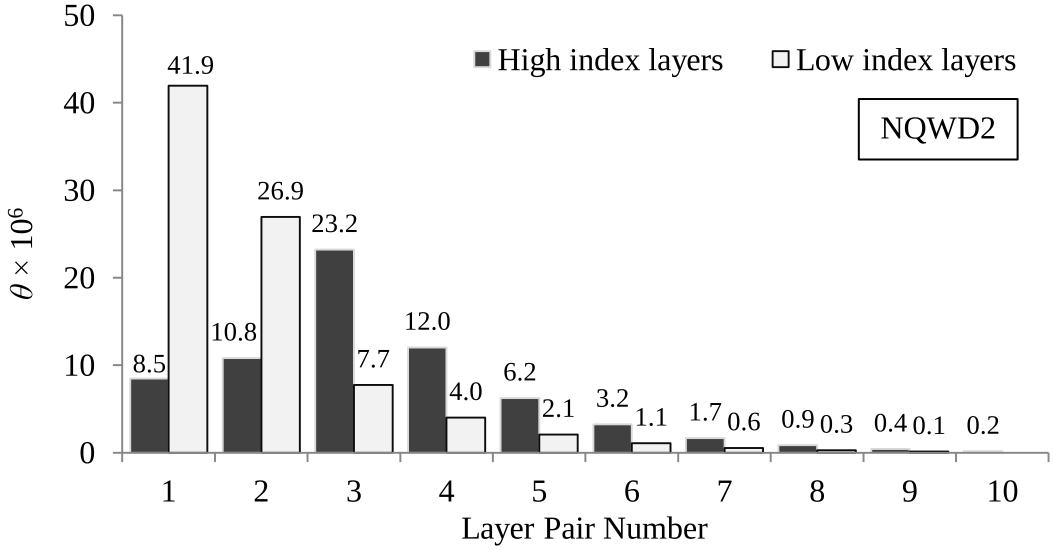

(c)

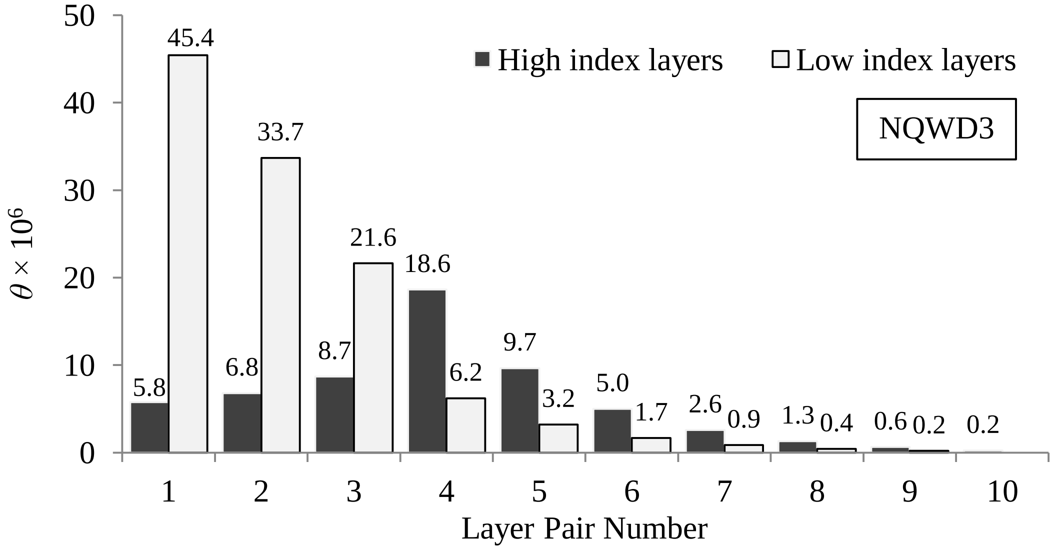

(d)

Figure 3.20 (continued) Absorption of laser by the coating layers for the multiple shot case; (a) QWD, (b) NQWD1, (c) NQWD2, (d) NQWD3, (e) NQWD4 and (f) NQWD5.

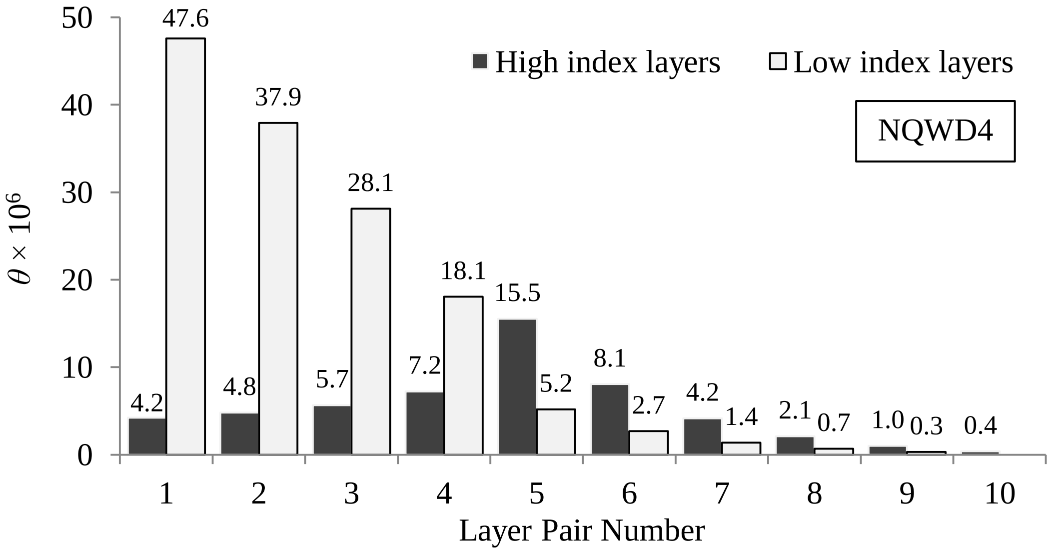

(e)

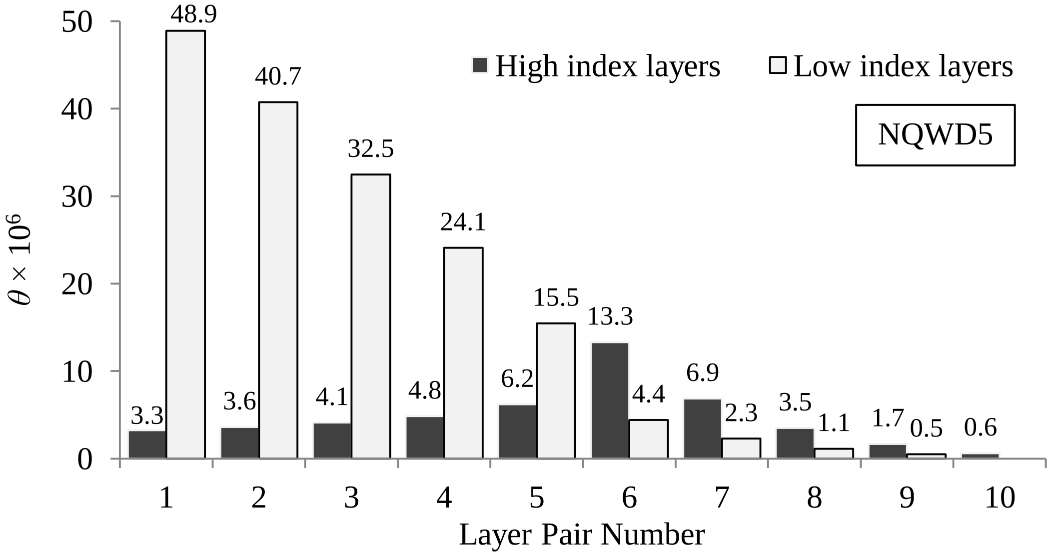

(f)

Figure 3.20 (continued) Absorption of laser by the coating layers for the multiple shot case; (a) QWD, (b) NQWD1, (c) NQWD2, (d) NQWD3, (e) NQWD4 and (f) NQWD5.

As seen in Figure 3.20, the amount of laser absorption by H layers are larger than that by L layers for QWD. Whereas for NQWD1, the laser absorption by the L_1 layer is larger than that of the H_1 layer (Figure 3.20). While more absorption is expected in L_1 layer (due to increased L_1 layer thickness) compared to H_1 layer, usage of NQWD1 also results increased laser absorption in the 2^{nd}, 3^{rd}, 4^{th} and 5^{th} layer pairs. The same trend can also be observed in Figure 3.20.c for the 3^{rd}, 4^{th} and 5^{th} layer pairs of NQWD2.

Although NQWD decreased the laser absorption in the H layers of the modified layer pairs (e.g., H_1 layer for NQWD1), higher absorption has been observed in the succeeding non-modified layers. Because the employment of NQWD method results penetration of laser energy inside coating stack and it causes higher laser energy absorption which is not favorable in terms of laser induced damage. As seen in Figure 3.19, employment of NQWD3, NQWD4 and NQWD5 have no positive effect on temperature distribution compared to temperature distribution of QWD.

3.3.2.2.1 Proposed New NQWD For The Laser Absorption Reduction

The purpose of the usage of NQWD method, as explained in previous chapters, is to shift square of the normalized EFI peaks from interfaces towards to low refractive index layers. By doing so interface temperatures are made to be reduced. On the other hand usage of NQWD layer thicknesses results higher absorption of laser energy through coating stack. As shown in previous subsection usage of three, four or five modified layer pair thickness causes higher interface temperatures for multiple shot laser irradiation case. In order to come up with resultant higher absorption drawback, a new NQWD is proposed in this subsection. In the new NQWD alternative (so called NQWD5-M) the first five layer pair thicknesses are modified similar to NQWD5. Different than NQWD5, all the modified layer pairs have identical (single) layer thickness, as given in Table 3.9.

Table 3.9 Coating thicknesses (nm) for QWD, NQWD5 and NQWD5-M

Layer	**QWD**	**NQWD5**	**NQWD5-M**
H_1	131	48	78
L_1	182	313	273
H_2	131	52	78
L_2	182	308	273
H_3	131	58	78
L_3	182	301	273
H_4	131	66	78
L_4	182	290	273
H_5	131	80	78
L_5	182	270	273

As seen in the table, all modified high index layers have 78 nm thicknesses and all modified low index layers have 273 nm thicknesses. The basic idea behind the method is to lessen amount of laser absorption while the EFI peaks are shifted from H/L film interfaces. For this purpose modified layer thicknesses are calculated in developed MATLAB code. Simply for each iteration, MATLAB code changes the quarter wave thicknesses and calculates laser absorption amounts for individual H and L layers. Then compares these absorption amounts with those of prior NQWDs. If the absorption amounts are lowered at the desired layer pairs compared to prior NQWDs, the iterations are stopped.

The primary expectation from NQWD5-M is the less amount of absorption of laser through coating stack as mentioned before. Percentage absorption of laser plot is given in Figure 3.21 for NQWD5-M. When Figure 3.21 is compared with Figure 3.20, it is obvious that laser absorption is decreased significantly compare to NQWD5.

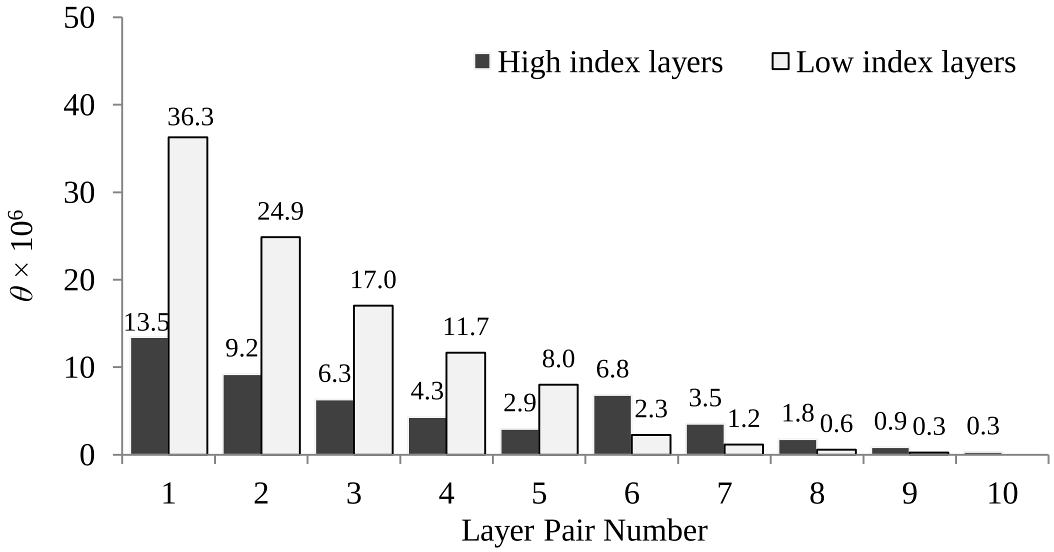

Figure 3.21 The relative amount of absorption of laser for each coating layer individually for NQWD5-M.

Comparing Figure 3.20 and Figure 3.21 one can realize that the total absorption at the 1st, and the 2nd layer pairs are lowered for NQWD5-M according to NQWD1. In addition, EFI peaks are shifted from the first five H/L interfaces with the usage of NQWD5-M. In NQWD1, EFI peak is only shifted from the first interface. It is obvious, the total absorption at 1st, 2nd and 3rd layer pairs are lower for NQWD5-M according to NQWD2, as well. Moreover EFI peaks are only shifted from the first and second interfaces for NQWD2.

Simulations are performed for the evaluation of proposed new design (NQWD5-M) and the resulting temperature distribution is given in Figure 3.22. This graph should be compared against the ones given in Figure 3.19.

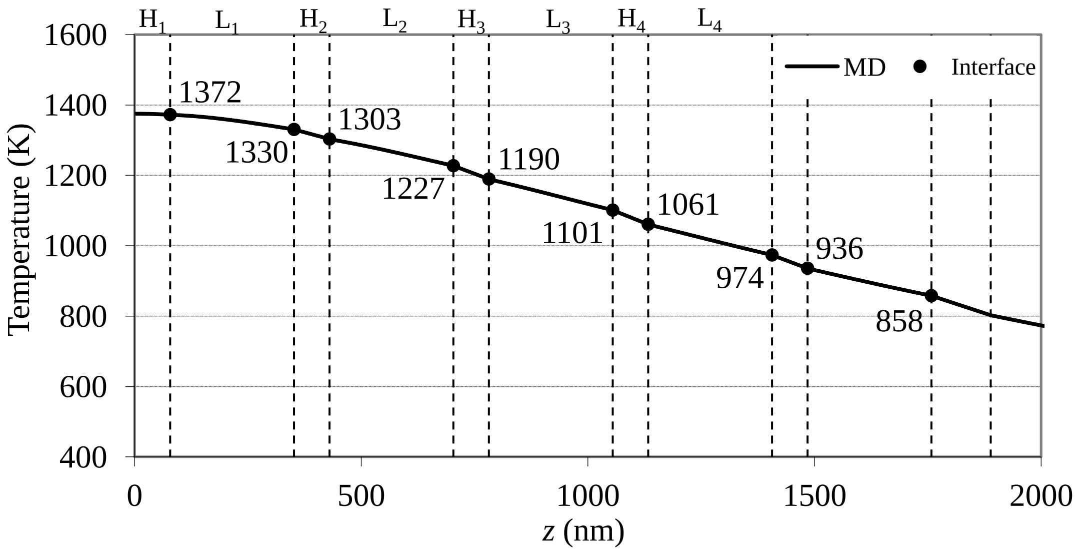

Figure 3.22 Temperature distributions along the *z*-axis for NQWD5-M.

As seen in Figure 3.22, the highest temperature is (1375 K) lowered according to both NQWD1 and QWD. In addition to that temperatures at the 1^{st}, 2^{nd}, 3^{rd} and 4^{th} interfaces are decreased according ones for QWD and NQWD1. It is obvious that NQWD5-M shows better thermal performance compared to both QWD and NQWD1 due to reduced laser absorption amounts at the 1^{st} and 2^{nd} layer pairs (where considerable amount of laser is absorbed). It should also be noted that the EFI peaks are shifted from H/L interfaces for the first five interfaces.

Considering temperature results and amount of laser absorption it seems that NQWD5-M meets requirements. Both the highest internal and interface temperatures are lowered whereas EFI peaks are shifted from interfaces as desired.

3.4 Upper Surface OC And Its Effect On Temperature Distribution

One of the important methods which is used to increase LIDT of the optical coatings is the upper surface OC layers or in other words protective upper surface layer [79]. The serviceable effect of OC layers on LIDT values was demonstrated by researchers [80-91]. Most of the researchers [80-85] used low refractive index material OCs with half wave optical thickness without reducing the desired reflectivity for HR coatings.

Carniglia *et al.* [80] measured that the half wave thick SiO_2 OC layer increases the LIDT value nearly 50% for the 15 layer (SiO_2/TiO_2) HR coating. They also showed that the square of the normalized EFI variation has an additional and increased peak (1.92) inside the OC while the square of the normalized EFI variation at the rest of the coating (in which highest peak is 0.82 at the first interface) is not affected. The serviceable effect of upper surface OC layers was explained as mechanical enforcement in another study by Hart *et al.* [81]. They claimed that mechanical strength of the HR coating is increased with the additional half wave thick OC. They also measured nearly 100% increment in LIDT value with the usage of half wave thick OC layer on the HR coatings.

The effect of OC optical thickness on LIDT performance was also studies by researchers to furtherly increase the serviceable effect [86-91]. In this regard, studies show that thicker OCs increase the mechanical strength of the coating, however it may causes stress provoked upper surface cracks.

Considering studies completed in the past, half wave OC layer is added to coating configuration NQWD5 (which is studied in chapter 3.3.1) and called as NQWD5OC. Numerical computations are repeated for the current configuration (NQWD5OC) and temperature distribution is obtained as given in Figure 3.23.

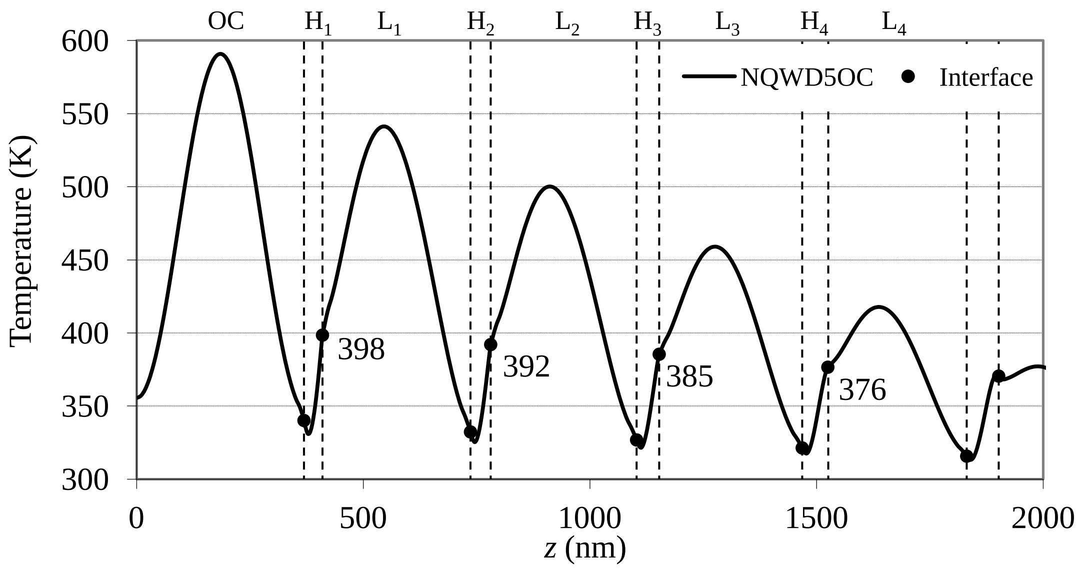

Figure 3.23 Temperature distributions along the *z*-axis for NQWD5OC.

As seen in Figure 3.23 temperature distribution has an additional peak which is approximately 590 K inside the OC layer. The rest of the distribution is not affected significantly when compared with Figure 3.14.e. The new (highest) peak is far from the OC/H_1 interface which is desired for a durable coating.

However OC has no positive effect on temperature distribution as seen in Figure 3.23, LIDT improvement effect of OC has been proved by experiments in literature. Therefore it is concluded, as mentioned in past studies, the primary serviceable effect of OC layers on LIDT is the mechanical enforcement against to the local heating induced delamination.

3.5 Investigation Of TMCs With NQWD Method

High LIDT value is one of the most important concerns for the coatings of high power laser optics. In order to increase LIDT value of such laser resistant coatings, electric field alteration studies and also temperature field design studies have been performed in the past [42, 55, 63, 74]. Recently, TMCs, in which two different high refractive index materials and one low refractive index material are used together, have been proposed for coatings of high power laser optics. The basic idea behind TMCs is to use highly laser resistant high refractive index materials such as HfO_2 or Y_2O_3 with the comparatively low stress high refractive index materials such as Ta_2O_5 or TiO_2 in the same coating stack, Figure 3.24.

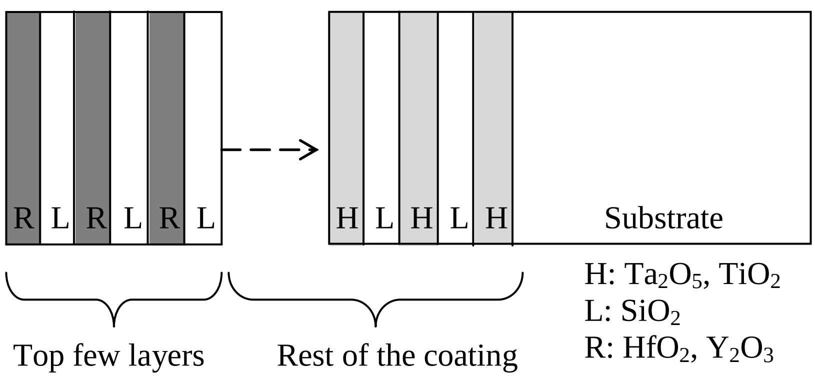

Figure 3.24 TMC structure schematic.

According to best of writer's knowledge, two recent studies had been performed for the investigation of TMCs for the high power laser optics. The first study was performed by Meng *et al.* [92]. TMC design of Meng *et al.* was constructed by HfO_2, TiO_2 and SiO_2 materials. They employed plasma sputtering deposition technique for the fabrication of the TMC stack. HfO_2 as the high refractive index material was used in the first three layer pair (where EFI values are high) together with the SiO_2 in order to obtain high laser damage resistance. For the rest of the coating TiO_2 was used as the high refractive index material which provides higher reflection compared to HfO_2. Finally they reported the LIDT values for the conventional 34 layer HR mirror (constructed from TiO_2/SiO_2 only) and 34 layer TMC HR mirror as 24.6 J/cm^2 and 39.6 J/cm^2, respectively. The second study that issues TMCs was published by Patel *et al.* [93]. In order to increase laser damage resistance of Ta_2O_5/SiO_2 coatings, Ta_2O_5 layers was replaced with HfO_2 and Y_2O_3 layers in the top few layers in that study. LIDT evaluations were performed according to 50% damage probability criteria. Results showed that the LIDT value was increased from 16 J/cm^2 to 22 J/cm^2 and 25 J/cm^2 when Y_2O_3 and HfO_2 materials are used in the top few layers, respectively.

However TMCs have been investigated by these two studies, no one applied NQWD method on TMCs before. In order to fill this lack in literature, non-quarter wave layer thicknesses are employed in TMCs in the current subsection. The usage of non-quarter wave layers is expected to be increase thermal performance and thermal performance of TMCs.

In order to investigate effects of NQWD method on thermal performance of TMCs, a 27 layer HR optical coating stack is used. The configuration of the HR coating is specified as $\{A/4L\ (RL)^3 4L(HL)^6 H/S\}$ where R represents the HfO_2 material in the first three layer pair, L represents the SiO_2, H represents the TiO_2 material, S represents the substrate and A represents the air. Numerical procedure which was described and used in previous chapter (chapter 3.3.1) is applied on both quarter and non-quarter wave TMC designs. Firstly, numerical studies are performed for the quarter wave thicknesses, Table 3.10. After than numerical studies are repeated for the non-quarter wave thicknesses, Table 3.10. These two designs are named as TMC-QWD and TMC-NQWD. As seen in table, only the first three layer pair (HfO_2/SiO_2)

thicknesses are changed for the TMC-NQWD which means that rest of the coating (TiO_2/SiO_2) still have quarter wave thicknesses. As known, the conventional quarter wave thicknesses provides theoretically highest reflectivity.

Table 3.10 Coating layer thicknesses (nm) for QWD and NQWD TMCs

		QWD	**NQWD**
For the first three layer pair	R	131	78
	L	182	273
For the rest of the coating	H	122.58	122.58
	L	182	182

* Shaded cells indicate that these layer thicknesses are modified

Temperature distributions are given in Figure 3.25 both for TMC-QWD and TMC-NQWD and it is obvious, employment of NQWD thicknesses results temperature reduction in HfO_2 layers. The peak temperature is decreased from ~585 K to ~450 K in the first layer pair and also the temperature peak is shifted inside to SiO_2 layer of the first layer pair. On the other hand, usage of NQWD thicknesses causes penetration of laser energy inside to inner layers and it corresponds to amount of laser absorption increment in the TiO_2/SiO_2 layer pairs. As seen in Figure 3.26, TiO_2 layers absorb more laser energy when NQWD thicknesses are used and it corresponds to higher peak temperature in the first TiO_2/SiO_2 layer pair. However, the peak temperature in the TMC-NQWD is ~490 K and it is still ~100 K lower than the peak temperature of the TMC-QWD.

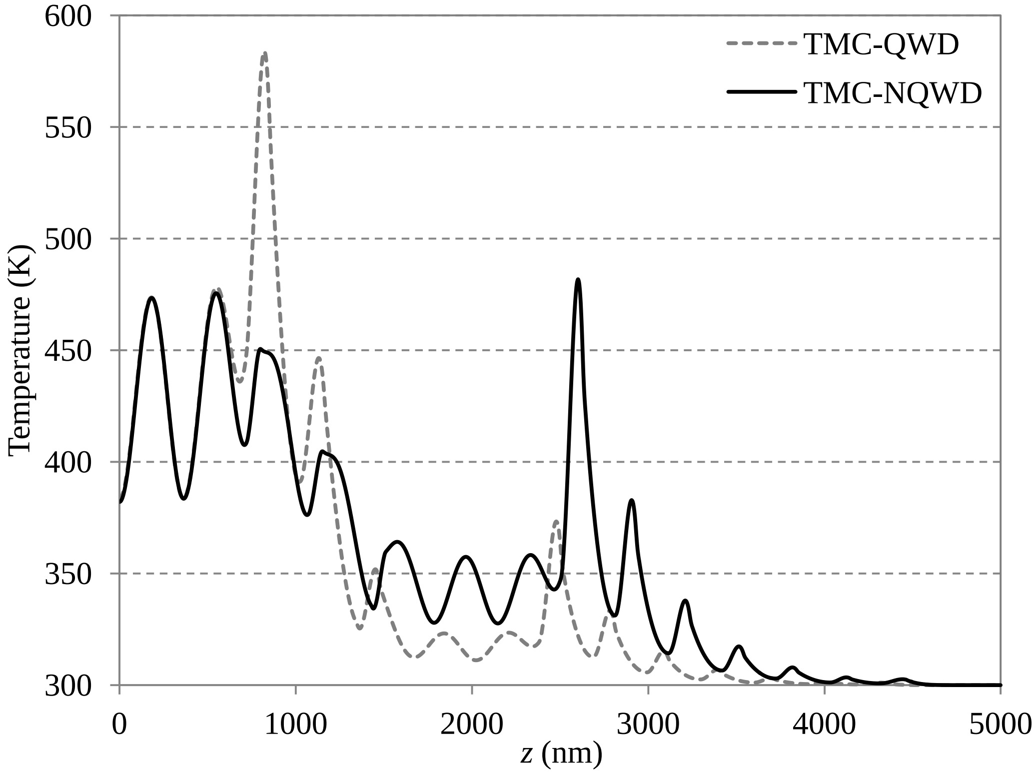

Figure 3.25 Temperature distributions along the *z*-axis for TMCs.

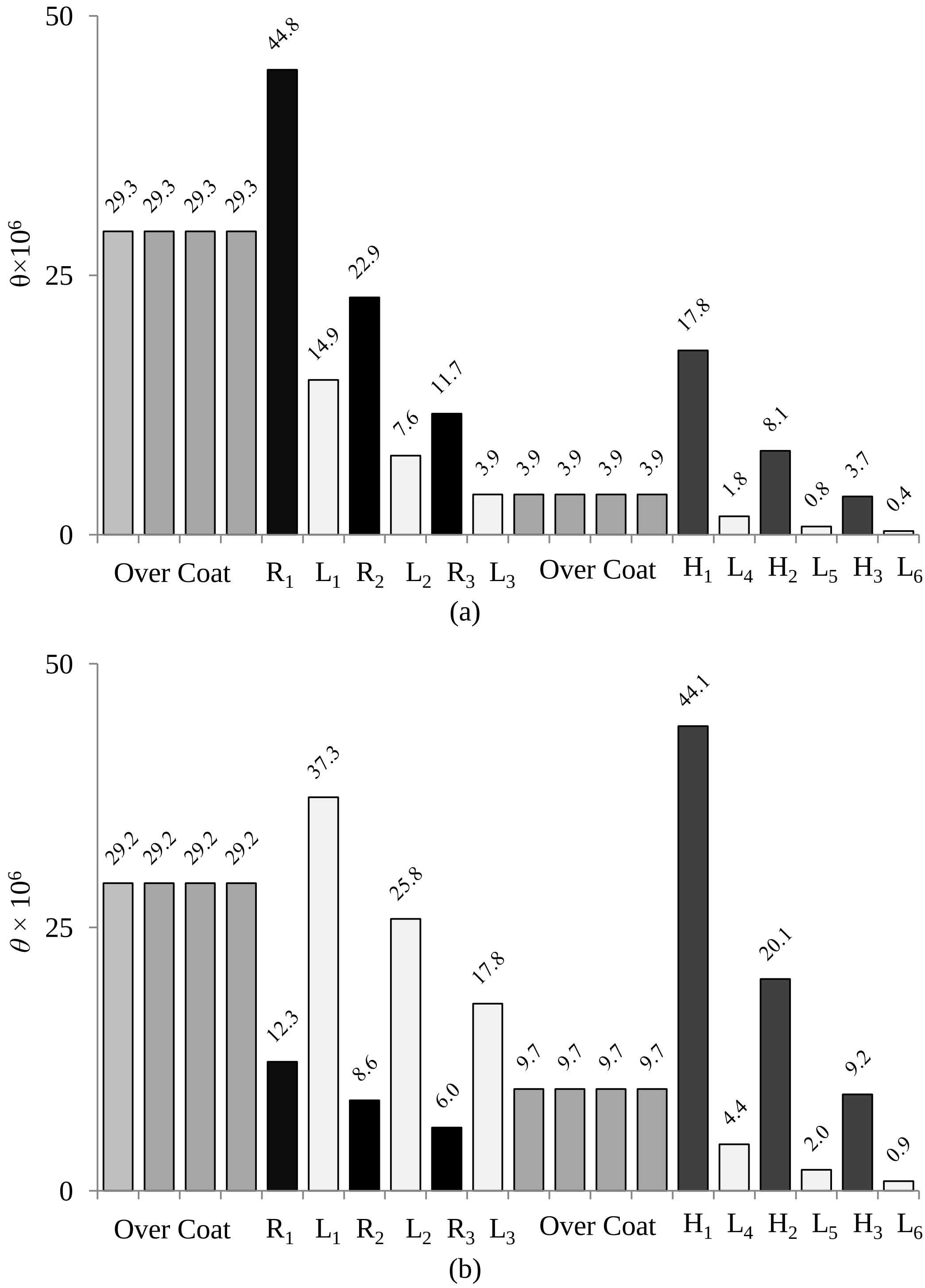

Figure 3.26 Absorption of laser by the coating layers; (a) TMC-QWD and (b) TMC-NQWD, (R: HfO_2, L: SiO_2, H: TiO_2).

CHAPTER 4

EXPERIMENTAL LIDT MEASUREMENT

LIDT performance is seen as the primary indicator of the durability (quality) of a coating. However, measurement of LIDT performance is not an easy task due to experimental parameters (such as laser spot size, laser peak power, laser temporal shape and etc.) which are difficult to control precisely during the tests. In order to overcome such difficulties, measurement procedures and terminologies are strictly defined by standard organizations such as ISO, IEEC and CEN [6].

It is observed both 1-on-1 and S-on-1 LIDT measurement techniques have been commonly used in the literature [94-96]. These techniques are standardized by ISO as ISO 11254-1 and ISO 11254-2 [97-98]. In both of the techniques, an optical specimen is shot by a laser in order to measure LIDT performance in a statistical way. A particular experimental setup is depicted by ISO for LIDT measurements as shown in Figure 4.1.

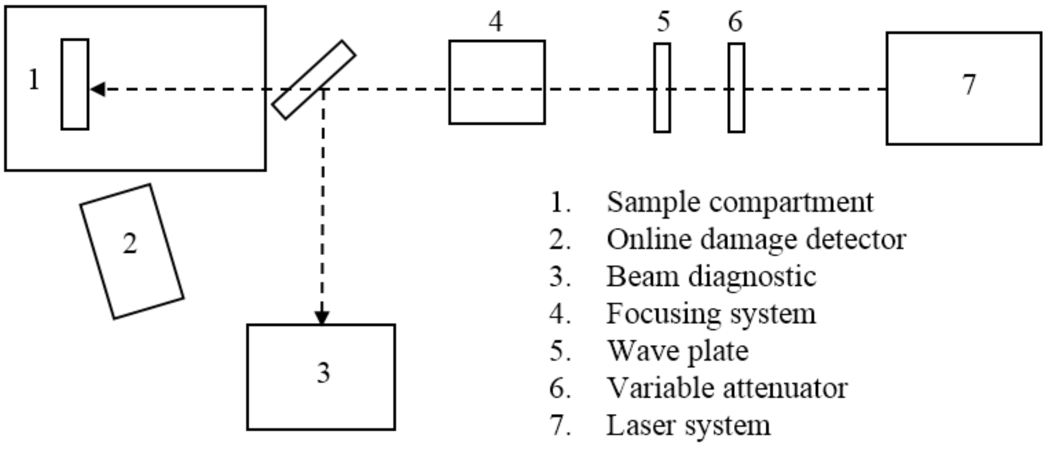

Figure 4.1 Simple schematic of S-on-1 laser damage testing setup [97].

The working mechanism of the setup is that the output of the laser is set to the predetermined energy level with a variable attenuator and delivered to specimen as shown in the simplified schematic. The optical specimen is settled in a manipulator which is used to move specimen (this movement provides the shot of different regions of specimen surface). During the tests, the laser beam is sampled with the help of beam splitter and directed to beam diagnostic unit for the simultaneous determination of the laser pulse energy and laser pulse temporal/spatial profile.

However both of the techniques use the same experimental setup, the procedure of 1-on-1 technique is simpler. In the case of 1-on-1 testing; the optical specimen surface is divided into sites as shown in Figure 4.2. Each site contains at least 10 sub regions. Each sub region is exposed to identical laser irradiance with predetermined pulse energy through only one pulse duration. After than regions are checked to identify whether the sub region is damaged or not, Figure 4.2.

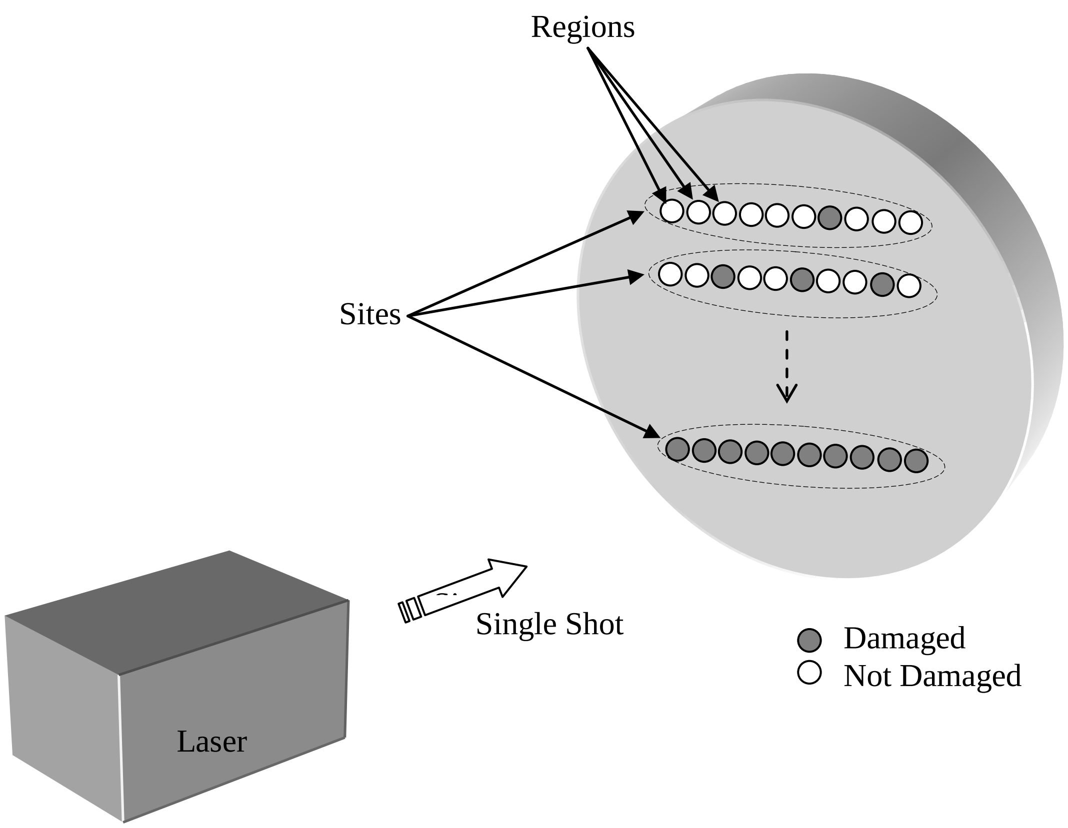

Figure 4.2 Optical specimen in 1-on-1 testing.

The damaged sub region is recorded with the corresponding pulse energy magnitude for the specimen. Thereafter test is repeated with the following site and in each following site, pulse energy will be increased to a higher level. The test will end when sub regions of all the sites are shot. After all, recorded damaged site counts and corresponding pulse energy levels are used to construct damage probability plot as illustrated in Figure 4.3.

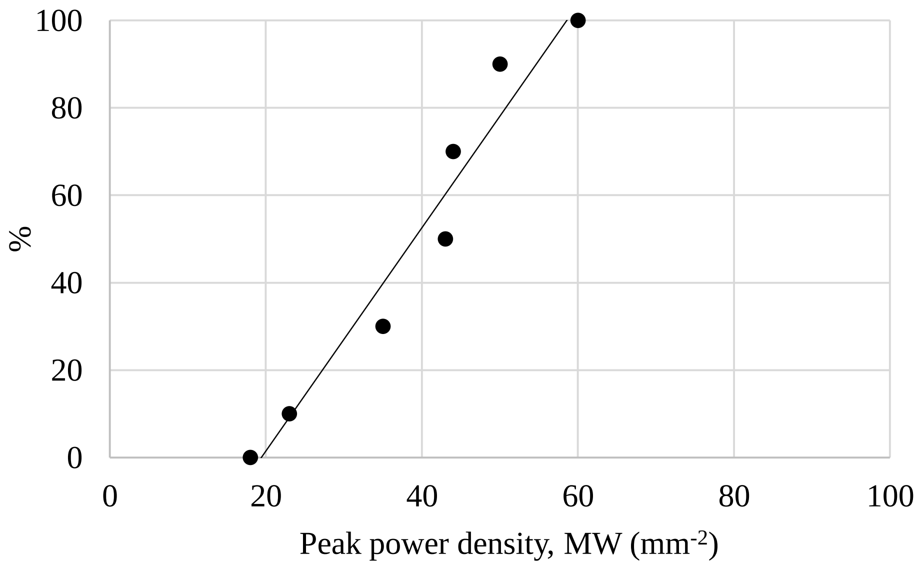

Figure 4.3 Damage probability chart [6].

Different than 1-on-1 testing, sub regions are irradiated with pulse trains of constant energy density and repetition frequency in the case of S-on-1 testing. The symbol “S” of the S-on-1 testing specifies the number of consecutive pulses. During the test each sub region of a site are exposed to S consecutive laser shots with identical fluence. Meanwhile surface of the specimen should be observed with an online damage detector throughout the test. After than the fluency will be increased and sequence will be repeated for sub regions of another site.

In the present study the 1-on-1 testing method is employed to find LIDT performance of numerically investigated HR coating configurations. In order to perform these 1-on-1 tests, firstly HR multilayer coatings are fabricated as detailed in the chapter 4.1. Then fabricated HR optical coatings are tested by following the 1-on-1 testing procedure in chapter 4.2. At the last part, in chapter 4.3, damage morphologies are investigated on the tested optical coating surfaces.

4.1 Manufacturing Of HR Multilayer Optical Coatings

Modified optical designs and their effects on thermal performance are investigated and studied through numerical simulations in the third chapter. Firstly, NQWD method is used to increase thermal performance of a conventional 19 Layer HR coating [63]. Based on the study of Gill *et al.* [58], high index coating layer thicknesses are decreased and low index coating thicknesses are increased to obtain the five NQWDs. In the second step, a new NQWD method is proposed for multiple shot laser irradiation case in order to overcome drawbacks of previous NQWDs [74]. In addition to these, the effects of upper surface OC layer and TMC designs on thermal performance are also studied in chapter 3.4 and chapter 3.5, numerically. In the current subsection HR multilayer coatings are manufactured so as to collaborate numerical studies with LIDT tests.

A limited number of HR multilayer coatings are fabricated because of the high cost of the production method and the coating materials. Fabricated coatings and corresponding layer thicknesses are given in Table 4.1, below.

Table 4.1 Layer thicknesses of the fabricated HR coatings

Layer ID	**QWD**	**NQWD1**	**NQWD2**	**NQWD5**	**NQWD1-M**	**NQWD2-M**	**NQWD5-M**	**QWD-OC**	**NQWD1-OC**	**NQWD1-M-OC**
OC	N.A.	N.A.	N.A.	N.A.	N.A.	N.A.	N.A.	726.48	726.48	726.48
H_1	131	80	66	48	78	78	78	131	80	78
L_1	182	270	290	313	273	273	273	182	270	273
H_2	131	131	80	52	131	78	78	131	131	131
L_2	182	182	270	308	182	273	273	182	182	182
H_3	131	131	131	58	131	131	78	131	131	131
L_3	182	182	182	301	182	182	273	182	182	182
H_4	131	131	131	66	131	131	78	131	131	131
L_4	182	182	182	290	182	182	273	182	182	182
H_5	131	131	131	80	131	131	78	131	131	131
L_5	182	182	182	270	182	182	273	182	182	182

*Shaded cells indicates that these thicknesses are modified
**N.A. indicates that the design has no OC

As seen in Table 4.1, one QWD and nine NQWDs are fabricated. For the NQWDs modified layer thicknesses are used. Modified layer thicknesses for NQWD1, NQWD2 and NQWD5 are calculated based on Gill *et al.*'s study. In the meantime, the MATLAB code is used for layer thickness calculations of NQWD1-M, NQWD2-M and NQWD5-M. The upper surface OC is also added on QWD-OC, NQWD1-OC and NQWD1-M-OC. As noted in the numerical studies section, the modification of first and second layer pair thicknesses, as done for NQWD1 and NQWD2, assessed as applicable while the other designs, for example NQWD5, are criticized due to the increased amount of laser absorption. These designs are fabricated in this chapter to investigate their LIDT performance.

.

All these HR multilayer stacks composed of HfO_2 and SiO_2 layers. These layers are deposited by electron beam physical vapor deposition (EB-PVD) system. Briefly, in EB-PVD technique, electrons are released from a tungsten filament (so called electron gun) and directed towards to coating materials surface with the help of quite powerful magnetic field. Such an electron bombardment results sudden evaporation/sublimation of coating material locally. Thereafter, sublimated/evaporated coating material is started to deposit on substrate surface inside the chamber.

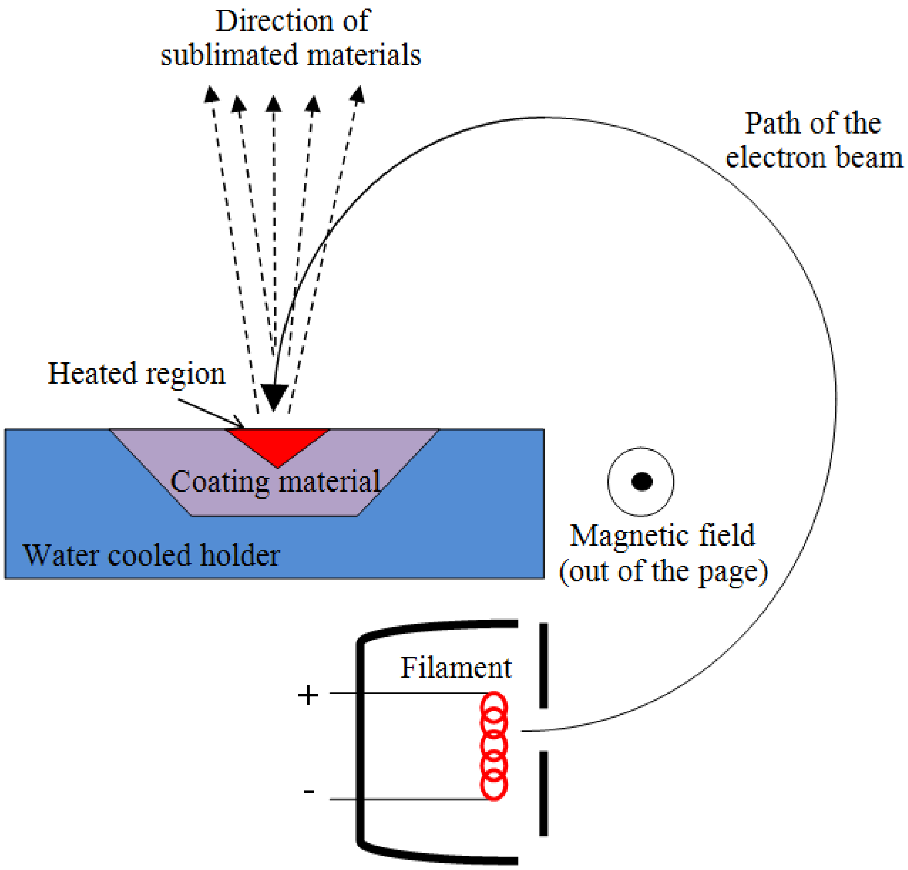

Figure 4.4 Schematic representation of the working mechanism of an electron gun [99].

Figure 4.5 Generic photographs of coating material in an electron gun pot (left) and electron gun (right) [100].

A commercial EB-PVD coating chamber which is Leybold Optics Syrus pro (Figure 4.6) is used for the production of HR multilayers. The coating chamber also involves Advanced Plasma Source (APS) pro for the additional ion bombardment [101].

Figure 4.6 Photographs of Leybold Optics Syrus pro [101]; external appearance (left), internal appearance and ignited APS (right).

In the APS system, Argon gas is used for the plasma generation. As explained in chapter 3.3, an additional ion bombardment by means of APS increases the quality (in other words laser resistance) of optical coatings greatly. The base pressure inside the coating chamber is vacuumed to 10^{-7} mbar before the deposition process is started. In addition, substrate surface is presputtered/etched through 120s with using plasma ion source in order to remove contaminations from substrate surface, if any. Then, substrate temperature is raised to 120 ºC and coating process is started. During the deposition processes of HfO_2 and SiO_2 layers, oxygen flow rate is adjusted to 50 sccm and 5 sccm, respectively. The rate of the thicknesses of the HfO_2 and SiO_2 layers are monitored using in situ online optical monitoring system OMS 5000. The used growth rates of HfO_2 and SiO_2 layers are 0.2 nm/s and 0.5 nm/s, respectively. Currents which are used to accelerate released electrons from electron gun are 300 mA and 60 mA for HfO_2 and SiO_2 layers.

4.2 Experimental Setup Installation Advancements

Experimental setup installation works has been continued in ASELSAN Inc. for LIDT measurements. Photographs related with the experimental setup installation are given in Figure 4.7. As seen in Figure 4.7, installation of setup is almost completed. Studies will be continued by fine tuning of the optic units for better focusing the laser beam. In addition sample compartment is controlled by manually in this setup and it increases the time for testing any sample.

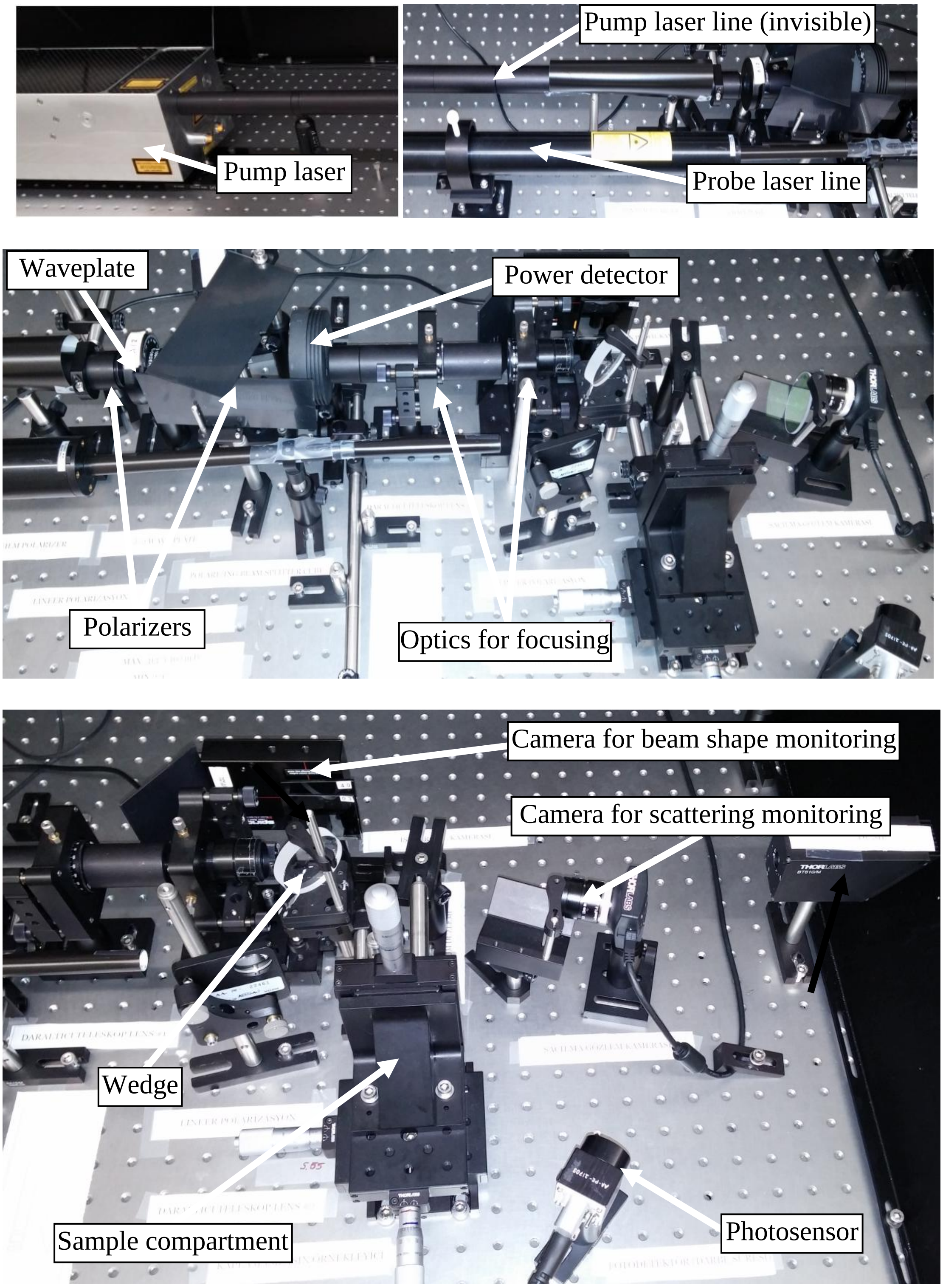

Figure 4.7 Photographs of experimental setup.

4.3 LIDT Test Results And Damage Morphology Investigations

Damage morphology investigations for thin film optical coatings have been studied since its essence is realized by the researchers. These investigations elucidate the relationship between damage morphology and LIDT. In addition to that, effect of optical design, thin film materials and laser parameters on LIDT value can also be clarified owing to damage morphology investigations.

In the literature laser irradiation induced damages on optical coatings were entitled and introduced into several groups according to their characteristic shapes [102-104]. Damage types for HfO_2/SiO_2 HR multilayers were defined in Genin and Stolz's [103] study within details. In that study four damage types are reported as pits, flat bottom pits, scalds and delaminations. Among these damage types it is known that pit type damages are resultant from nodule ejections (expulsions) [102-106]. In fact, nodules or in other words nodular defects are formed during the thin film deposition process due to irregularities on substrate surface or preferential nucleation sites (seeds) [106]. Briefly, during the laser irradiation, nodules cause local laser absorption and this severe absorption causes sudden temperature increase inside nodules. Due to the local and sudden temperature rise, coating materials melt at that local spot and cause nodule ejection, Figure 4.8 [105].

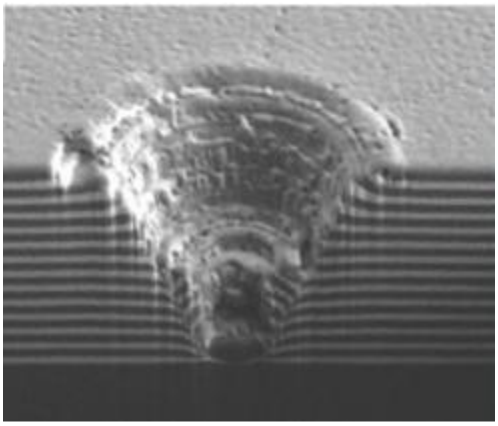

Figure 4.8 Cross sectional view of pit type damage morphology obtained by Nomarski microscope after Focused Ion Beam (FIB) characterization [105]. Adapted from "The effect of an electric field on the thermomechanical damage of nodular defects in dielectric multilayer coatings irradiated by nanosecond laser pulses," by X., Cheng, J., Zhang, T., Ding, Z., Wei, H., Li, and Z., Wang, 2013, *Light: Science & Applications*, *2*(6), p. e80. Copyright 2015 by the Copyright Clearance Center.

Flat bottom pit, which is another damage type for HR thin films, is resultant from nanoabsorbing centers at the film/film interfaces and they are not resultant from substrate surface irregularities or preexisting seeds [103, 107-108]. The origin of nanoabsorbing center is not fully understood, because these centers cannot be detected before the LIDT tests with optical microscopy. Dijon [108] defines these absorbing centers as invisible and almost punctual. It is stated in Wang *et al.*'s [107] study; during the laser irradiation, temperature and pressure at the absorbing center suddenly increases due to excessive laser energy absorption and creates small cavity by melting the coating material. Then, the coating material that surrounds the small cavity exposed to free electron injection and heat. The heat and electron injection causes big tensile stress on coating layers and finally coating layers are blistered. As given in Figure 4.9, a small cavity is seen at the bottom of the cylindrically blistered damaged site as a characteristic indicator of the flat bottom pit damage. In addition to these explanations, Ristau [104] also simply stated that; the flat bottom pit type damage contours (Figure 4.10) can be formed due to excessive laser absorption resultant overheating of the coating layers.

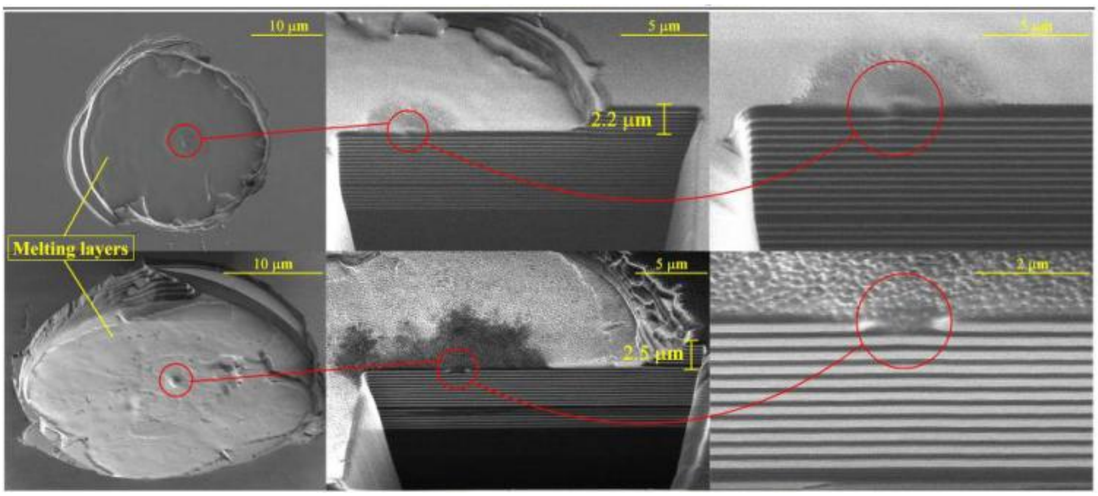

Figure 4.9 Top view and cross sectional views of flat bottom pit type damage contours obtained by Nomarski microscope after FIB characterization [107]. Adapted from "Interfacial damage in a Ta_2O_5/SiO_2 double cavity filter irradiated by 1064 nm nanosecond laser pulses" by Z., Wang, G., Bao, H., Jiao, B., Ma, J., Zhang, T., Ding, and X., Cheng, 2013, *Optics Express*, *21*(25), p. 30623. Copyright 2015 by the Copyright Clearance Center.

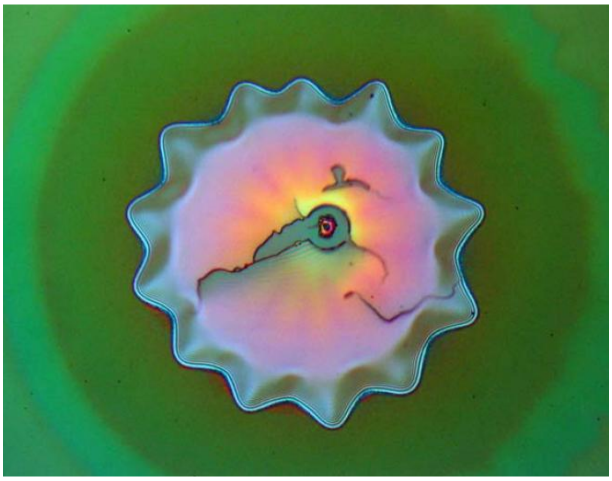

Figure 4.10 Top view of the flat bottom pit type damage contours obtained by Nomarski microscope [104]. Adapted from “Laser damage thresholds of optical coatings,” by D., Ristau, M., Jupé, and K., Starke, 2009, *Thin Solid Films*, *518*(5), p.1607. Copyright 2015 by the Copyright Clearance Center.

Scald type damage contours can also be seen on optical thin films due to plasma formation in front of the outer surface of the coating. The reason of plasma formation, in front of coating, possibly will be the electric field enhancement due to dust particles [103, 110]. Due to the plasma formation and corresponding local extensive temperature increase, coating surface is damaged by forming scalds, (Figure 4.11).

Removal of outer layers due to laser irradiation is defined as delamination [103]. Delamination of the outer layers is caused from internal laser absorption [104]. For conventional HR coatings EFI strength is higher at the outer layers, especially at the H/L interfaces. As mentioned in Genin and Stolz’s work, overlayer (outer layer) removed from the surface in case of delamination which is different than scald type damage. It is believed that delamination starts due to instantaneous heating of the coating material and it causes removal of the outer layers totally [104, 111] whereas damage starts from the air side of the outer layer for the scalds.

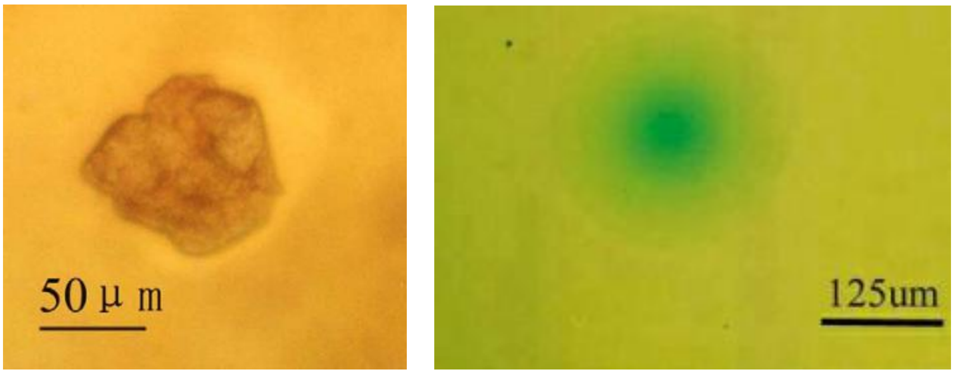

Figure 4.11 Top view of scald type damage contours obtained by Nomarski microscope (left) [109] Adapted from "Roles of absorbing defects and structural defects in multilayer under single-shot and multi-shot laser radiation," by Y., Zhao, W., Gao, J., Shao, and Z., Fan, 2004, *Applied Surface Science, 227*(1), p. 275. Copyright 2015 by the Copyright Clearance Center and (right) [110].

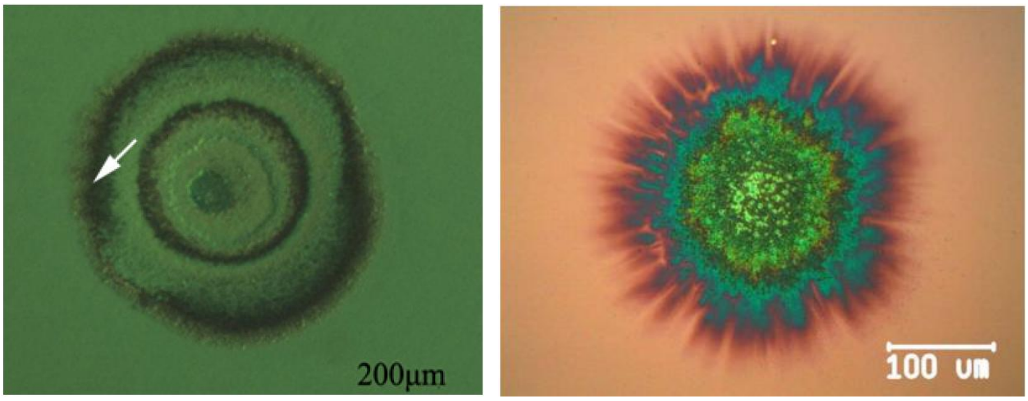

(a) (b)

Figure 4.12 Top view of delamination type damage contours obtained by Nomarski microscope (left) [111] Adopted from "Damage morphology change condition and thermal accumulation effect on high-reflection coatings at 1064nm," by Z., Liu, J., Luo, Y., Zheng, P., Ma, Z., Zhang, Y., Wei, and S., Chen, 2014, *Optics Express, 22*(9), p. 10151 and (right) [104]. Adapted from "Laser damage thresholds of optical coatings," by D., Ristau, M., Jupé, and K., Starke, 2009, *Thin Solid Films, 518*(5), p.1607. Copyright 2015 by the Copyright Clearance Center.

Damage morphology investigations in this chapter are used to collaborate numerical simulations with the experimentally measured LIDT values. In order to achieve this, damaged sites which are formed during the 1-on-1 LIDT measurements are scanned using a Nomarski differential interference contrast (DIC) microscope [112-113]. As explained in chapter 3, one of the primary goals of this dissertation is to enhance thermal performance of the HR coatings by manipulating the electric field and corresponding temperature field inside the coating stacks.

It is believed that investigation of damages together with the LIDT values provides us much more information about the effectiveness of the performed modifications.

4.3.1 1-on-1 LIDT Measurements On The HR Coatings

HR coatings which are fabricated using EB-PVD technique are tested by following the 1-on-1 LIDT measurement procedure with the help of Lidaris Inc. As remembered, the coating identities and corresponding layer thicknesses are given in Table 4.1. 1-on-1 test method is considered as appropriate for the damage morphology investigations and so preferred instead of S-on-1 test method. Because repetitive shots of S-on-1 testing will totally corrupt damage sites and the origin of damage will become degenerated.

4.3.1.1 1-on-1 Test Result Of The QWD

The 1-on-1 test results are given in the Figure 4.13 and a trend line is fitted on data for QWD. Even though LIDT measurement is a statistical test and results have to be given in such a probability chart, results will be evaluated by inspecting damage contours as well. It is thought that delamination and flat bottom pit type damage contours and corresponding laser fluencies are meaningful for the evaluation of the layer thickness modifications. Because, layer thickness modifications change laser absorption distribution inside the coating stack that changes the temperature field as presented in numerical simulations. Herein, nodule ejection and scald type damage contours will be disregarded, since such damages resultant from substrate irregularities, seeds and dust particles as explained in previous pages.

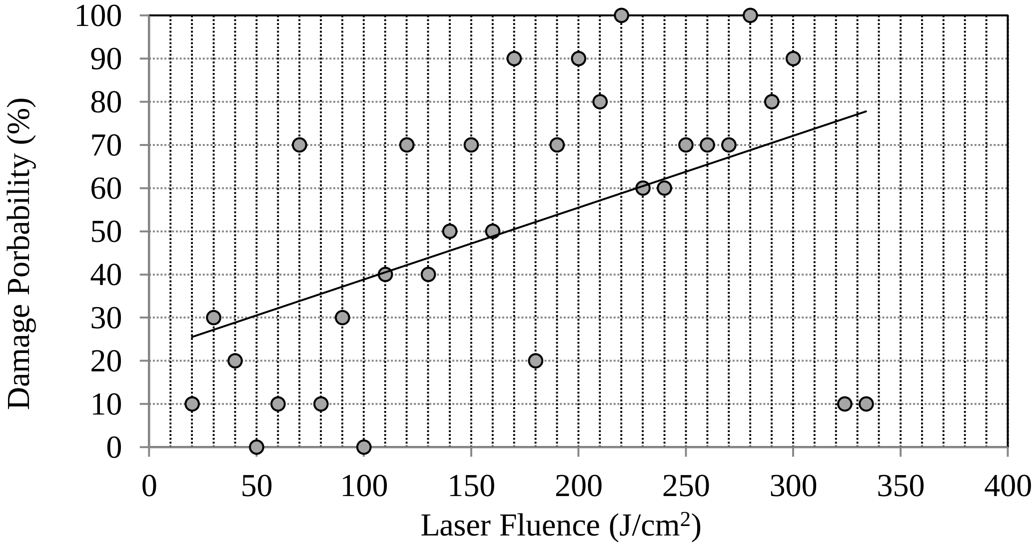

Figure 4.13 Percentage damage probability chart of the fabricated QWD

The lowest damage fluence in the chart is 20 J/cm^2 but the contour of this damage is a kind of scald, so this damage will be disregarded. The following lowest damage fluence is 30 J/cm^2. In this level, three damages are detected but only one of them is inspected. Because the contour of that damage is delamination type, as seen in Figure 4.14.

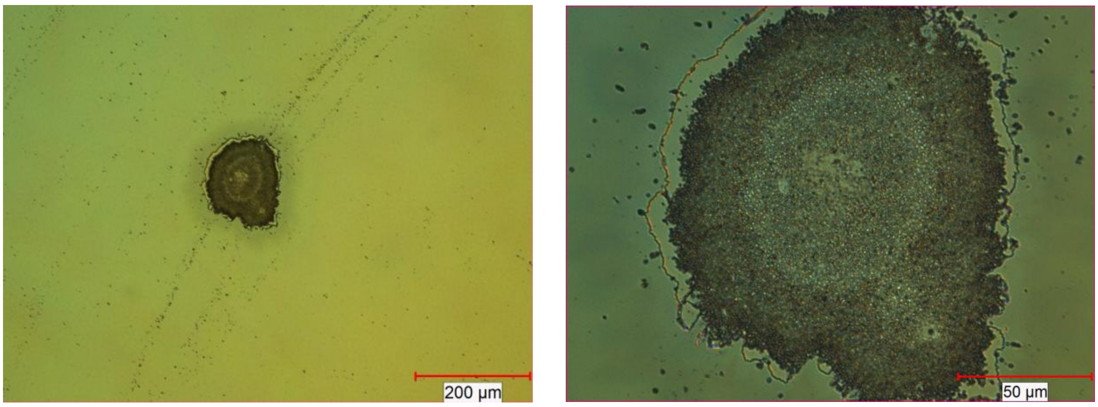

(a) (b)

Figure 4.14 Delamination type damage at 30 J/cm^2 laser fluence on QWD; (a) 100x magnification (b) 500x magnification.

In addition to that damage, other (delamination type) contours are also inspected under Nomarski DIC microscope. It is seen that damages have two noticeable features. The first feature is the fracture of the outermost (H_1) layer as seen in Figure 4.15. It is known that owing to the prior numerical calculations for the QWD design, the highest EFI peak occurs at the first H/L interface (Figure 3.11.a) and it causes the highest interface temperature rise at that point, Figure 3.6. Accordingly, the sudden rise of the temperature and corresponding pressure increase cause the fracture of the H_1 layer by leaving a fracture mark behind. The second feature is the melted and resolidified center region, Figure 4.16. The first HfO_2 (H_1) layer and maybe the first SiO_2 (L_1) layers are melted due to excessive laser absorption.

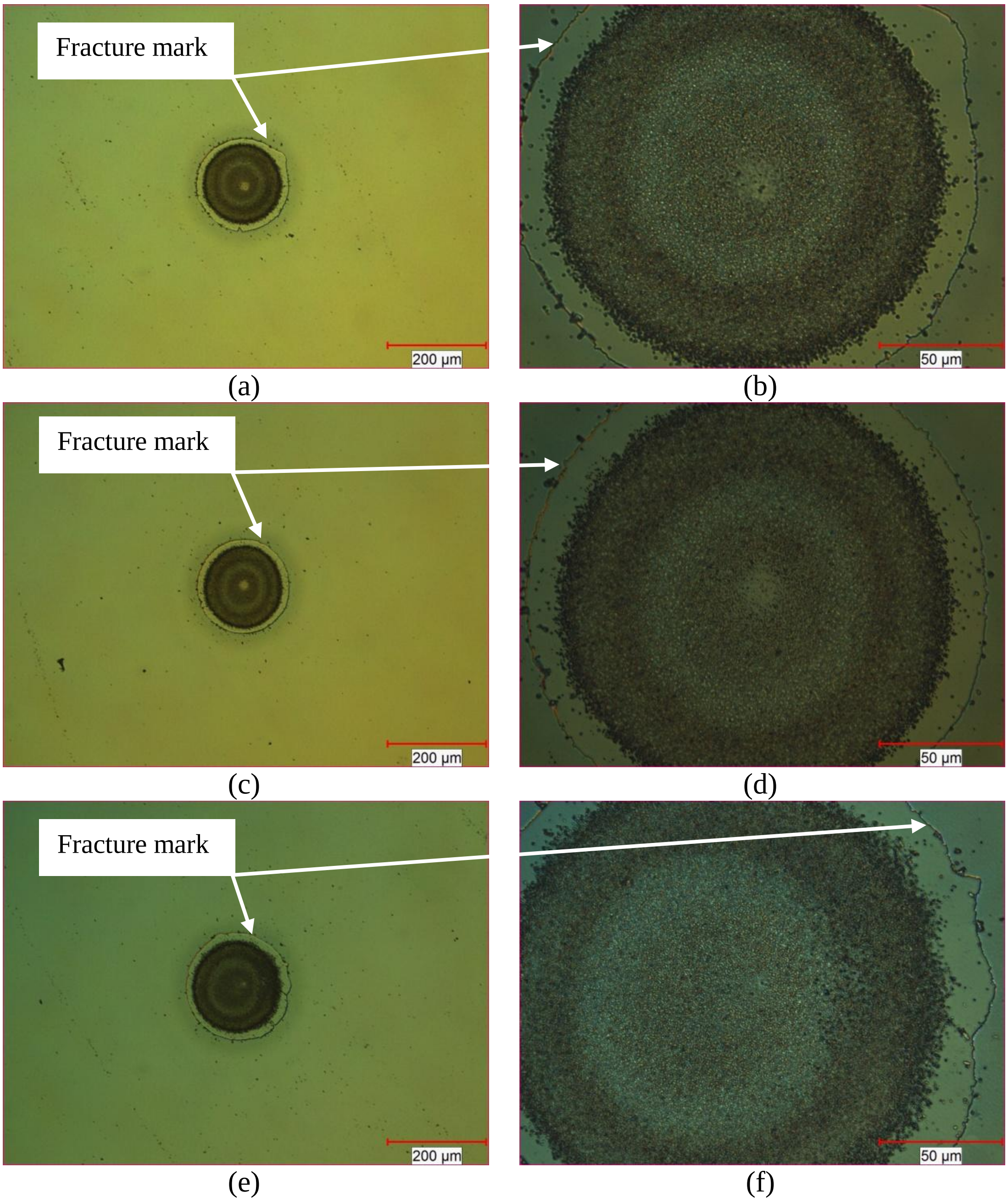

Figure 4.15 Delamination type damage contours on QWD surface; (a) at 70 J/cm^2 laser fluence-100x magnification, (b) at 70 J/cm^2 laser fluence-500x magnification, (c) at 90 J/cm^2 laser fluence-100x magnification, (d) at 90 J/cm^2 laser fluence-500x magnification, (e) at 120 J/cm^2 laser fluence-100x magnification, (f) at 120 J/cm^2 laser fluence-500x magnification.

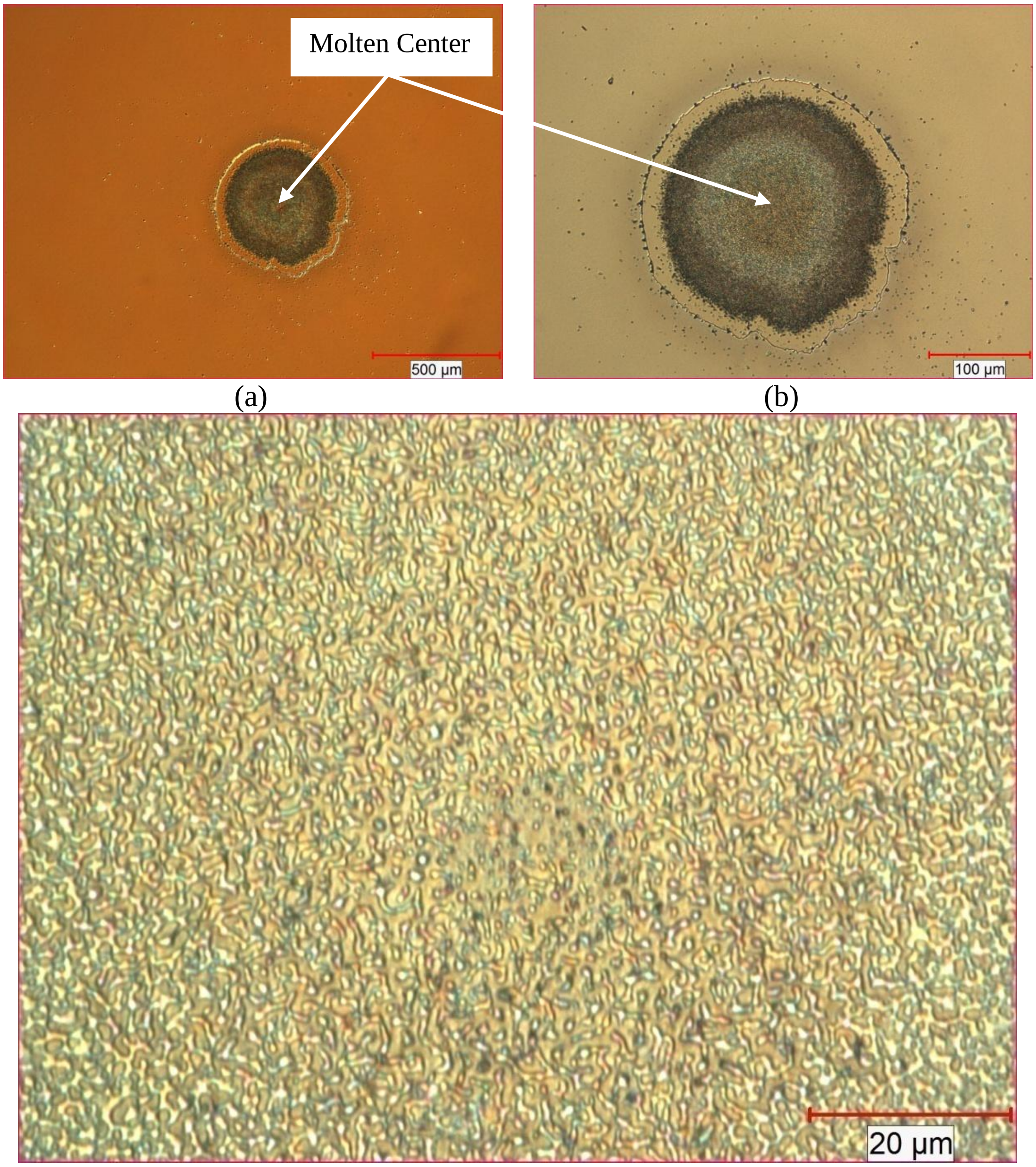

(a) (b)

(c)

Figure 4.16 Delamination type damage at 140 J/cm^2 laser fluence on QWD surface; (a) 50x magnification, (b) 200x magnification, (c) 1000x magnification.

The first noticeable feature of the damage mechanism is also scrutinized by performing white light interferometry (WLI) measurements. Two damage contours are investigated using a (Zygo 7100) white light interferometer [114-115] and three dimensional damage pictures are obtained. Furthermore damage depth graphics are also obtained on a reference line that crosses the damage crater. Results are given in Figure 4.17 and Figure 4.18.

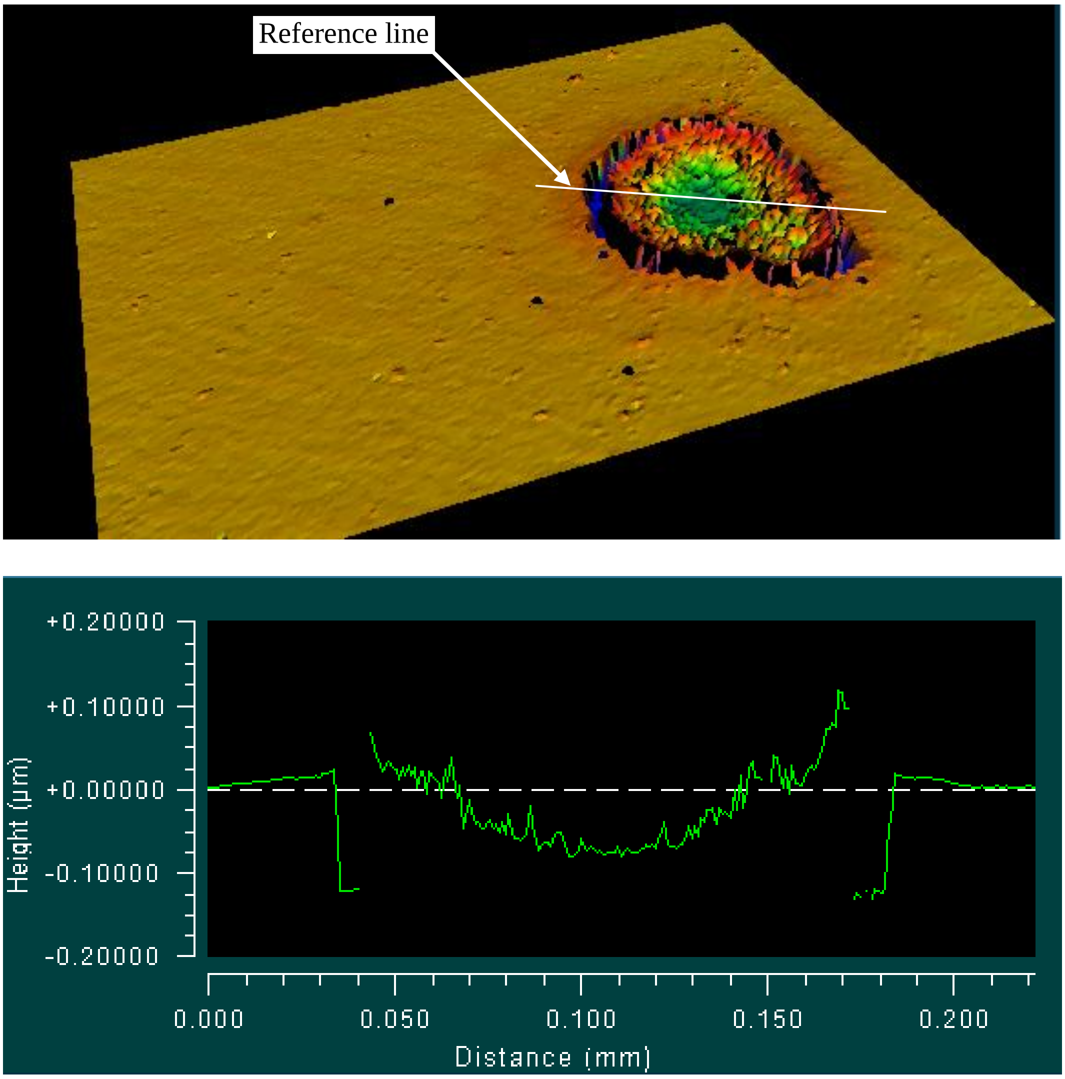

Figure 4.17 WLI measurements of the delamination type damage (corresponds to Figure 4.14) for QWD. 3-D appearance at the top view and depth measurement through a reference line at the bottom view.

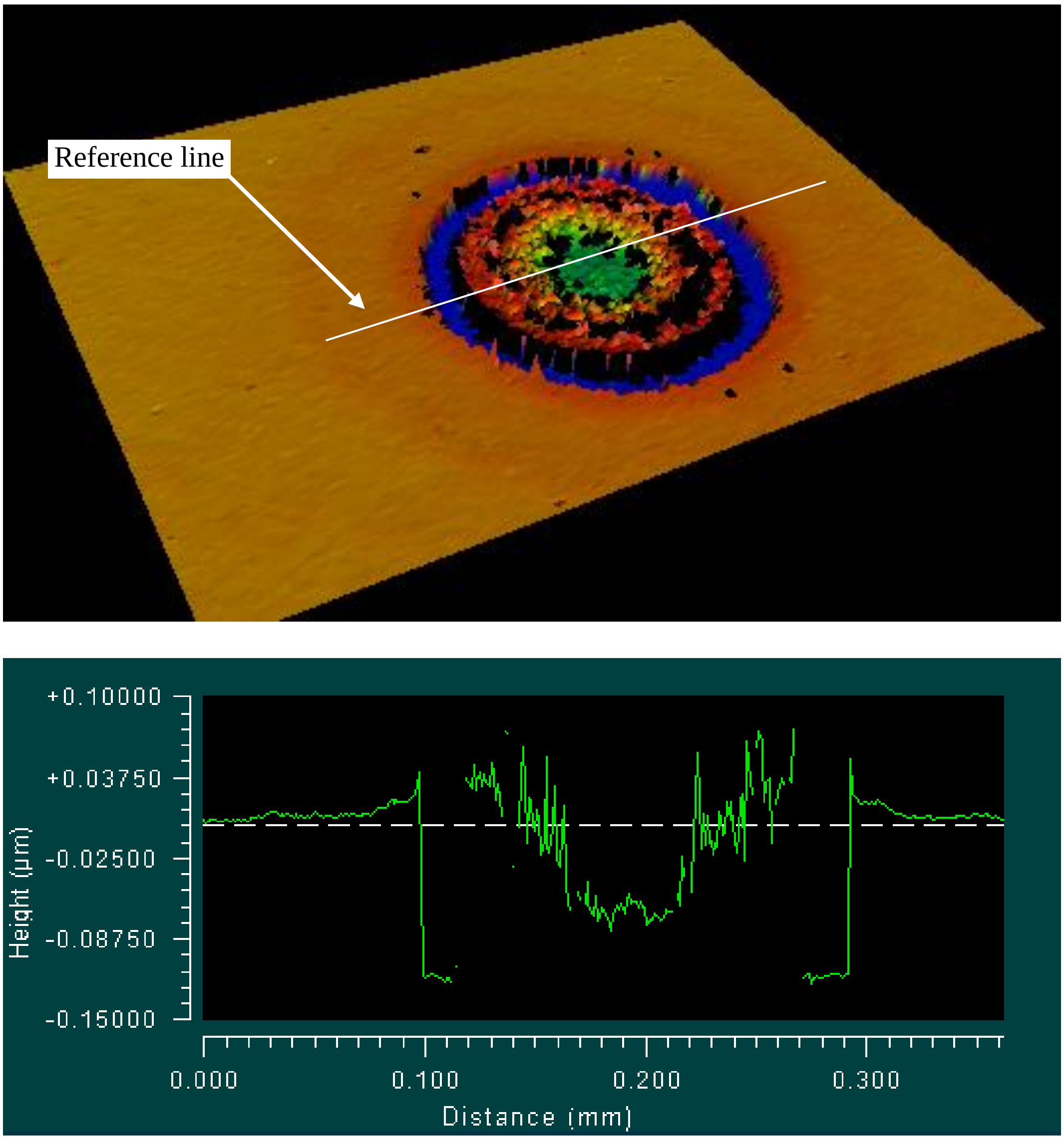

Figure 4.18 WLI measurements of the delamination type damage (corresponds to Figure 4.15.a) for QWD. 3-D appearance at the top view and depth measurement through a reference line at the bottom view.

As seen in Figure 4.17-Figure 4.18, the depth of the fracture mark is about to 125 nm. As known (Table 4.1), the thickness of the H_1 layer is 131 nm for QWD. Hence, the starting points of the damages are probably the first interface. These outcomes support our numerical simulations, as stated in the subsection 3.1.1 the highest interface temperature is calculated at the first H/L interface on the QWD. In addition, the depths are ~70 nm in both of the damage centers which means that some part of H_1 layer is sublimated and/or exploited from this region and remaining part is melted and resolidified.

4.3.1.2 1-on-1 Test Result Of The NQWD1

Damage probability chart of NQWD1 is formed after 1-on-1 test and presented in Figure 4.19.

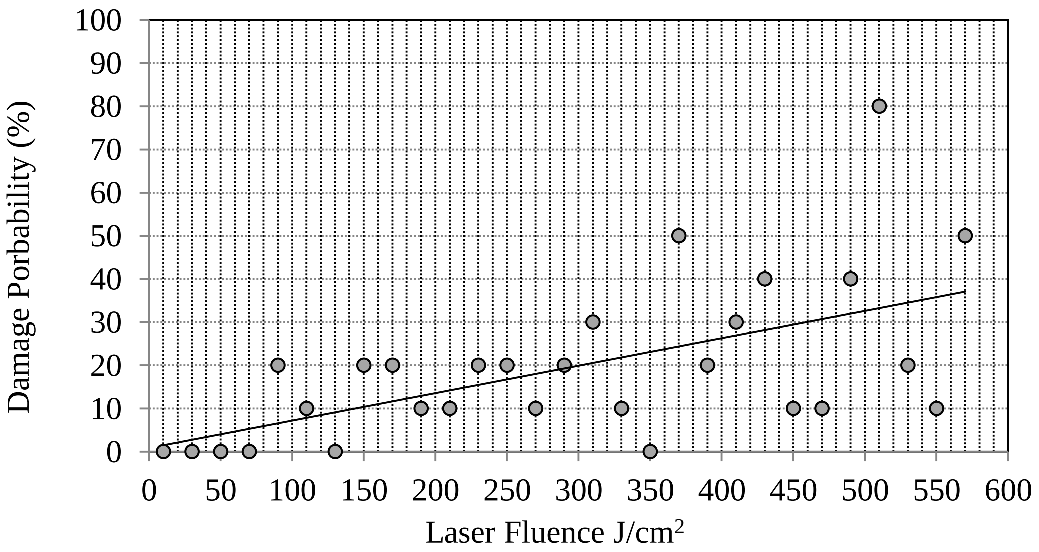

Figure 4.19 Percentage damage probability chart for NQWD1.

Considering Figure 4.19, one can easily realize that the lowest fluence is 90 J/cm^2 at which damages are occurred. Both of the damages which are formed at 90 J/cm^2 fluence level are delamination type as seen in Figure 4.20.

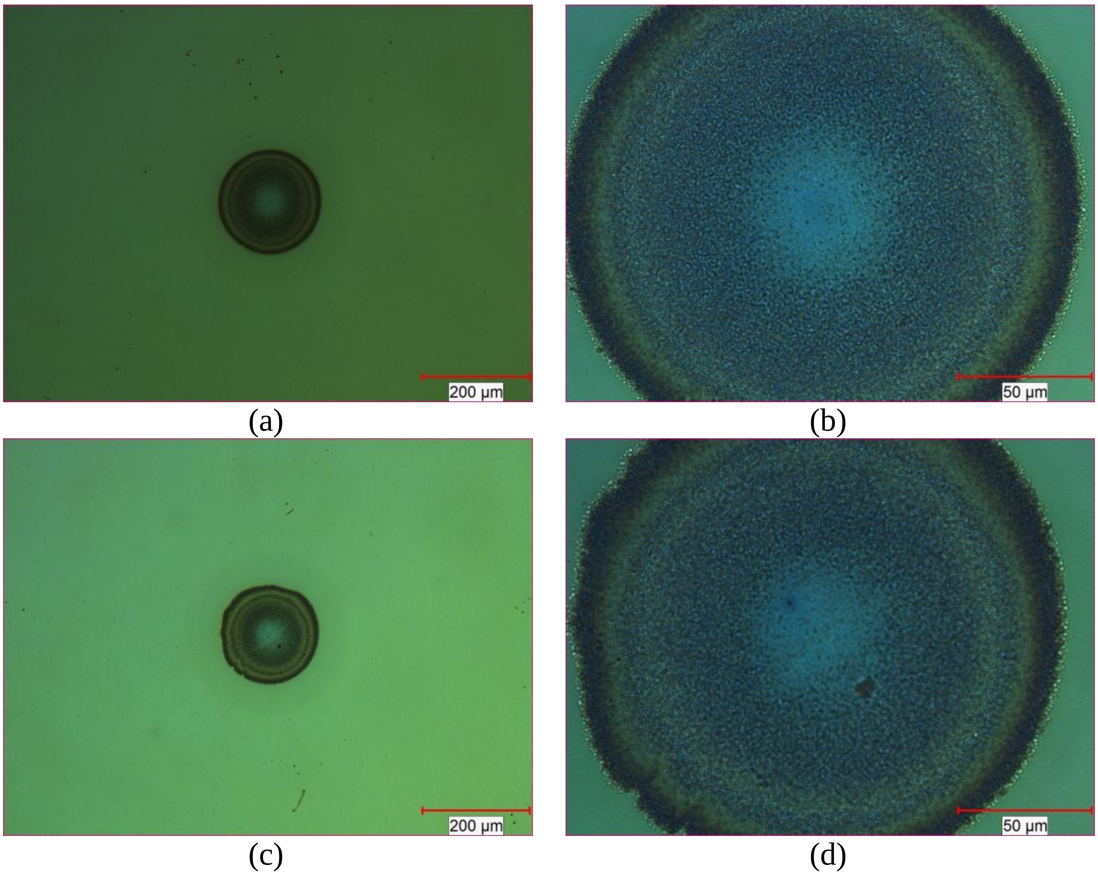

Figure 4.20 Delamination type damage contours at 90 J/cm^2 laser on NQWD1; (a) 1st damage-100x magnification, (b) 1st damage-500x magnification, (c) 2nd damage-100x magnification, (d) 2nd damage-500x magnification.

Delamination type damages have also seen at higher laser fluence levels. The noticeable feature of these damages is the concentric ring like shapes. As seen in Figure 4.21, at least three concentric rings can be easily detected. Reasons that form the concentric rings are cleared up after WLI measurements. As explained in numerical studies section, the first layer pair thickness modification shift the temperature peak inside the low index layer and also the peak temperature value is decreased. In accordance with that the sharp fracture mark is not observed on the damages of NQWD1.

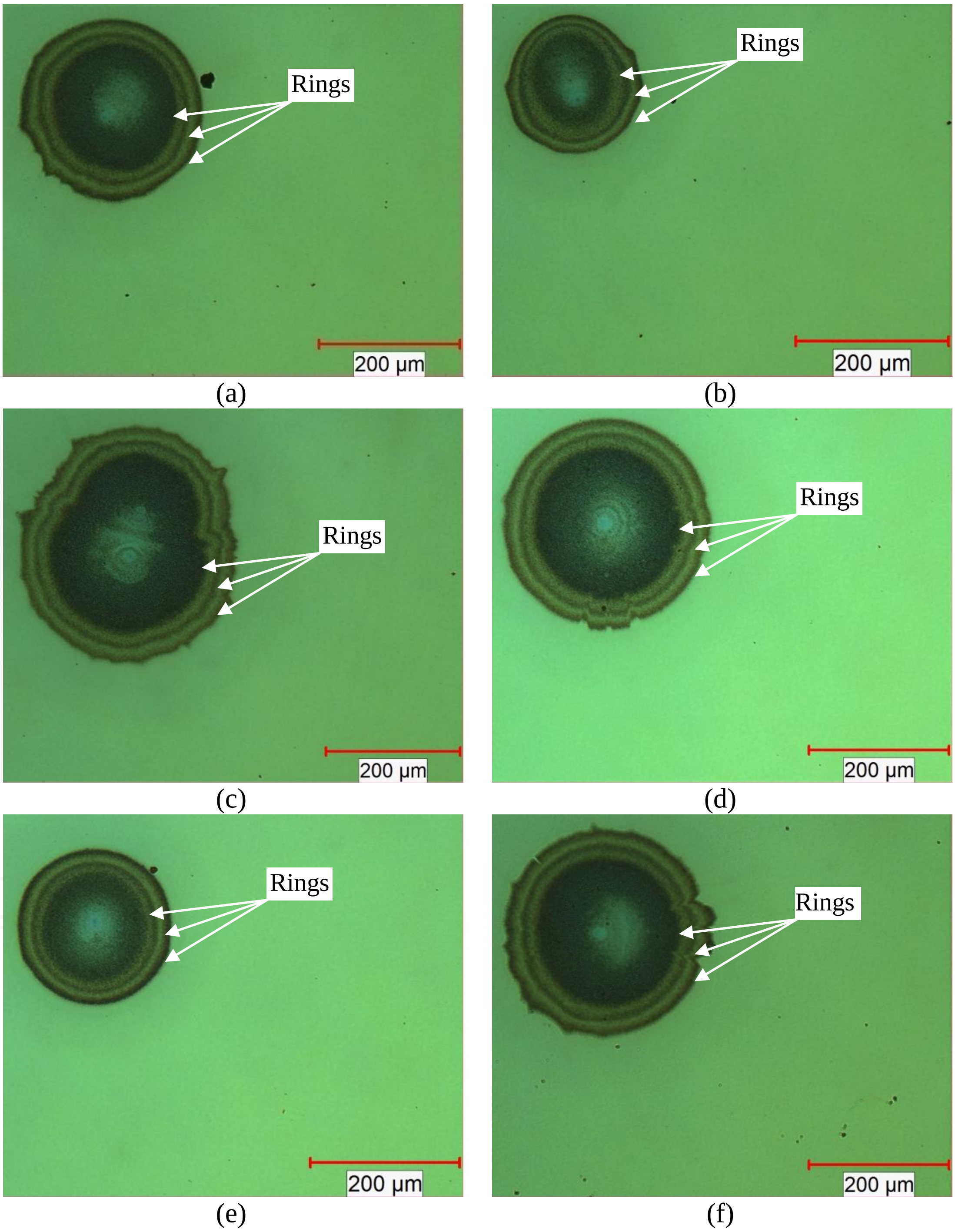

Figure 4.21 Delamination type damage contours on NQWD1 surface (100x magnification); (a) at 110 J/cm^2 laser fluence, (b) at 150 J/cm^2 laser fluence, (c) at 150 J/cm^2 laser fluence, (d) at 170 J/cm^2 laser fluence, (e) at 170 J/cm^2 laser fluence, (f) at 190 J/cm^2 laser fluence.

WLI measurements are performed for the damages of NQWD1 to collect more data about damage contours. The concentric rings (noticeable features) are explicitly seen in the WLI measurements as given in Figure 4.22 and Figure 4.23.

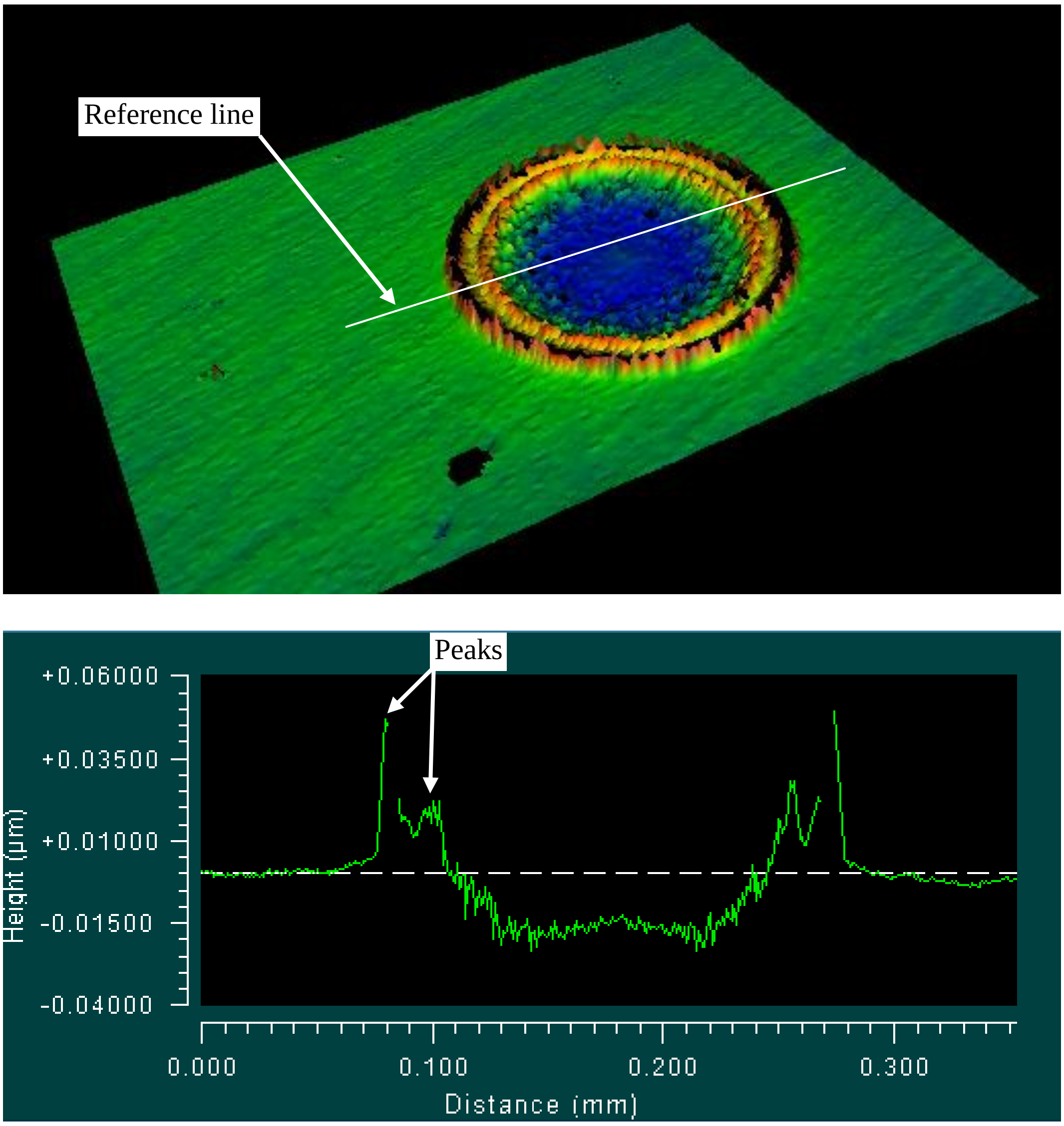

Figure 4.22 WLI measurements of the delamination type damage (corresponds to Figure 4.20.a) for NQWD1. 3-D appearance at the top view and depth measurement through a reference line at the bottom view.

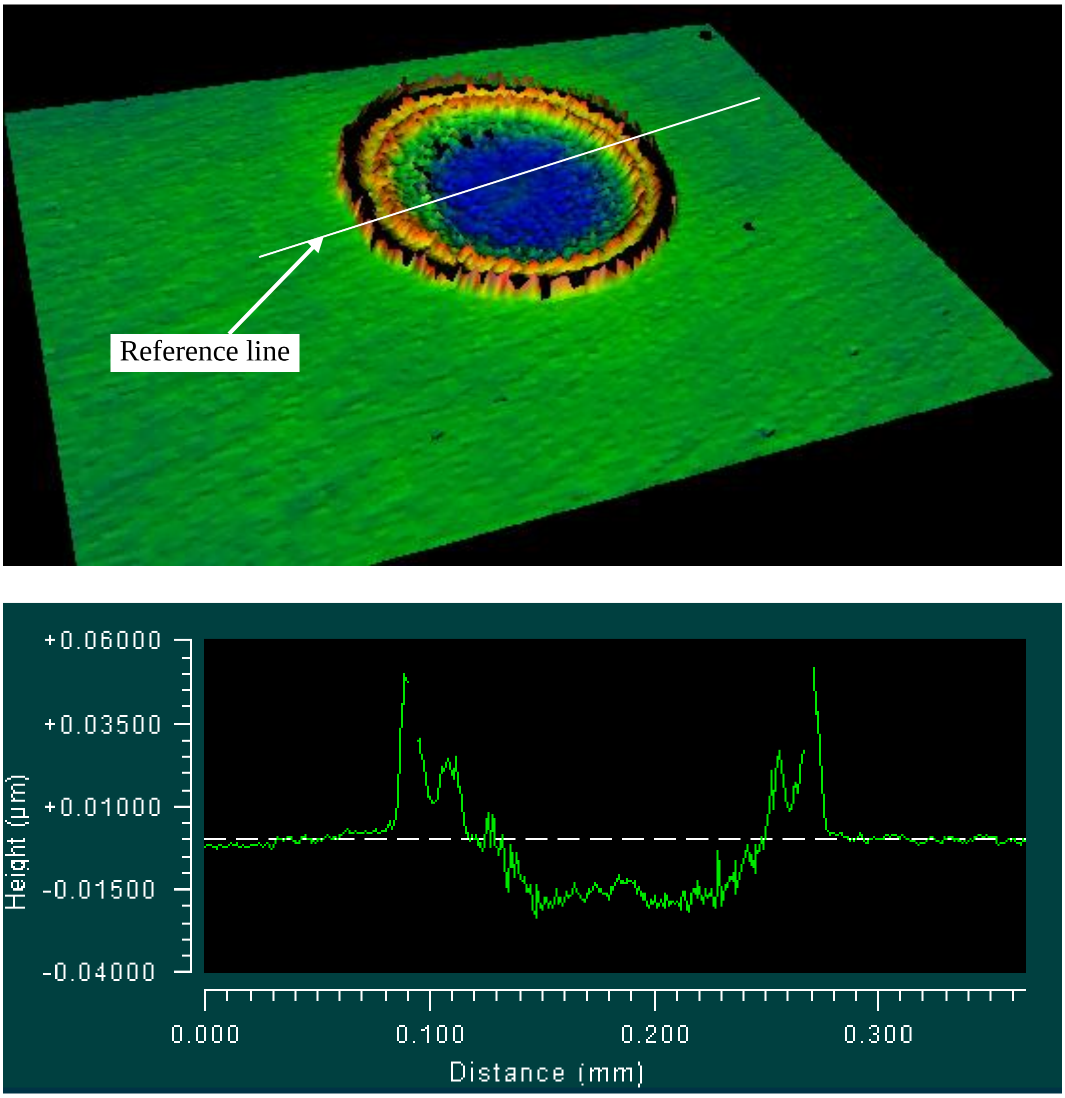

Figure 4.23 WLI measurements of the delamination type damage (corresponds to Figure 4.20.c) for NQWD1. 3-D appearance at the top view and depth measurement through a reference line at the bottom view.

Measurements show that there are two peak regions exist between concentric rings. The heights of the inner and outer peaks are ~25 nm and ~50 nm respectively. Horizontal distance between peaks are ~20 nm. The depths of the center regions are ~25 nm. It is conceived that due to sudden temperature rise and corresponding pressure rise at the coating layers especially at the 1st layer pair, some part of the H_1 layer (hafnia) is sublimated. This movement may produce these sharp peaks. As presented in the numerical part of the present study, the EFI peak is suppressed in the L_1 layer for the NQWD1. For this reason the peak temperature is damped inside the first L layer as shown in Figure 3.14.a. Even though both the QWD and NQWD1 damages have concave shape at the damage centers, the depths of NQWD1 damages are smaller. The possible reason of the depth difference is the reduced temperature rise by the increased L_1 layer thickness. The damping of temperature rise reduces the amount of sublimated hafnia at the damage centers for NQWD1.

4.3.1.3 1-on-1 Test Result Of The NQWD2

Damage probability result of NQWD2 is given in Figure 4.24.

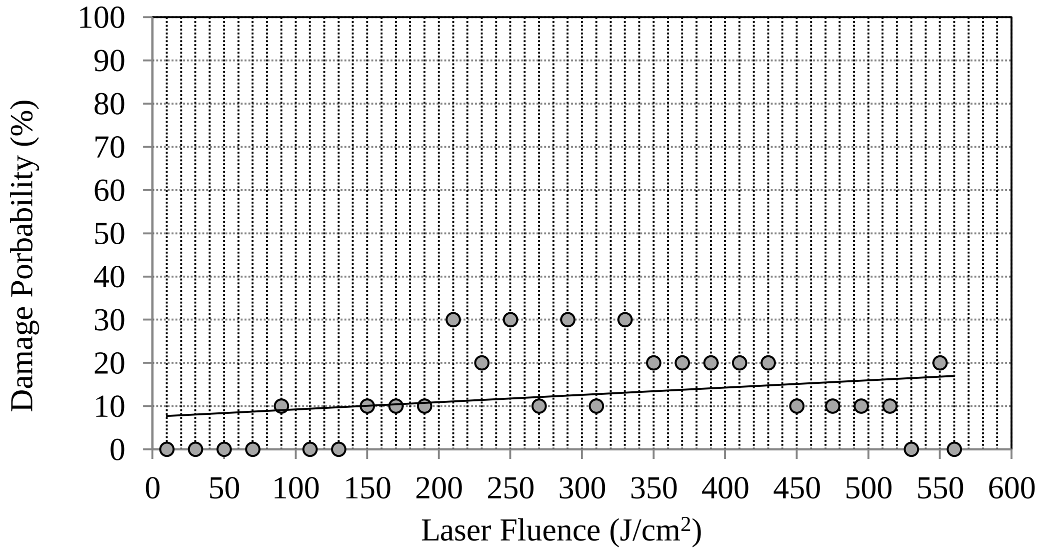

Figure 4.24 Percentage damage probability chart of the fabricated NQWD2

The lowest laser fluence is 150 J/cm^2 at which delamination type damage is seen (Figure 4.24). The damage contour is given in Figure 4.25. If one presumes, the threshold value is the lowest laser fluence level that causes a delamination type damage, NQWD2 has the highest threshold among all the designs.

Delamination type damages have also seen at higher fluence levels for NQWD2 like NQWD1, Figure 4.26. Another similarity is the disappeared fracture mark on the damages of NQWD2.

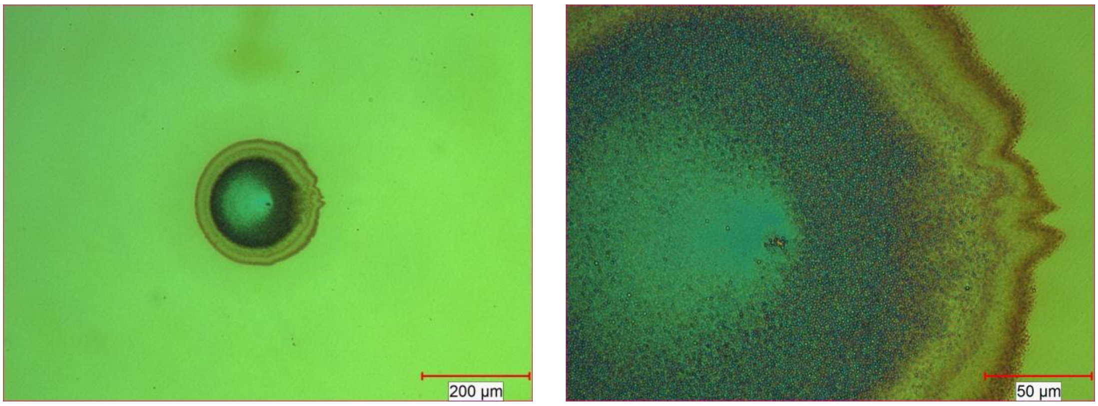

(a) (b)

Figure 4.25 Delamination type damage on NQWD2 surface at 150 J/cm^2 laser fluence; (a) 100x magnification, (b) 500x magnification.

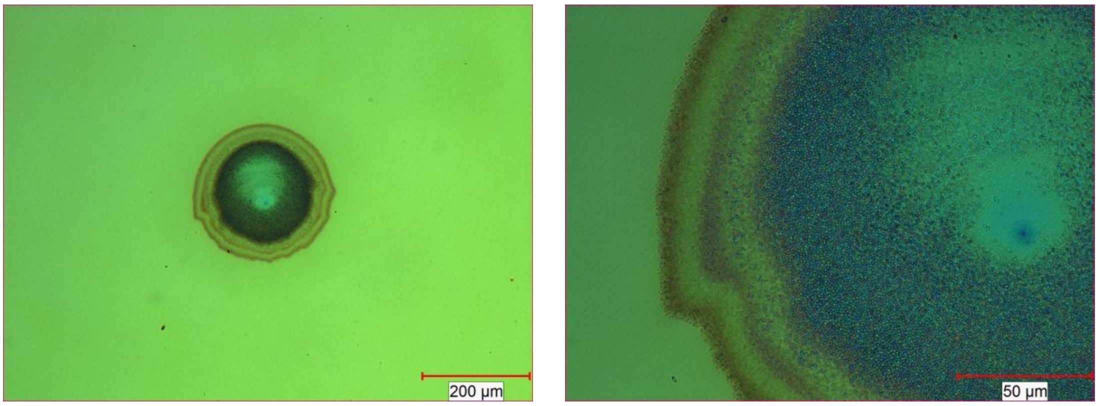

(a) (b)

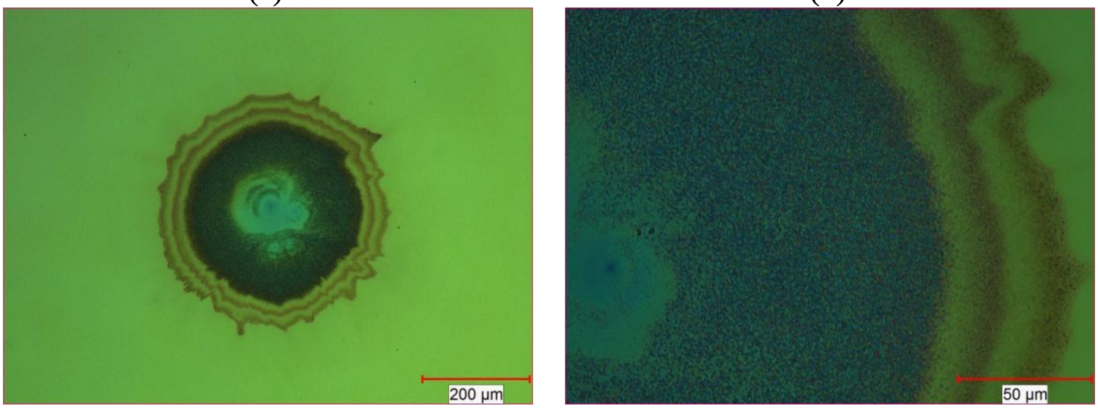

(c) (d)

Figure 4.26 Delamination type damage contours on NQWD2; (a) at 170 J/cm^2 laser fluence-100x magnification, (b) at 170 J/cm^2 laser fluence-500x magnification, (c) at 210 J/cm^2 laser fluence-100x magnification, (d) at 210 J/cm^2 laser fluence-500x magnification.

For the two of NQWD2 damages, WLI measurements are performed, Figure 4.27 and Figure 4.28.

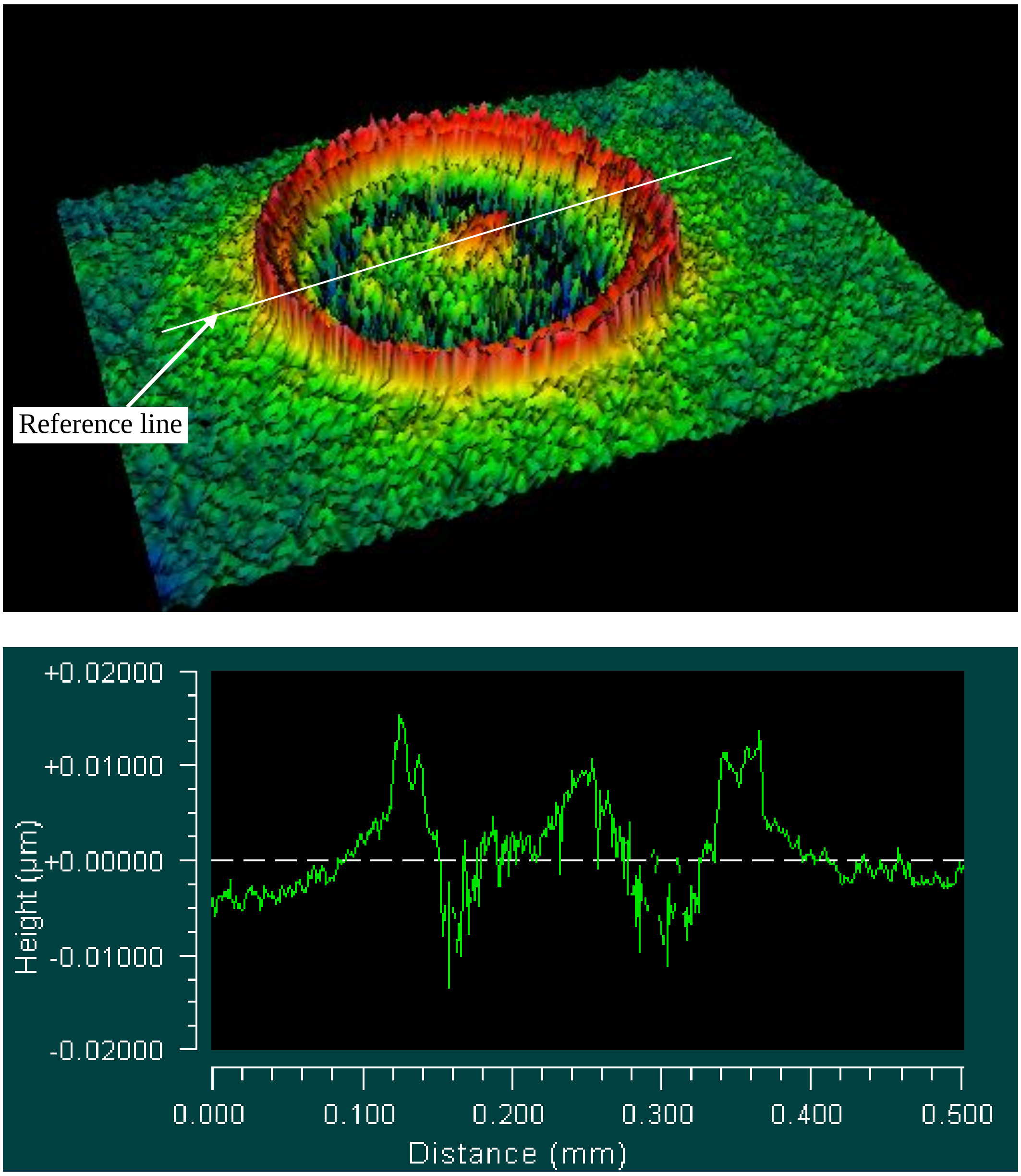

Figure 4.27 WLI measurements of the delamination type damage (corresponds to Figure 4.25) for NQWD2. 3-D appearance at the top view and depth measurement through a reference line at the bottom view.

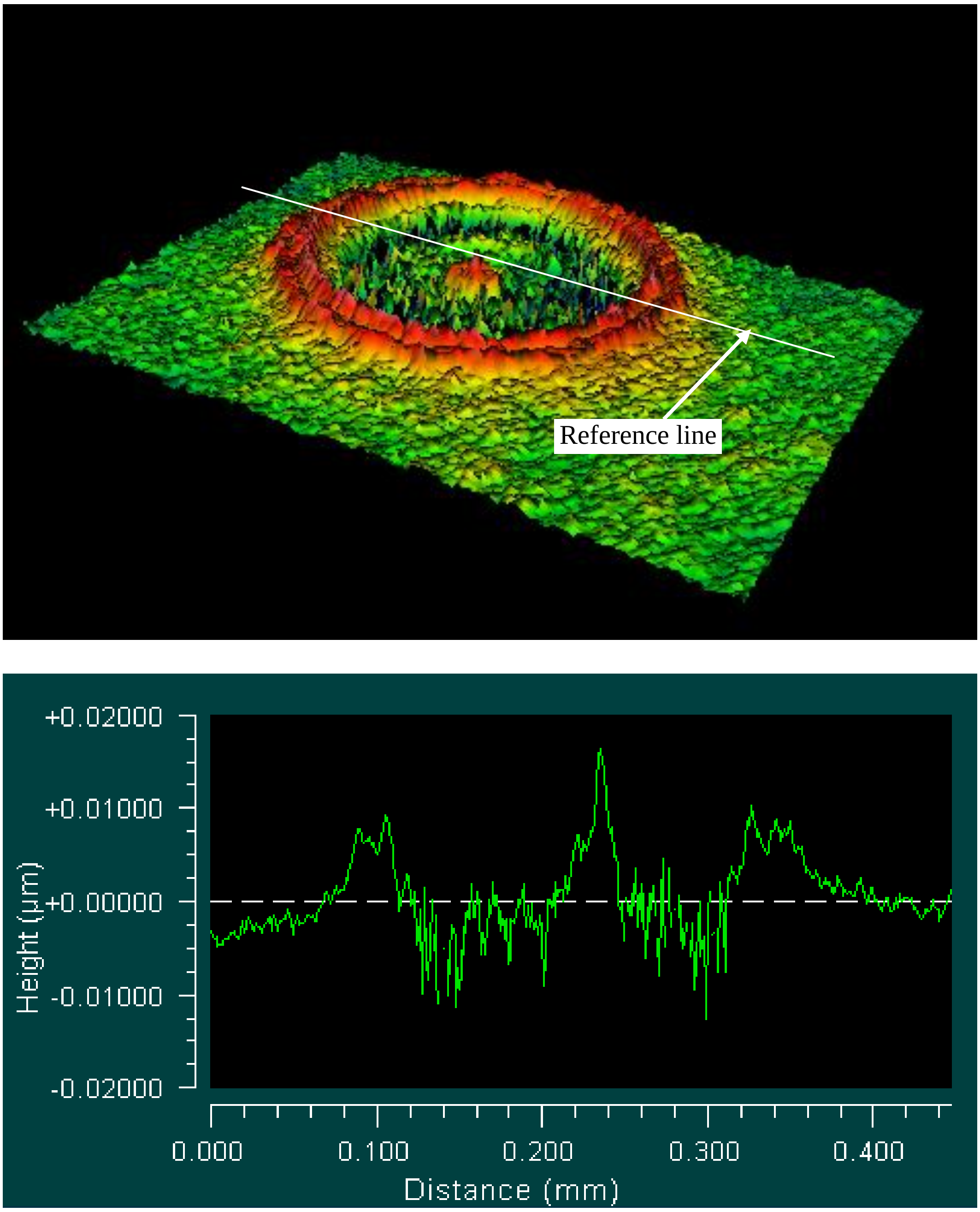

Figure 4.28 WLI measurements of the delamination type damage (corresponds to Figure 4.26.a) for NQWD2. 3-D appearance at the top view and depth measurement through a reference line at the bottom view.

Even though concentric ring like shapes are observed at WLI measurement similar to NQWD1 damages, there are convex shapes occurred at the center regions of NQWD2 damages. The heights of those convex shapes are about to 15 nm. It is known, the thicknesses of the L_1 and L_2 layers are increased as seen in Table 4.1 and it results shifting of the first and second EFI peaks from interfaces. Accordingly as presented in the numerical studies section (Figure 3.14.b) the temperature peaks of the first and the second layer pairs are shifted into the L_1 and L_2 layers. Therefore the suppressed temperature peaks, inside the low index layers, prevents the formation of the fracture mark as expected. Moreover damped temperature rise (particularly at the 1^{st} layer pair) is not strong enough to explode or sublimate any portion of the H_1 (hafnia) layer from the center region of the damages.

4.3.1.4 1-on-1 Test Result Of The NQWD5

Damage probability chart is given in Figure 4.29 for NQWD5. The lowest fluence is 90 J/cm^2 at which delamination type damage is detected, Figure 4.30. The following delamination damage is detected at 150 J/cm^2, Figure 4.31.

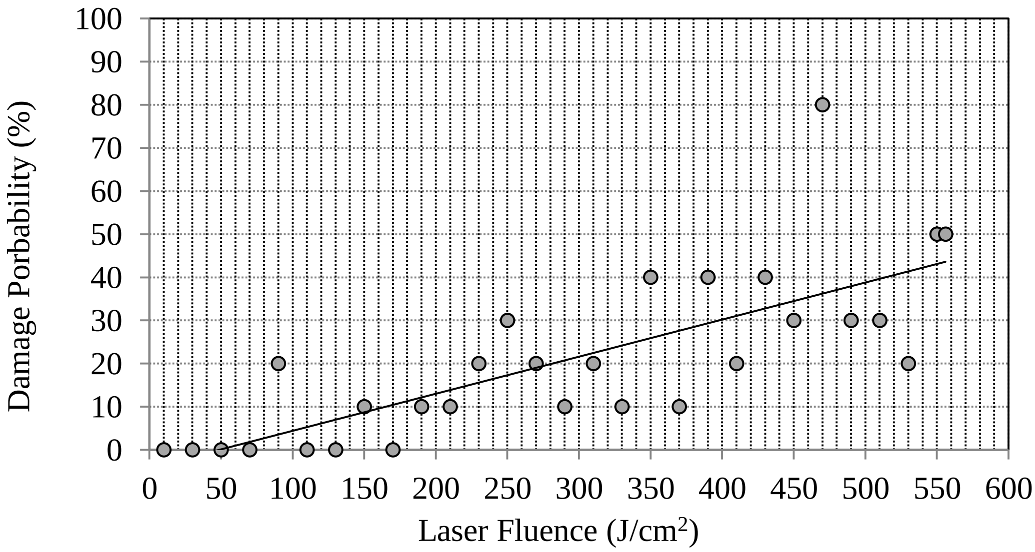

Figure 4.29 Percentage damage probability chart of the fabricated NQWD5.

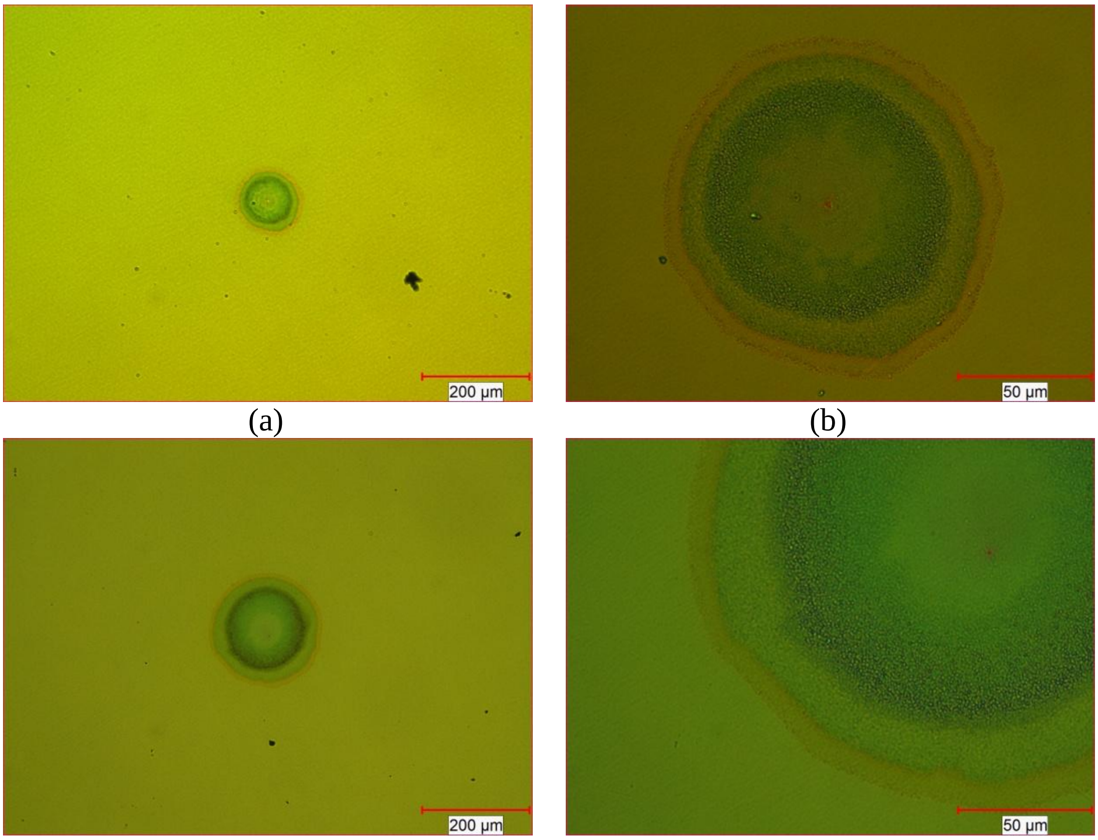

(a) (b) (c) (d)

Figure 4.30 Delamination type damage contours on NQWD5 at 90 J/cm^2 laser fluence; (a) 1st damage-100x magnification, (b) 1st damage- 500x magnification, (c) 2nd damage-100x magnification, (d) 2nd damage- 500x magnification.

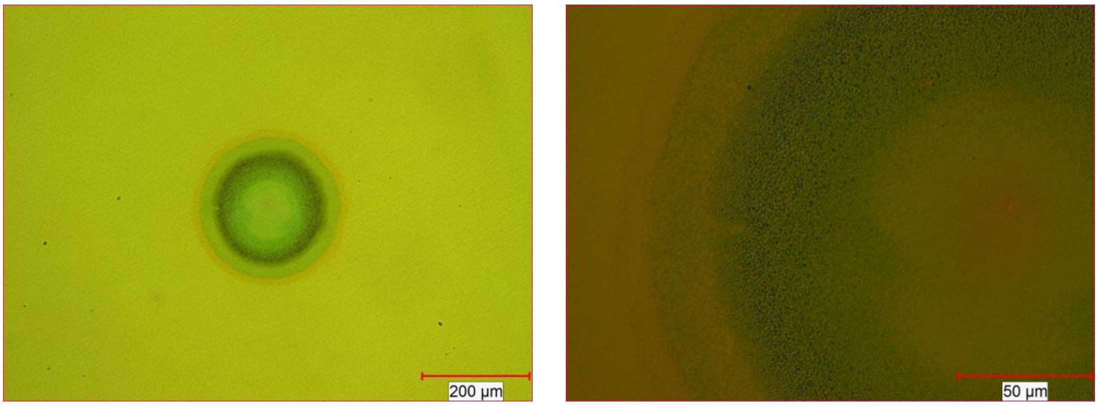

(a) (b)

Figure 4.31 Delamination type damage on NQWD5 at 150 J/cm^2 laser fluence; (a) 100x magnification, (b) 500x magnification.

As seen in Figure 4.30 and Figure 4.31 damages have faded appearance compared to damages seen on NQWD1 and NQWD2 surfaces. As stated in the numerical studies section, the first five layer pairs are modified for NQWD5 and local reflectivity is decreased at that layers. Hence, the possible reason of this obscurity is the reduced reflectivity (or in other words the increased transmissivity) at the modified layers.

Flat bottom pit type damage contour is also detected at 230 J/cm^2 laser fluence on NQWD5 surface, Figure 4.32. A nanoabsorbing center at the interface may be responsible for such kind of damage.

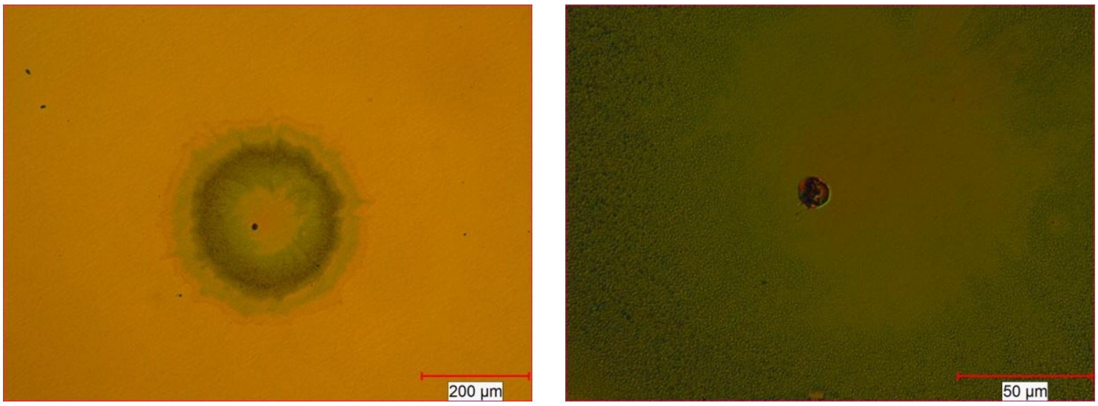

(a) (b)

Figure 4.32 Flat bottom pit type damage on NQWD5 at 230 J/cm^2 laser fluence; (a) 100x magnification, (b) 500x magnification.

WLI measurements are also performed for the damages on NQWD5, Figure 4.33 and Figure 4.34. During the WLI process, measurements are hardly obtained compared to prior measurements. The reason of that measurement difficulty is conducted to increased internal reflections due to employment of non-quarter wave layers at the first five layer pairs.

Center regions of the NQWD5 damages are convex similar to NQWD2. However, the heights of these peaks are advanced for NQWD5. As noted in the numerical studies section (Figure 3.15), the EFI peak magnitude and the amount of laser absorption (particularly in L_1 layer) is increased for the NQWD5 top layers compared to NQWD1 and NQWD2. It is thought that the increased absorption and the corresponding temperature rise cause the higher convex peaks at that centers at the end of the tests.

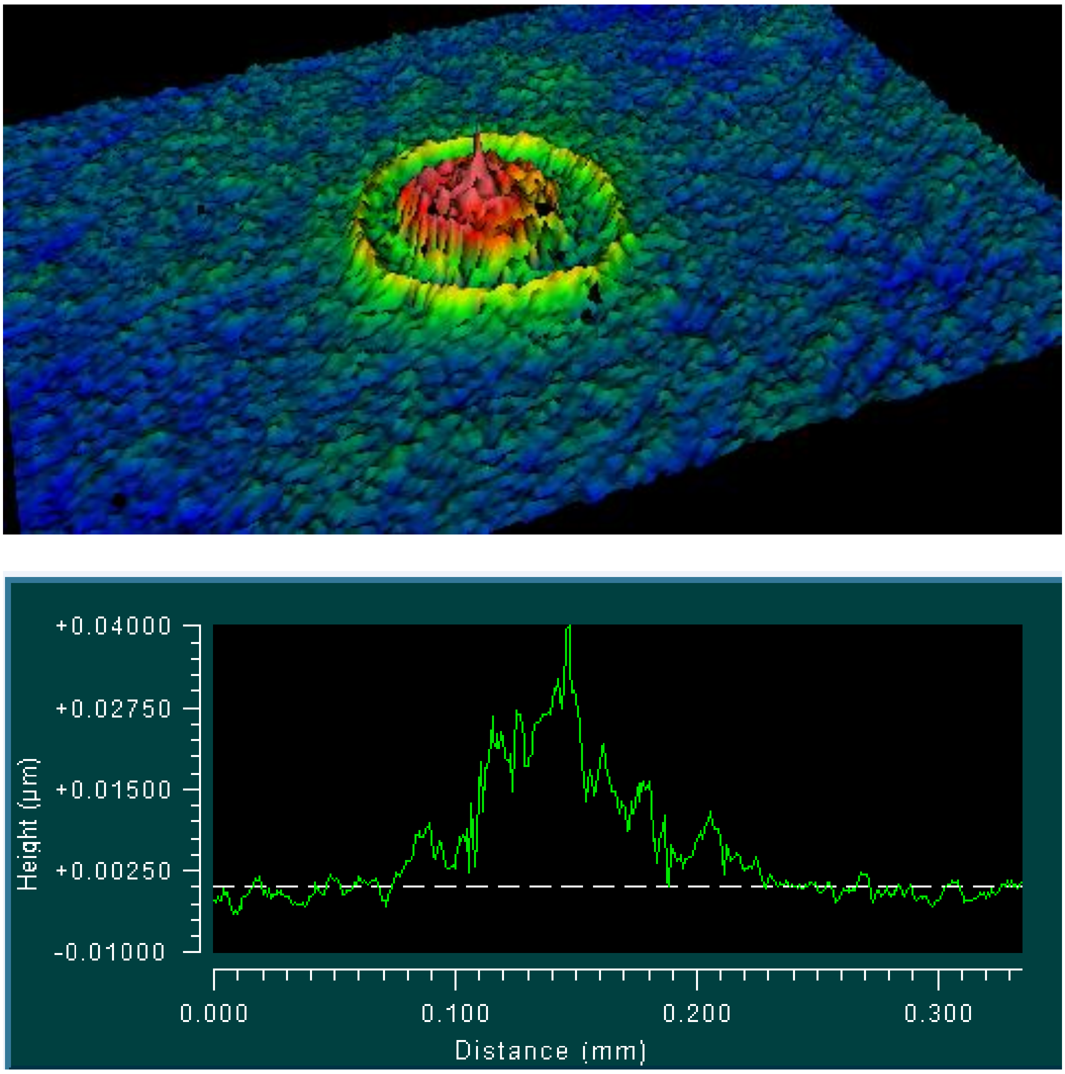

Figure 4.33 WLI measurements of the delamination type damage (corresponds to Figure 4.30.a) for NQWD5. 3-D appearance at the top view and depth measurement through a reference line at the bottom view.

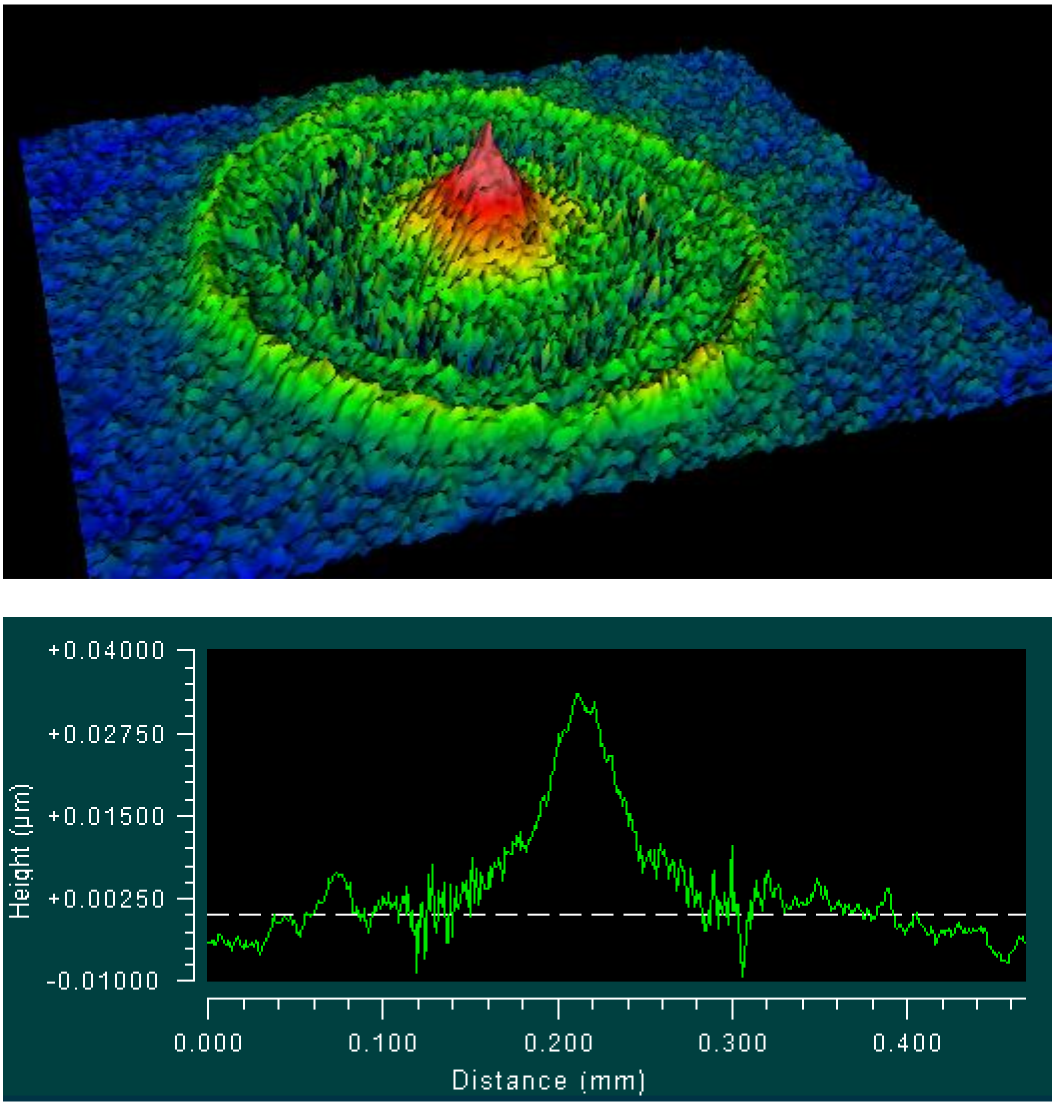

Figure 4.34 WLI measurements of the delamination type damage (corresponds to Figure 4.30.c) for NQWD5. 3-D appearance at the top view and depth measurement through a reference line at the bottom view.

4.3.1.5 1-on-1 Test Result Of The NQWD1-M

Damage probability chart of NQWD1-M is given in Figure 4.35.

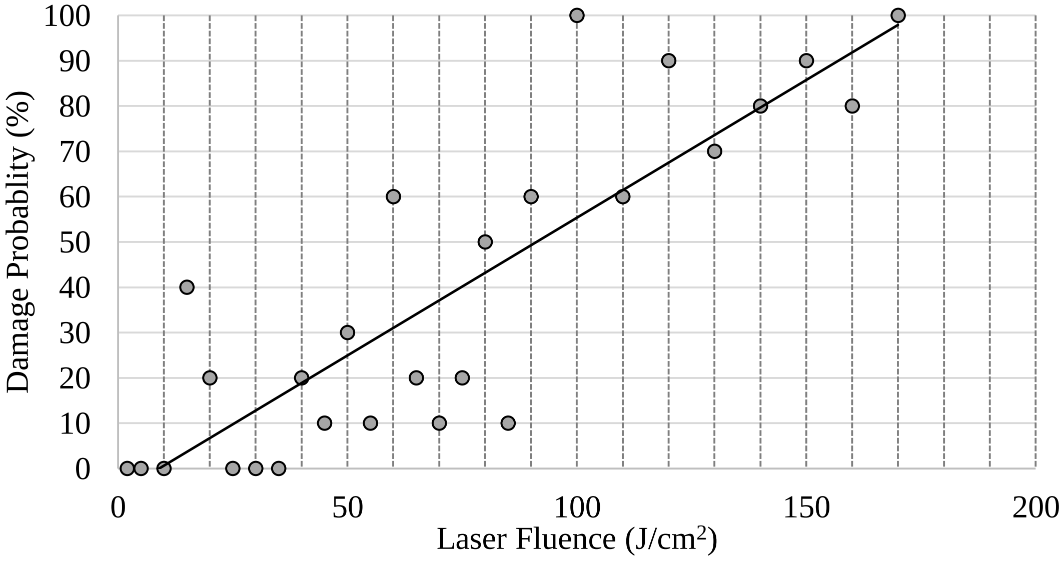

Figure 4.35 Percentage damage probability chart of the fabricated NQWD1-M

The lowest fluence level is 50 J/cm^2 at which delamination type damage is seen, Figure 4.36. Concentric rings can be perceived in the damage (Figure 4.36) similar to damages of prior NQWDs.

(a)

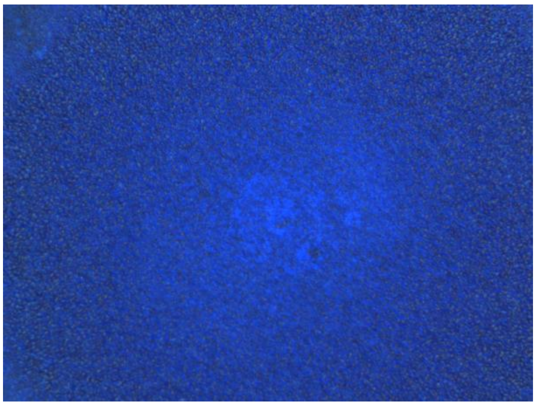

(b)

Figure 4.36 Delamination type damage contours on NQWD1-M at 50 J/cm^2 laser fluence; (a) 100x magnification, (b) 500x magnification.

Considering the lowest laser fluence value, one can say that NQWD1-M laser resistance is higher than the base design (QWD). As noted in the chapter 3.3.1 modification of the first H and L layers enable the suppression of the first EFI peak.

Hence, no fracture marks is observed on the NQWD1-M damages similar to NQWD1 damages. Delamination type damages have seen at higher fluence levels for NQWD1-M as well, Figure 4.37. The concentric ring like shapes are also seen in these damaged regions.

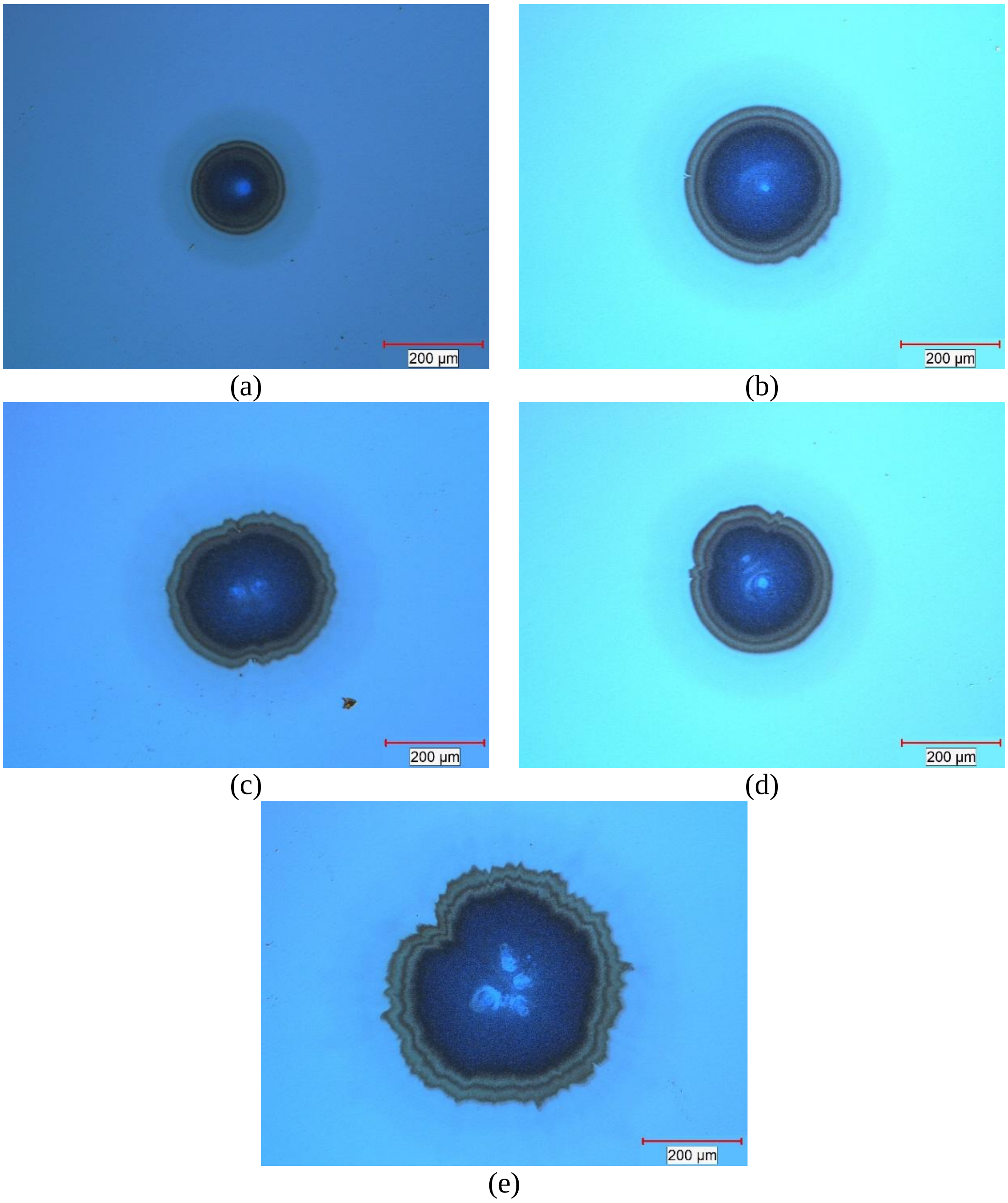

Figure 4.37 Delamination type damage contours on NQWD1-M surface (100x magnification); (a) at 60 J/cm^2 laser fluence, (b) at 65 J/cm^2 laser fluence, (c) at 80 J/cm^2 laser fluence, (d) at 85 J/cm^2 laser fluence, (e) at 90 J/cm^2 laser fluence.

WLI measurements also repeated for NQWD1-M damages. Results are given in Figure 4.38-Figure 4.39.

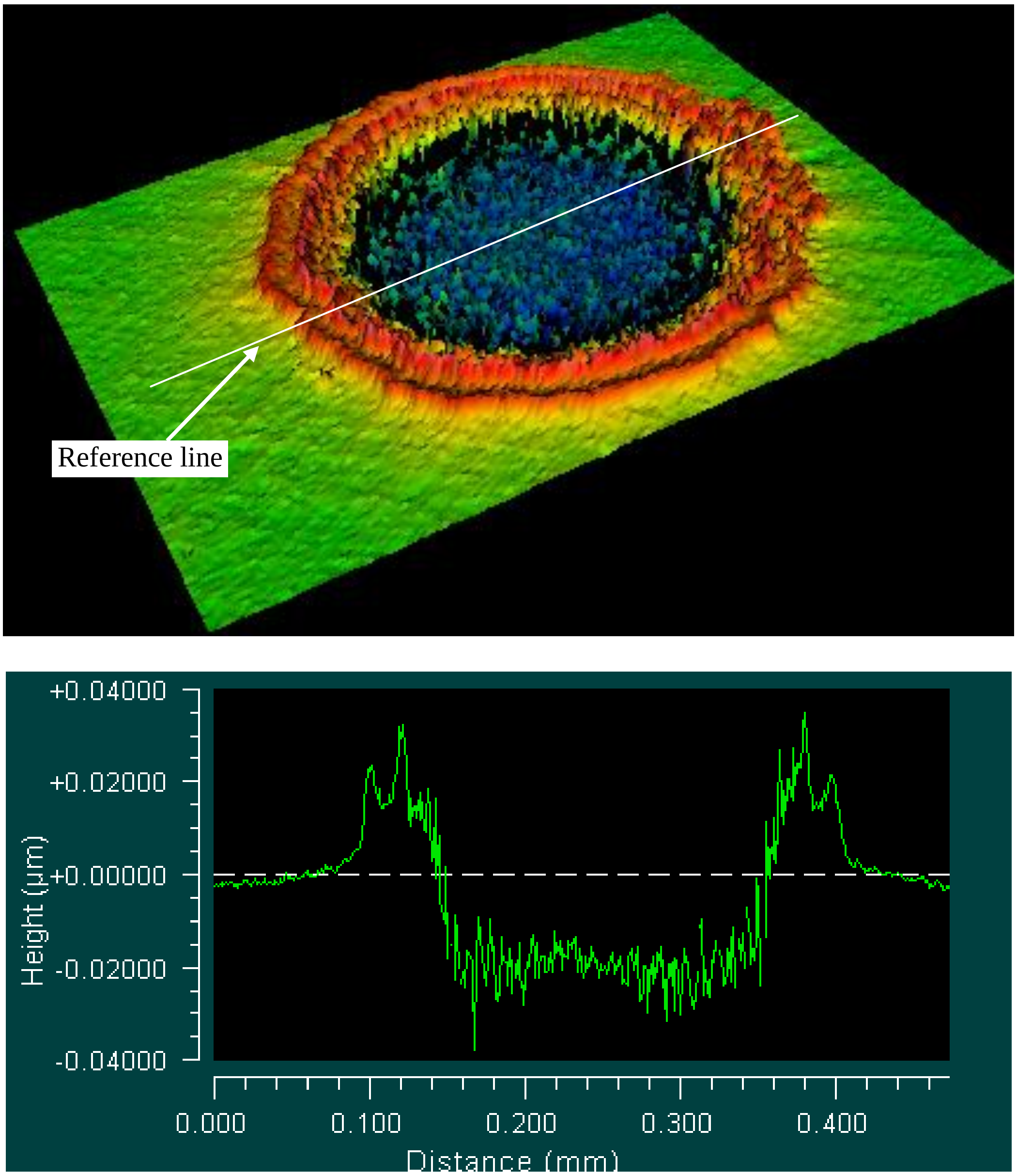

Figure 4.38 WLI measurements of the delamination type damage (corresponds to Figure 4.36) for NQWD1-M. 3-D appearance at the top view and depth measurement through a reference line at the bottom view.

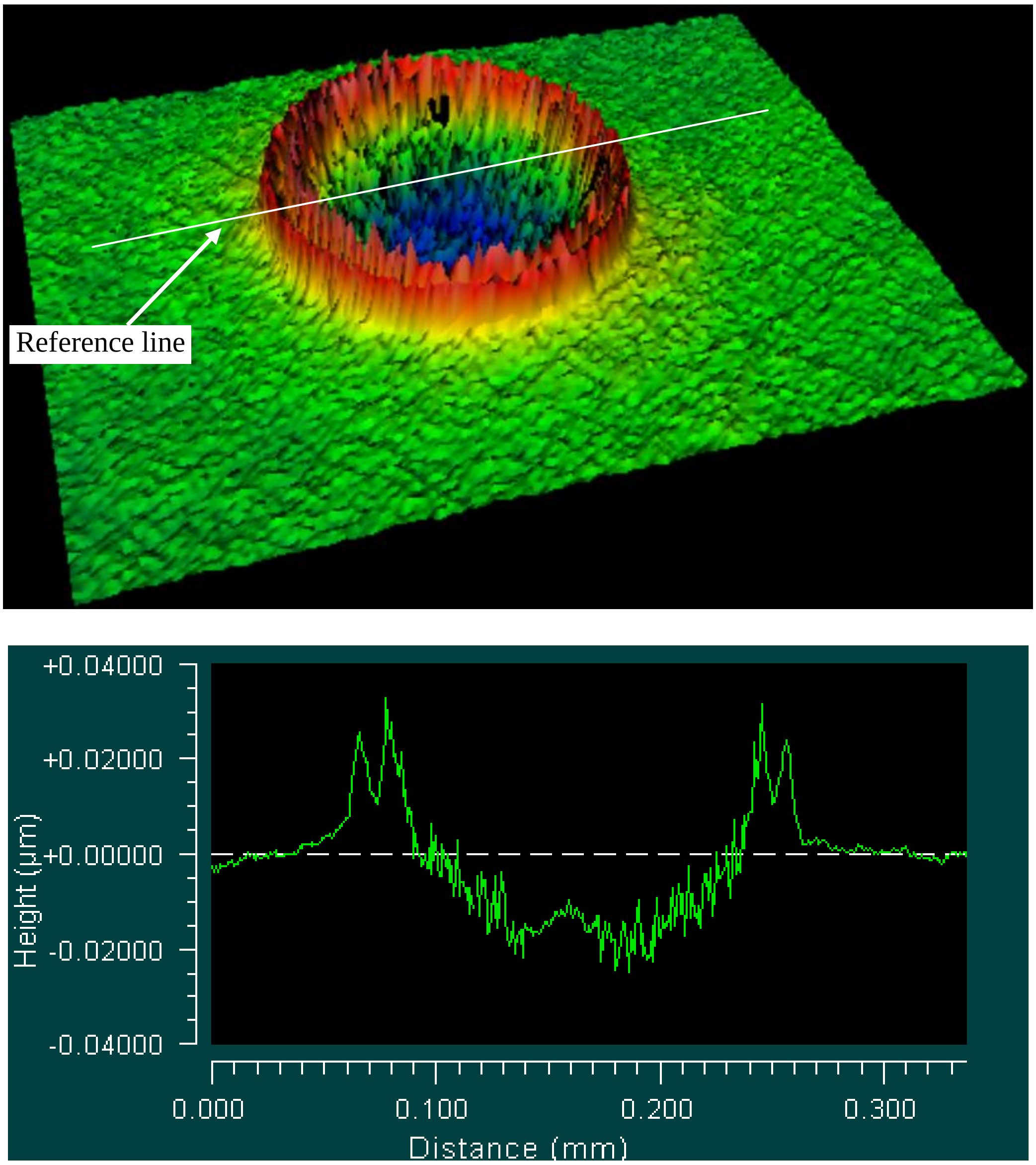

Figure 4.39 WLI measurements of the delamination type damage (corresponds to Figure 4.37.a) for NQWD1-M. 3-D appearance at the top view and depth measurement through a reference line at the bottom view.

WLI measurements show that the center regions are concave for NQWD1-M damages. The depths of concave regions are about to 20 nm. As presented before, similar concave regions were also measured for NQWD1 damages. Similar to NQWD1, 1st layer pair thicknesses are modified for NQWD1-M and it damps the temperature rise inside the L_1 layer as revealed in numerical simulations. Due to this effect, amount of exploded or sublimated hafnia from the damage center is decreased.

4.3.1.6 1-on-1 Test Result Of The NQWD2-M

Damage probability chart is given in Figure 4.40 for NQWD2-M.

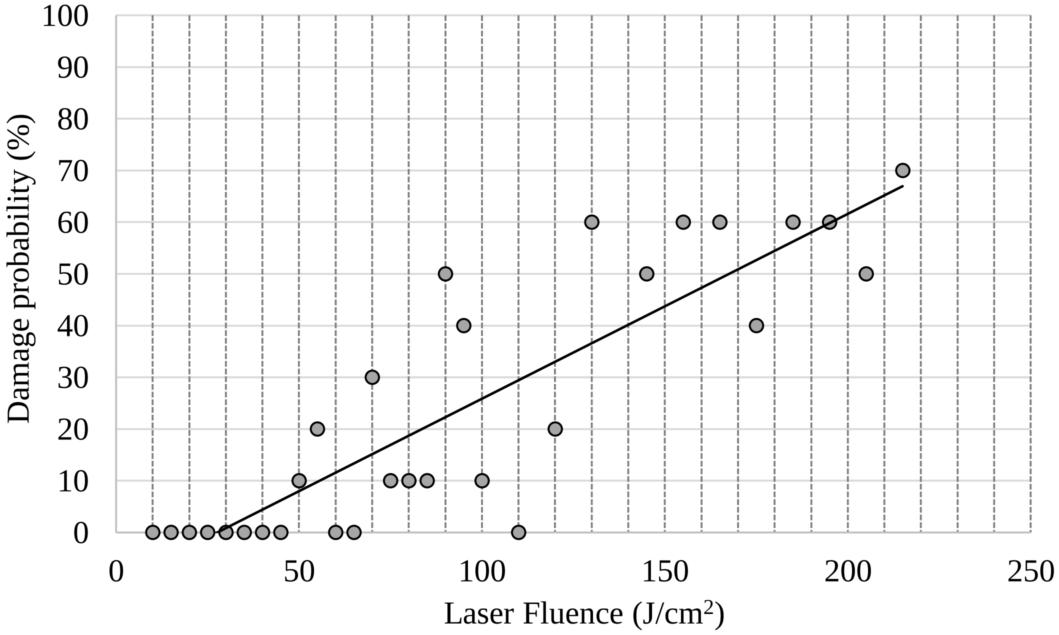

Figure 4.40 Percentage damage probability chart of the fabricated NQWD2-M

The lowest fluence is 50 J/cm^2 at which delamination type damage is detected, Figure 4.41. Delamination type damages have also seen for higher laser fluence levels, Figure 4.42.

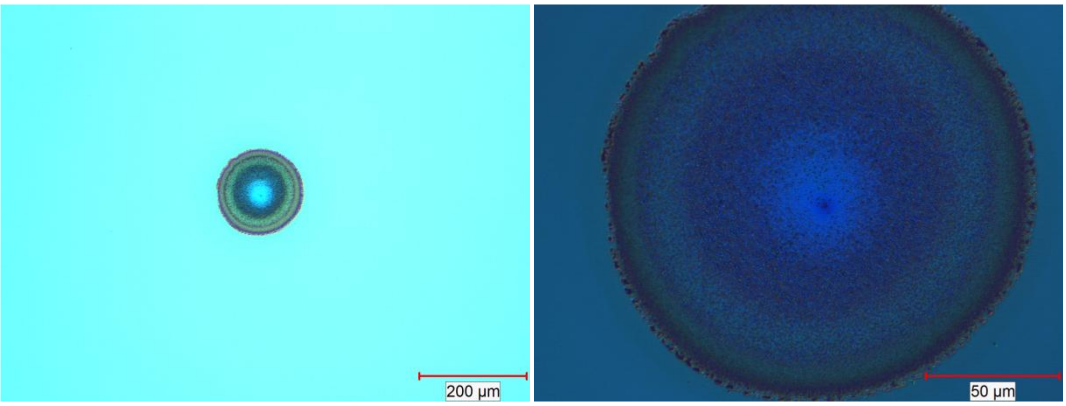

(a) (b)

Figure 4.41 Delamination type damage contours on NQWD2-M at 50 J/cm^2 laser fluence; (a) 100x magnification, (b) 500x magnification.

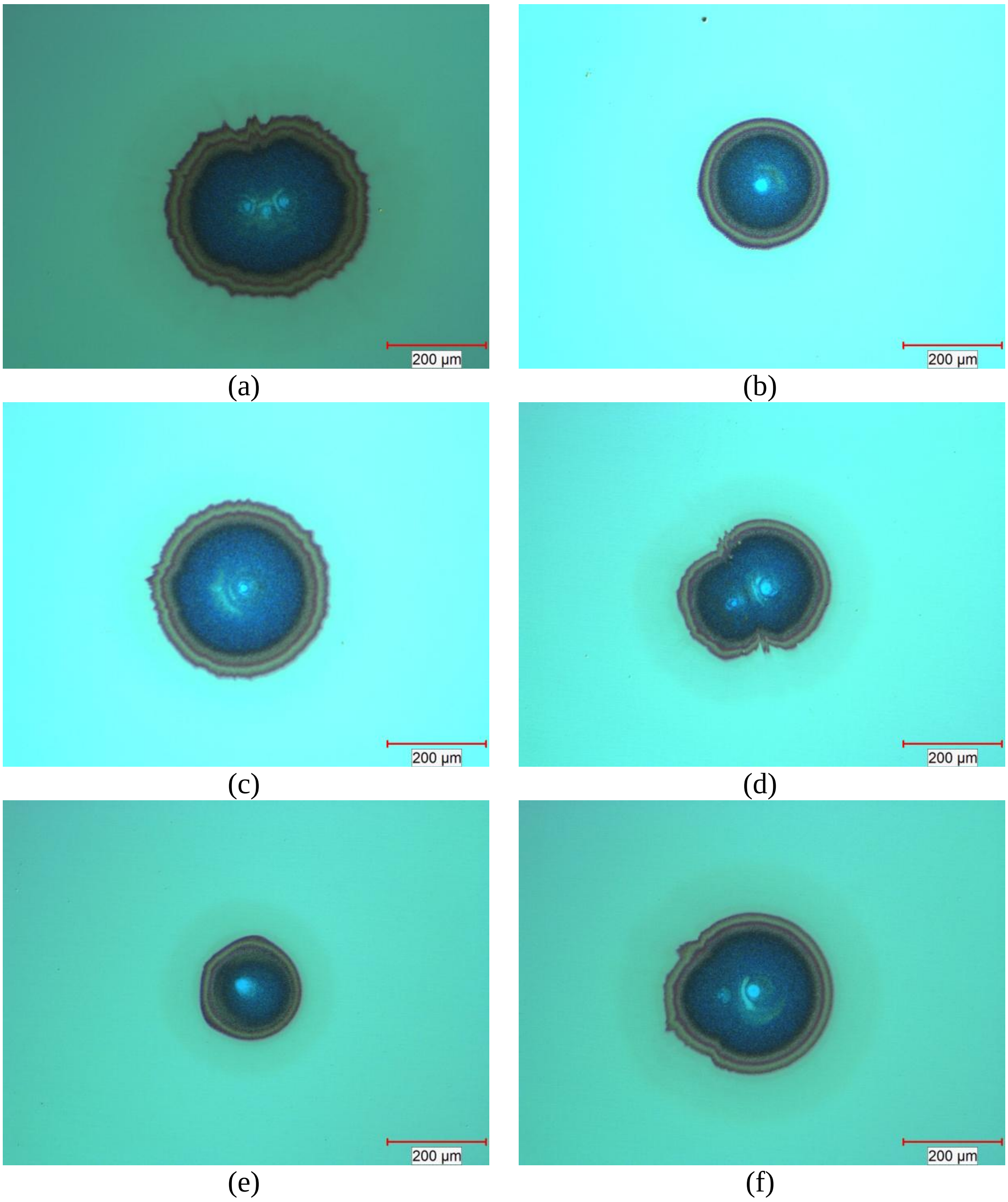

Figure 4.42 Delamination type damage contours on NQWD2-M at 100x magnification; (a) at 75 J/cm^{2}laser fluence level, (b) at 80 J/cm^{2}laser fluence level, (c) at 85 J/cm^{2}laser fluence level, (d) at 95 J/cm^{2}laser fluence level, (e) at 120 J/cm^{2}laser fluence level, (f) at 130 J/cm^{2}laser fluence level.

WLI measurements are also performed for the NQWD2-M damages. Results are given in Figure 4.43-Figure 4.44.

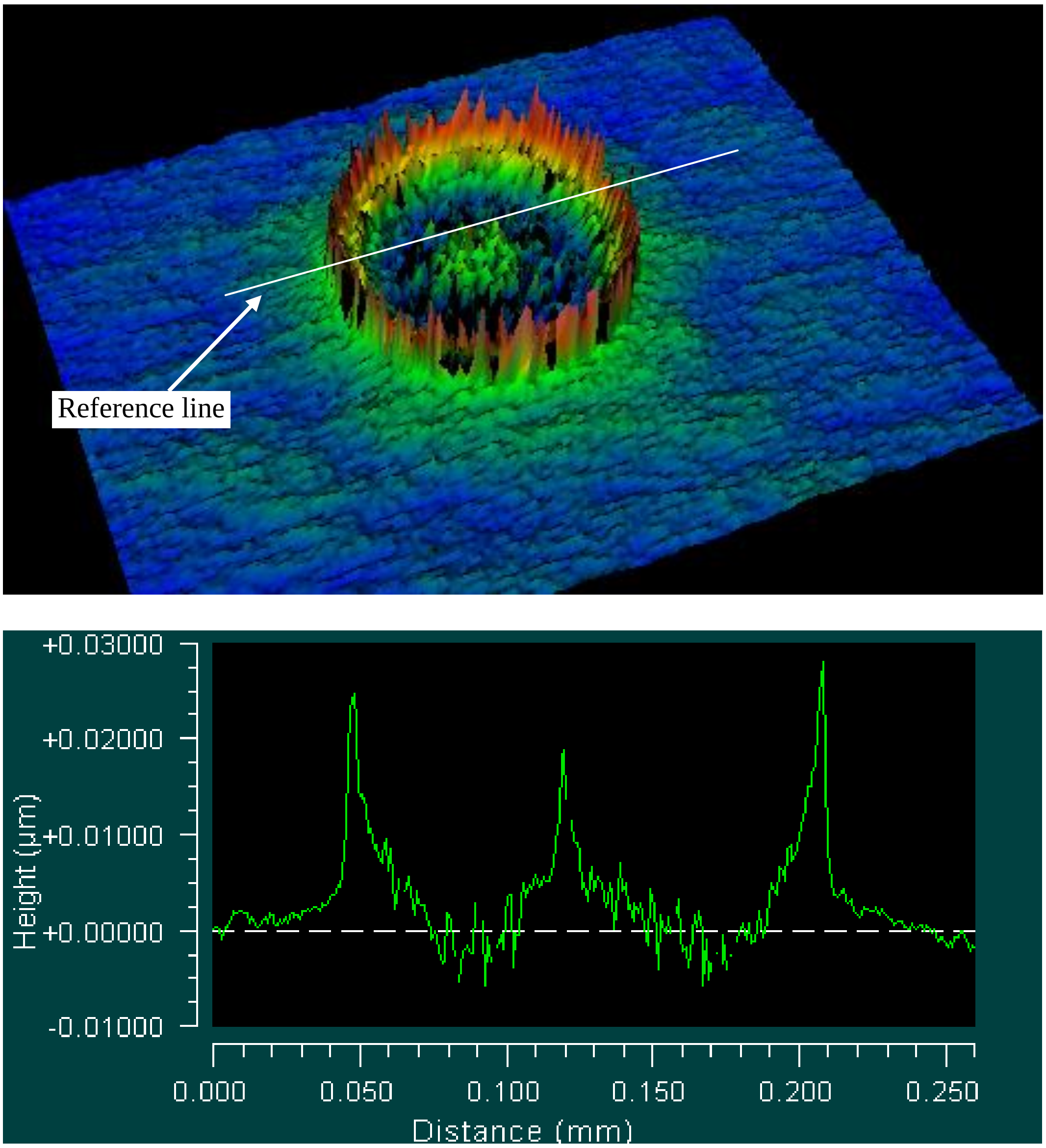

Figure 4.43 WLI measurements of the delamination type damage (corresponds to Figure 4.41) for NQWD2-M. 3-D appearance at the top view and depth measurement through a reference line at the bottom view.

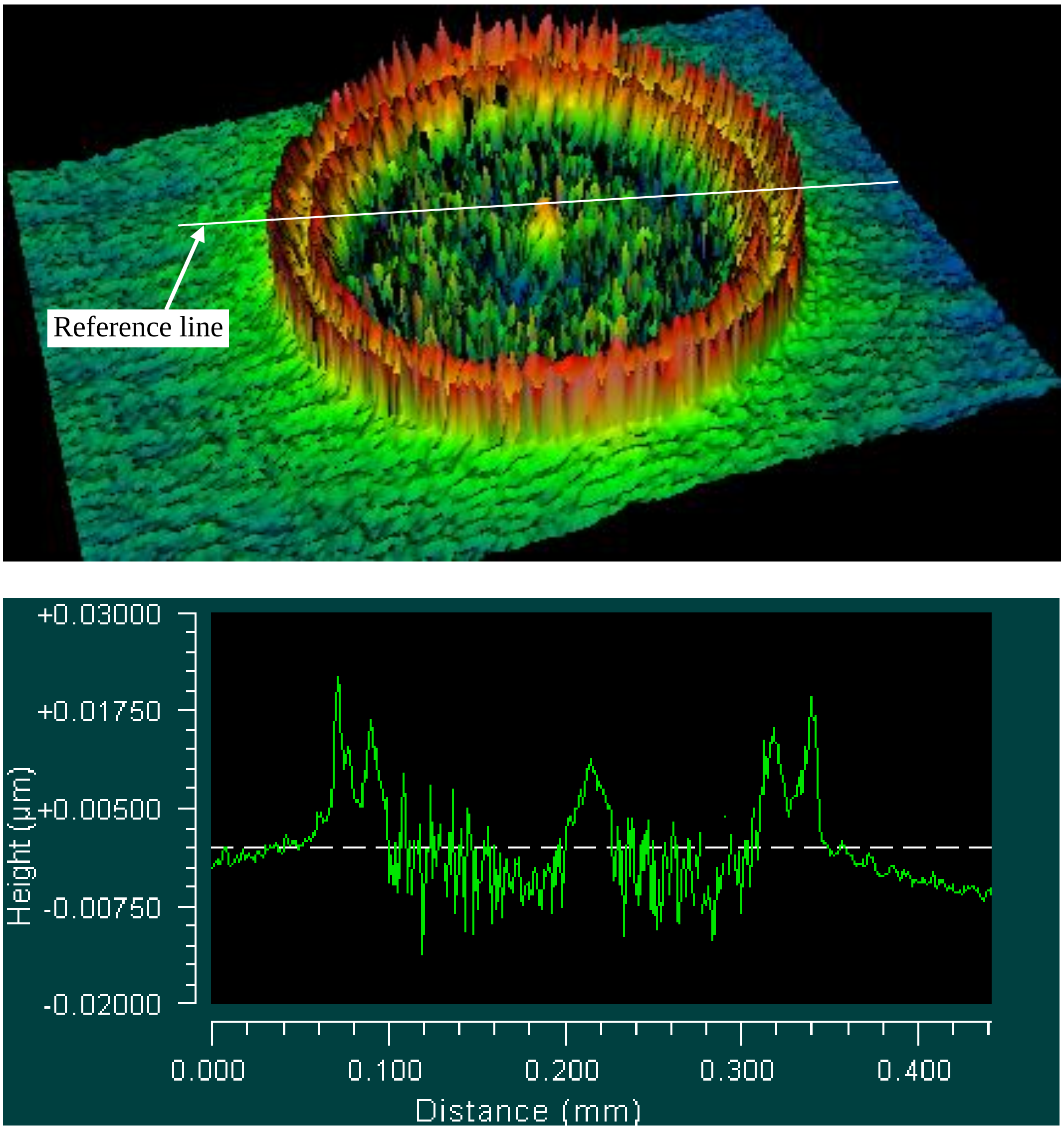

Figure 4.44 WLI measurements of the delamination type damage (corresponds to Figure 4.42.b) for NQWD2-M. 3-D appearance at the top view and depth measurement through a reference line at the bottom view.

WLI measurements reveal that the damage contours of NQWD2-M and NQWD2 have similarities. The center regions of the damages are convex for both of the designs. The peak heights of the convex damage centers are about to 17 nm and 12 nm in Figure 4.43-Figure 4.44. Similar peak heights also measured for NQWD2 damages. As explained for NQWD2, increased thicknesses of L_1 and L_2 layers damped the sudden temperature rise which is also commented in numerical studies chapter. Accordingly, the damped temperature rise is not strong enough to explode or sublimate any portion of H_1 layer.

4.3.1.7 1-on-1 Test Result Of The NQWD5-M

Damage probability chart is given for NQWD5-M in Figure 4.45.

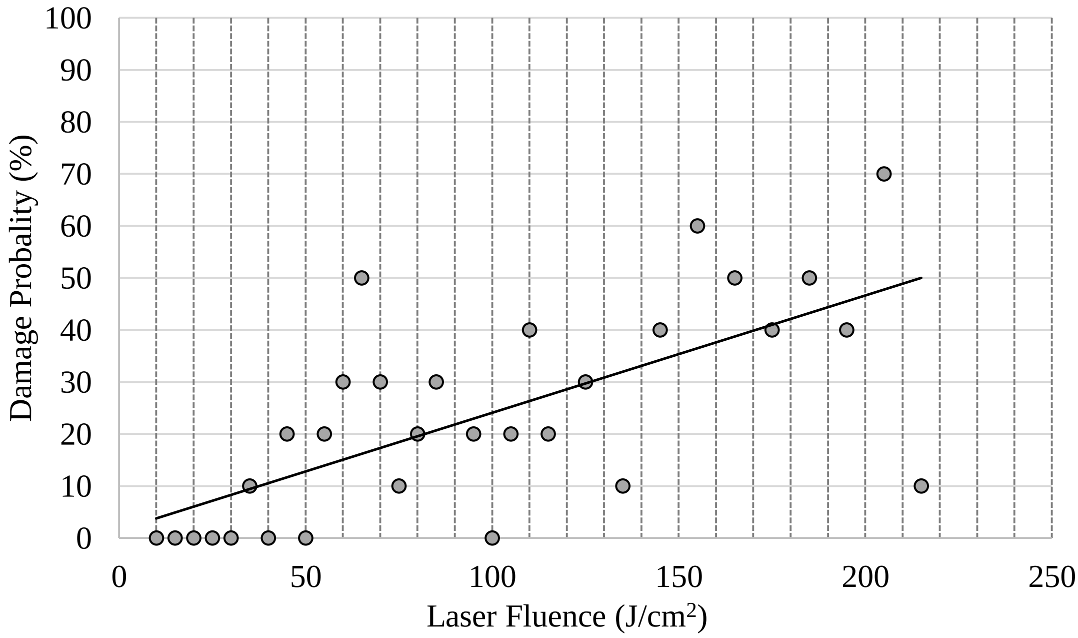

Figure 4.45 Percentage damage probability chart of the fabricated NQWD5-M

The lowest laser fluence level is 45 J/cm^2 at which delamination type damage is seen for NQWD5-M.

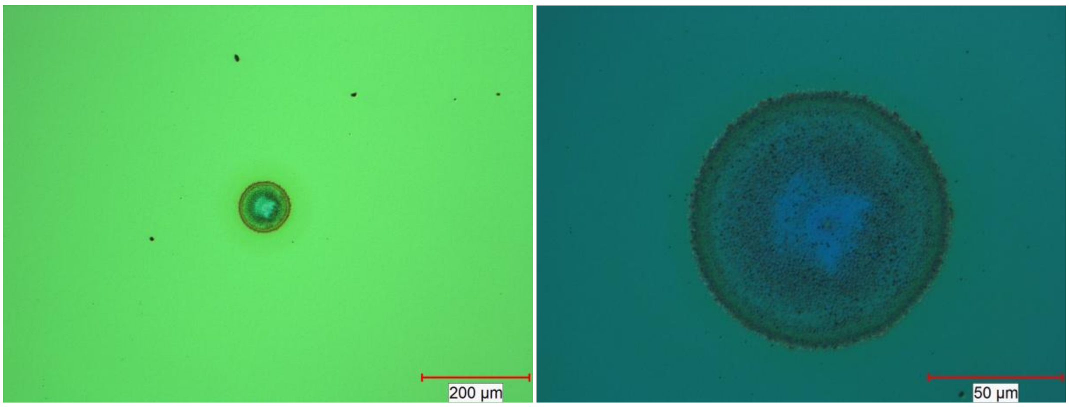

(a) (b)

Figure 4.46 Delamination type damage contours on NQWD5-M at 45 J/cm^2 laser fluence; (a) 100x magnification, (b) 500x magnification.

Similar damages are also seen at higher laser fluence levels as seen in Figure 4.47.

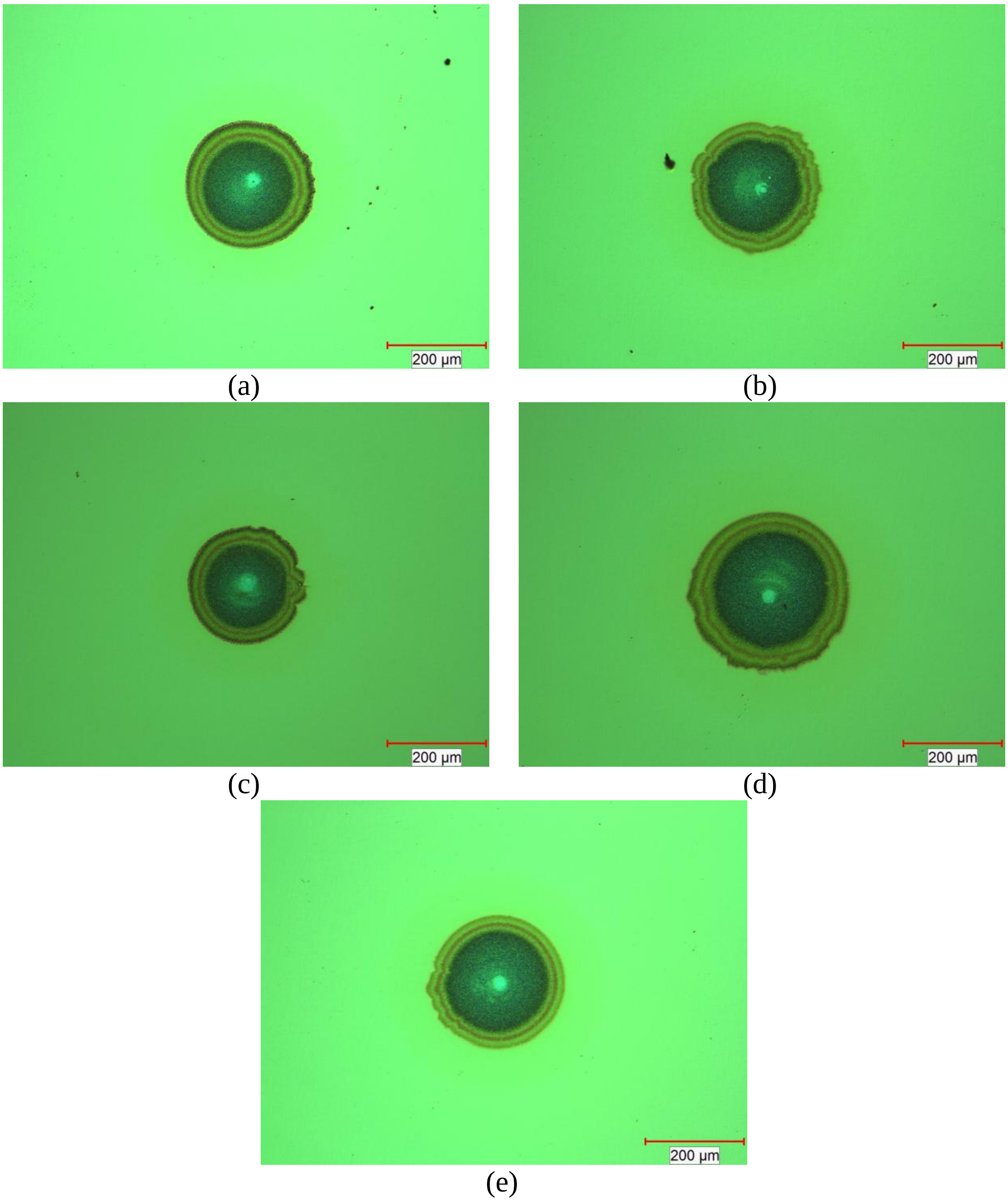

Figure 4.47 Delamination type damage contours on NQWD5-M at 100x magnification; (a) at 65 J/cm^{2}laser fluence level, (b) at 70 J/cm^{2}laser fluence level, (c) at 75 J/cm^{2}laser fluence level, (d) at 80 J/cm^{2}laser fluence level, (e) at 110 J/cm^{2}laser fluence level.

Flat bottom pit type damage is also seen at 55 J/cm^2 laser fluence level as given in Figure 4.48.

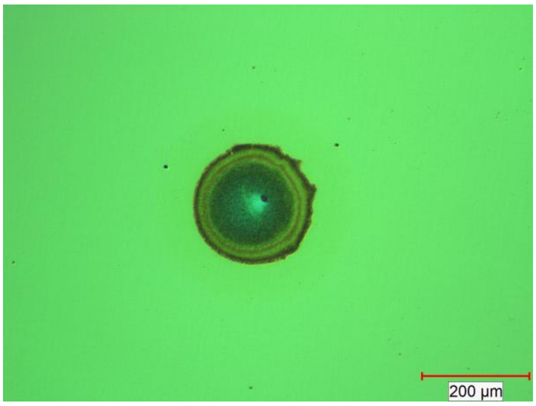

(a)

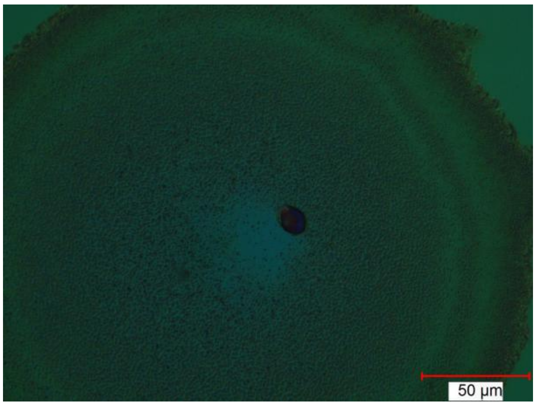

(b)

Figure 4.48 Flat bottom pit type damage on NQWD5-M at 55 J/cm^2 laser fluence; (a) 100x magnification, (b) 500x magnification.

WLI measurements are performed for NQWD5-M damages but unfortunately no reliable data is obtained. The possible reason of this trouble is conducted to the decreased local reflectivity at the modified layers. The internal reflections may affect the depth measurement of damage craters with the WLI system. Therefore the Nomarski images can only be used for the evaluation of NQWD5-M. Considering Nomarski images, it is thought that the EFI suppression at first five layer pair acts the laser resistance of the coating. Considering the lowest laser fluence level (in which delamintaion type damage is seen), the laser resistance of the NQWD5-M is increased compared to QWD.

4.3.1.8 1-on-1 Test Result Of The Designs With OC Layers

Damage probability charts are given in Figure 4.49, Figure 4.50 and Figure 4.51 for QWD-OC, NQWD1-OC and NQWD1-M-OC, respectively.

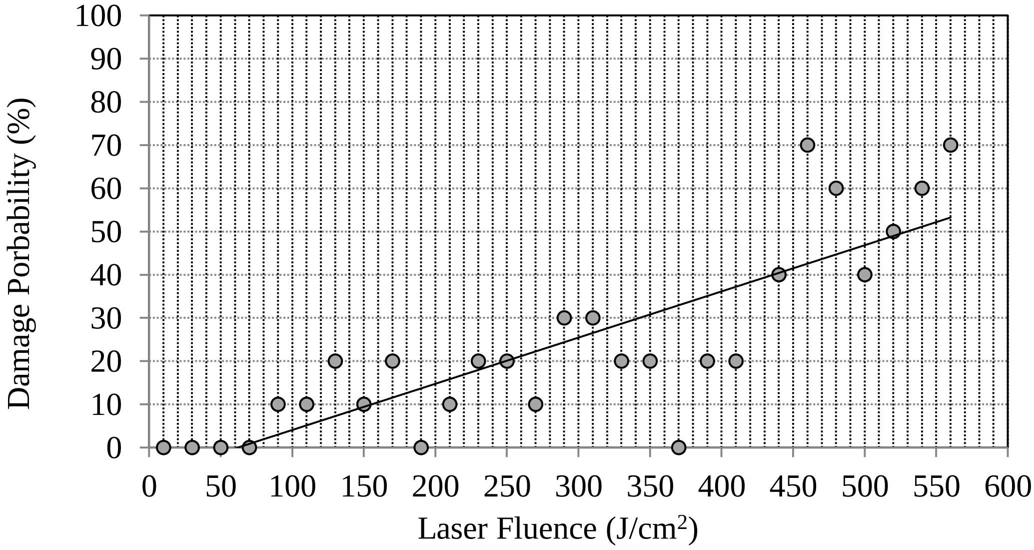

Figure 4.49 Percentage damage probability chart of the fabricated QWD-OC

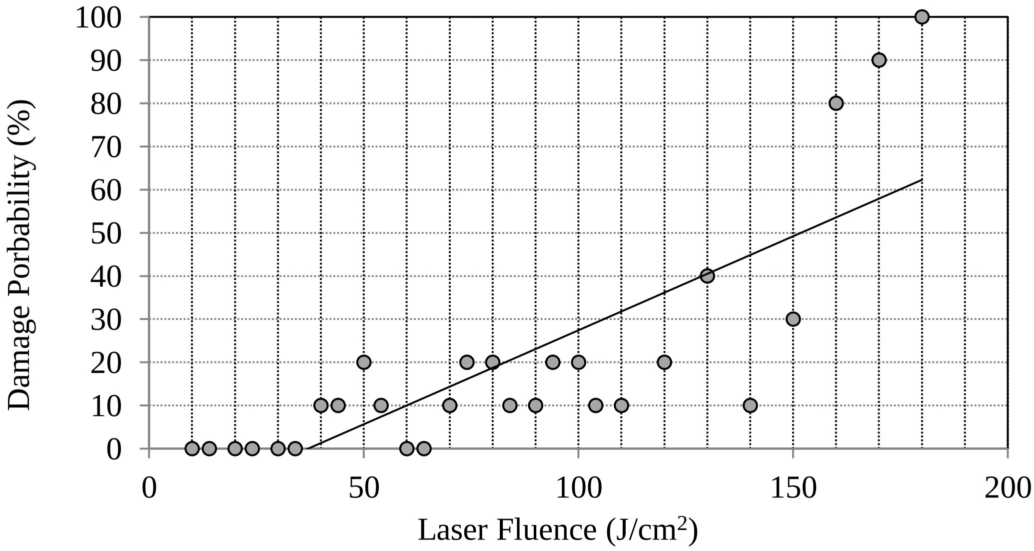

Figure 4.50 Percentage damage probability chart of the fabricated NQWD1-OC

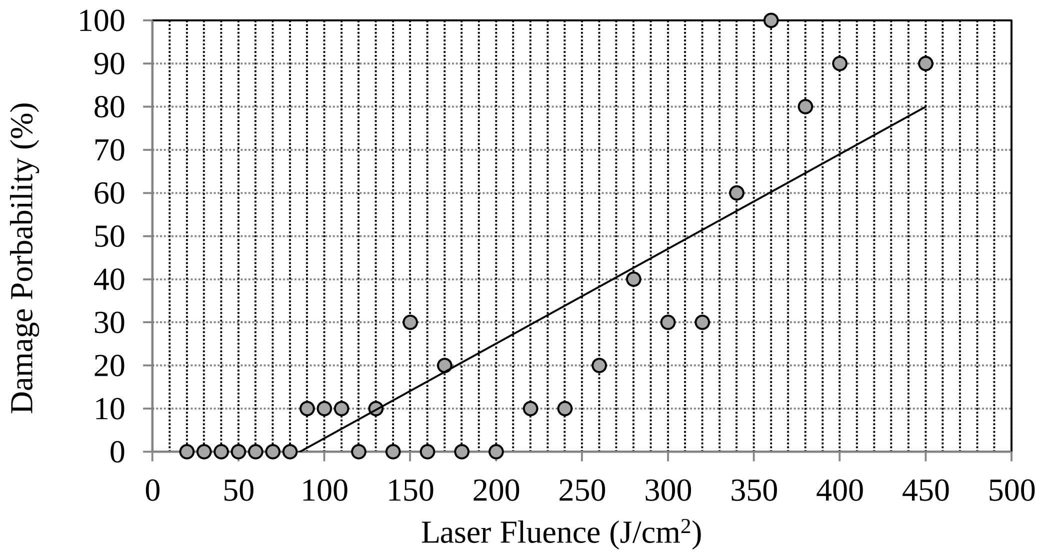

Figure 4.51 Percentage damage probability chart of the fabricated NQWD1-M-OC

Due to usage of OC layers, damages are almost invisible and cannot be visualized using available Nomarski DIC microscope as done in previous pages. Only a few damages have been scanned as being instances, Figure 4.52.

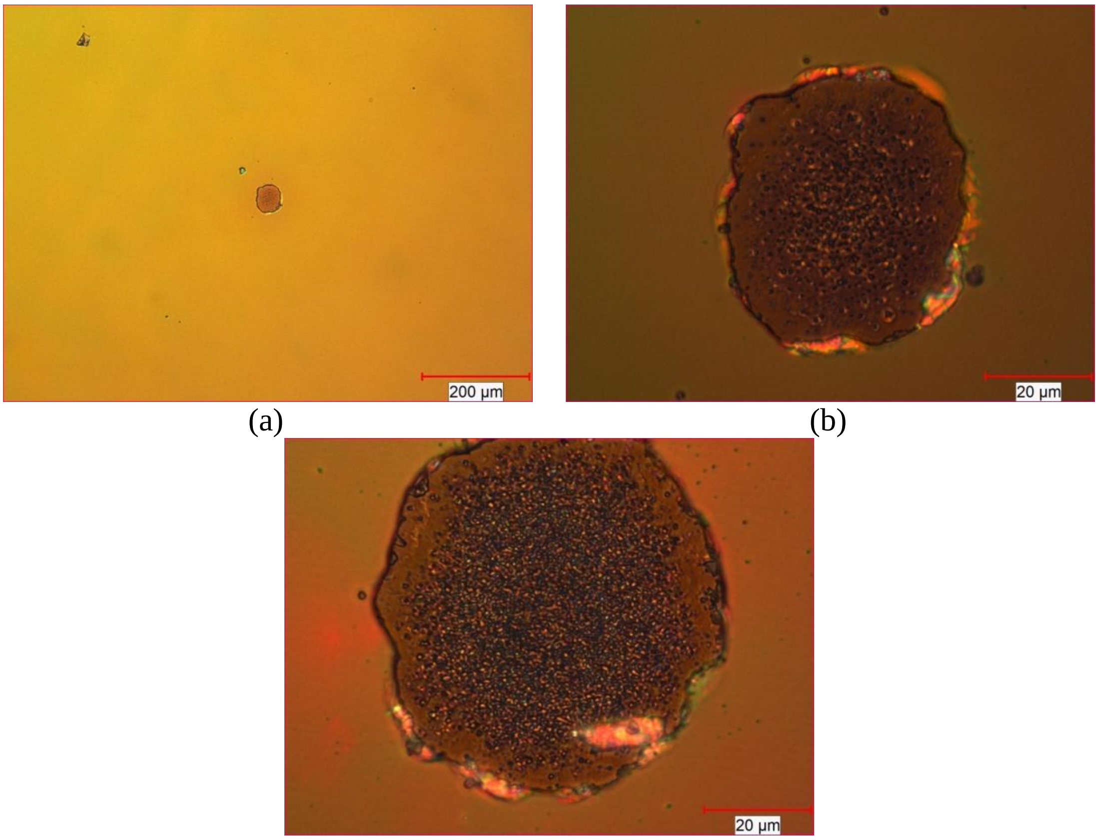

(a) (b) (c)

Figure 4.52 Exemplary damage appearances on coatings that have OCs at the outer most layer; (a)1st sample image-100x magnification, (b) 1st sample image-1000x magnification, (c) 2nd sample image-1000x

Scanned damage contours cannot be sorted as pit type, delamination type and etc. because of their vaguely appearance. Herein, OC layers fetter the formation of typical damage contours. As commented on numerical studies part, the OC layers have no effect on temperature distribution; however these layers may increase mechanical rigidity. Due to lack of damage visualization, effectiveness of the OCs have to be evaluated using the damage probability charts that are given above.

4.3.1.9 Discussion Of 1-on-1 LIDT Test Results

Damage probability charts and inspected damaged sites reveal that both non-quarter wave layers and OC layers increase the LIDT performance, as long as stacks do not contain any preexisting inclusions, small voids and/or contaminations (metal particles). Those imperfections originate before or during the coating process. For example, metallic particles (resultant from surface finish process) can stick on substrate surface before the deposition. Besides, non-oxidized coating materials (e.g. Hf metal) or coating material lumps (resultant from improper evaporation process) may diffuse into layers of the stack during the deposition process. If such kind of undesirable imperfections stay in the coating structure, NQWDs couldn't show expected performance. Because usage of modified layers enable the penetration of laser energy inside the coating and it may increases the probability of the damages resultant from imperfections, as seen in Figure 4.53. These damages are observed on a design that contains non-quarter wave layers at the top five layer pairs. In accordance with this perspective, usage of more and more non-quarter wave layers (e.g. NQWD5) is precarious as stated in the numerical part of the study.

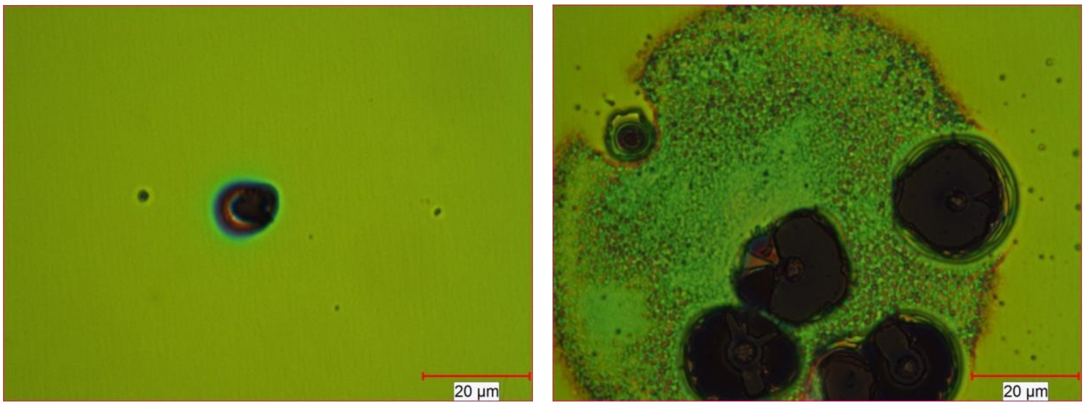

(a) (b)

Figure 4.53 Imperfection driven multi core damages; (a) 20 J/cm^2 laser fluence-1000x magnification and (b) 32 J/cm^2 laser fluence -1000x magnification.

Investigation of tested HR coatings indicated that the damage morphologies and LIDT performances are changed with the usage of non-quarter wave layers. Herein, the most remarkable feature of the QWD is considered as the sharp fracture mark. This feature is vanished when the EFI peaks are suppressed in the low refractive index layers. For example, the temperature peak is shifted inside to L_1 layer and it reduces the temperature peak value as calculated in numerical simulations (Figure 3.14) for NQWD1. Similar to NQWD1, no fracture mark is observed on NQWD2 damages due to decreased temperatures inside the low index layers as presented in the numerical studies section, Figure 3.14.b. On the other hand, NQWD2 damage profiles are different than the NQWD1 damages. Because the second layer pair thicknesses are also modified and that corresponds the absorption distribution change as calculated and shown in Figure 3.15. In the meantime, LIDT performance of NQWD5 is found similar to NQWD1. However, the increased amount of laser absorption through the coating layers with the usage of NQWD5 results differences in damage profiles. Moreover, NQWD5 is criticized in the numerical studies section due to increased laser absorption through coating layers. Herein, increased amount of absorption may cause lowered LIDT performance if the coating stack contains imperfections at the inner layers as illustrated in Figure 4.53.

On the other hand, designs with OC layers cannot be totally analyzed because of damage morphology scanning absence. As noted in the numerical studies section (chapter 3.4), OC layers have no positive effect on temperature distribution, however these layers may add mechanical rigidity to stacks. Accordingly, it is commented at the end of subsection 4.1.8, the OC layers mechanically enforce the coating structure and due to this enforcement the spread of damage morphologies are impeded. However, it is obvious that LIDT values of the QWD and NQWD1-M are increased with the usage of OC layers.

CHAPTER 5

CONCLUSIONS AND FUTURE RECOMMENDATIONS

5.1 Summary

In this dissertation, the laser induced temperature distribution on (optical) thin films are investigated through numerical and experimental studies. In the first chapter, the motivation of the present study is given as investigation of effects of optical design modifications on thermal performance of HR multilayer thin films. Then, heating effect of laser irradiation and corresponding heat transfer mechanism is explained both for bulk materials and multilayer optical coating stacks. In the objective of the dissertation part, the lack in the literature on the systematical assessment of the benefits and drawbacks of the optical design modifications linked to thermal performance, is pointed out. Then the objective of the present study is given as a versatile investigation of modified optical designs and their effects on thermal performance.

In the second chapter, material properties which are thermal conductivity and refractive index are discussed for thin films. In this respect, a wide literature review is given for thin film thermal conductivity. Measurement techniques, obtained thin film thermal conductivity results and important comments which are pointed by researchers are summarized for optical thin film materials. Herein the poor thermal conductivity of thin films is conducted to two main reasons that are microstructural irregularity and interface resistance. In addition to that a short literature review is also given for refractive index, particularly change of extinction coefficient with the type of production process is emphasized.

Numerical computation of the temperature rise due to absorption of laser energy is discussed at the beginning of the third chapter. Remarkable studies are reviewed and examples which are studied in literature about laser induced heating on multilayer films are presented. Important parameters such as time scale, thin film thicknesses and governing equations are illustrated. Then, a validation study is performed to examine capability of finite volume solver for the calculation of temperature distribution on multilayer thin films. The validation study reveals that temperature results of the ANSYS Fluent are in well agreement with the reference study. Then, QWD and NQWD methods are discussed. Their effects on thermal performance are analyzed with respect to temperature distributions. Investigation on thermal performance of NQWD method are extended with the multiple shot laser irradiation simulations in chapter 3.3. In addition to that a new alternative design is also proposed in the chapter 3.3 (so called NQWD5-M). The basic idea behind the proposed method is to lessen amount of absorption increment while the EFI peaks are shifted from H/L film interfaces. Moreover a new high refractive index material, HfO_2, is used in multiple shot irradiation studies. The advantages of HfO_2 material compared to TiO_2 are given with respect to reviewed studies from literature in the third chapter. Remarkable studies which aims enhancement of HfO_2 material laser resistance are also summarized.

Usage of OC layers which is another method employed in literature is studied in the chapter 3.4. TMCs are studied in the third chapter (3.5) together with the NQWD method. Numerical simulations are repeated for the thermal performance comparison of two TMC designs (TMC-QWD and TMC-NQWD) in terms of temperatures and laser absorption amounts.

Experimental studies are presented in the fourth chapter. At the beginning of this chapter, 1-on-1 and S-on-1 LIDT measurement techniques are introduced. Simplified scheme of the experimental set up, testing procedure and evaluation methods of LIDT results are summarized briefly. As a result for this part, 1-on-1 measurement technique is considered as suitable for the experimental parts of the present study. In the first subsection of the forth chapter, fabrication studies are explained for produced HR multilayers. The fabrication method and coating chamber are presented. Parameters which are used during the coating process are also reported. In chapter 4.2, the LIDT measurement setup which is settled down in ASELSAN Inc. is demonstrated. In the last subsection of the chapter four, damage morphology investigations and LIDT test results are studied. At the beginning of this subsection, a small literature survey is given and damage types are identified. Then performed 1-on-1 LIDT test results of fabricated HR multilayer stacks are evaluated owing to damage morphologies. Damage contours are visualized using Nomarski DIC microscope and Zygo WLI system. Delamination and flat bottom pit type damage contours and corresponding laser fluencies are taken into considerations for the evaluation of the layer thickness modifications.

In addition to these numerical and experimental works, a computer code is composed as well, in order to calculate square of the normalized EFI variation in MATLAB instead of commercial software MacLeod and Excel. Detailed calculation steps of the square of the normalized EFI variation are given in Appendix A.

5.2 Conclusions

The present study showed that, the temperature distribution on multilayer optical thin films can be analyzed with using the numerical methods. It is believed, thermal performance improvement efforts can be examined with these numerical studies even in the design stages. Herein, three optical design modification methods are studied numerically. Firstly, NQWD method or in other words the effect of usage of non-quarter wave layers on temperature distribution is scrutinized. It is observed the peak temperature (at most 24.6%) and the highest interface temperature (at most 21.6%) at top layers can be decreased by manipulating the layer thickness. Unfortunately the layer thickness modifications cause penetration of more laser energy inside the inner layers that increases the internal laser absorption. Due to this reason usage of too many non-quarter wave layer pairs is criticized. This drawback is also observed for the multiple shot laser irradiation simulations. Hence, a new NQWD is proposed to reduce the laser absorption increment. The newly proposed design (for which layer thicknesses are calculated using an in-house code) decreased the amount of absorption in the inner layers compared to prior designs and resulted in lower internal and interface temperatures (at most 15.4%).

Upper surface OC layers are also studied but no positive effect on temperature distribution is observed. Lastly TMC designs are examined by the numerical simulations. It is observed, temperatures can be decreased at the top laser resistant (HfO_2/SiO_2) layer pairs by modifying a few top layer pair thicknesses. On the other hand, modification of top layer pairs caused temperature increase in HR inner layer pairs. However, the peak temperature value in the multilayer stack is (18.3%) decreased.

In the meantime, LIDT measurement results are also assessed on the fabricated multilayer coatings. Herein damage probability charts, damage morphology visualizations and performed numerical simulations are used for evaluations. It is observed that both non-quarter wave and OC layers increase the LIDT performance. The usage of non-quarter wave layers changed the damage characteristics due to altered temperature distribution as noted in the temperature distribution simulations. For example, the fracture mark which is observed for the QWD is avoided due to shifted EFI peak from the first H/L interface as planned in the numerical studies section. In addition to that the damage profiles are changed due to damped temperature rise by the low refractive index layers in accordance with the calculated temperature distributions on the design alternatives. As pointed out in numerical simulations low refractive index layers have higher thermal conductivity and lower extinction coefficient, therefore damage profiles are changed in the experiments due to changed temperature field distribution in the modified layers as indicated in simulations. Moreover it is comprehended NQWDs can provide desired performance only if, multilayer coatings do not contain impurities (resultant from coating processes). If the coating stack contains densely and randomly distributed imperfections such as metal particles, voids or nodules, the LIDT value of the NQWDs will decrease significantly. Hence, usage of too many non-quarter wave layer pairs in the design is precarious as stated in the numerical studies section. Besides, if the coating structure contains rarely distributed impurities, their effects on LIDT performance should also be taken into consideration. Especially damages seen at the low laser fluence irradiations should be inspected. The effect of layer pair thickness modifications can only be evaluated fairly by inspecting damage characteristics seen at the low laser fluence levels. Damage diameter and the depth are the primary parameters for the inspection. If inspections indicate that the damage is resultant from an impurity like a nodule or void it should be disregarded during the evaluation of alternative NQWDs. In the meantime, it is observed that OCs mechanically enforce the coating structure and due to this enforcement the spread of damage morphologies are impeded. However, it is obvious that LIDT performance of the QWD and NQWD1-M are increased with the usage of OC layers.

5.3 Future Recommendations

Considering both numerical and experimental studies, usage of non-quarter wave and OC layers are proposed for the thermal performance enhancement. However, the number of modified layer pairs have to be carefully determined. Results which are reported in the previous sections reveal that no need to use more and more non-quarter wave layers to increase LIDT of the coatings. Because usage of more non-quarter wave layers causes the penetration of more laser energy in to coating stack that increases probability of damage. Accordingly, modification of the first and may be the second layer pairs are adequate to change temperature field distribution as desired. Similarly non-quarter wave layers can be employed in the laser resistant layers of TMC designs. By doing so, the laser resistance of these layers can be improved as desired. Besides, experimental LIDT measurements and complementary damage morphology investigations are recommended for the identification of damage types and damage characteristic profiles. Nomarski DIC microscope is appraised as a useful evaluation tool for identification of damage types. WLI systems are also suggested for damage profile investigation. Employment of these devices is believed to be beneficial for fair evaluation of design modifications on optical thin films.

REFERENCES

1. Jeong, Y. C., Boyland, A. J., Sahu, J. K., Chung, S. H., Nilsson, J., & Payne, D. N. (2009). Multi-kilowatt single-mode ytterbium-doped large-core fiber laser. *Journal of the Optical Society of Korea*, *13*(4), 416-422.

2. Snavely, R. A., Key, M. H., Hatchett, S. P., Cowan, T. E., Roth, M., Phillips, T. W., ... Campbell, E. M. (2000). Intense high-energy proton beams from petawatt-laser irradiation of solids. *Physical Review Letters, 85*(14), 2945.

3. Joint High Power Solid-State Laser. (2010). Retrieved from http://www.northropgrumman.com/Capabilities/SolidStateHighEnergyLaserSystems/Pages/JointHighPowerSolidStateLaser.aspx. [Last accessed on January 2016].

4. Area Defense Anti-Munitions (ADAM). (2012). Retrieved from http://www.lockheedmartin.com/us/products/ADAM.html. [Last accessed on January 2016].

5. ROX-OEM-Series-uLRF-Module.pdf. (2015). Retrieved from http://voxtel-inc.com/files/2015/04/ROX-OEM-Series-uLRF-Module-Revision-EVK-04152015-Model-EVKI-NABC-100-uJ-200-um-long-form.pdf. [Last accessed on January 2016].

6. Wood, R. M. (2003). *Laser-induced damage of optical materials*. CRC Press.

7. Ristau, D., Jupé, M., & Starke, K. (2009). Laser damage thresholds of optical coatings. *Thin Solid Films*, *518*(5), 1607-1613.

8. Shao, J., & Fan, Z. (2005, September). Laser thin films with very high damage threshold. In *Optical Systems Design 2005* (pp. 596312-596312). International Society for Optics and Photonics.

9. Bloom, A. L., & Costich, V. R. (1976). 5.5 Design for high power resistance. In *Laser Induced Damage in Optical Materials*, 1975: Proceedings of a Symposium (Vol. 604). US Department of Commerce, National Bureau of Standards.

10. Yu, J., Xiang, X., He, S., Yuan, X., Zheng, W., Lü, H., & Zu, X. (2014). Laser-Induced Damage Initiation and Growth of Optical Materials. *Advances in Condensed Matter Physics*, 2014.

11. Ristau, D. (Ed.). (2014). *Laser-Induced Damage in Optical Materials*. CRC Press.

12. Cheng, J. C., Zhang, S. Y., & Wu, L. (1995). Excitations of thermoelastic waves in plates by a pulsed laser. *Applied Physics A*, *61*(3), 311-319.

13. Lu, Y., Zhang, S., & Cheng, J. (2000). Theoretical study of transient thermal conduction and temperature distribution generated by pulsed laser. *Applied Physics B*, *70*(1), 85-90.

14. Mi, X. B., Gao, H. D., & Zhang, S. Y. (2004). Two-dimensional transient thermal analysis of diamond/Si structures heated by a pulsed circular Gaussian laser beam. *International journal of heat and mass transfer*, *47*(10), 2481-2485.

15. Shuja, S. Z., Yilbas, B. S., & Khan, S. (2009). Laser consecutive pulse heating and phase change: influence of spatial distribution of laser pulse intensity on melting. *International Journal of Thermal Sciences*, *48*(10), 1960-1966.

16. Wang, X., Shen, Z. H., Lu, J., & Ni, X. W. (2010). Laser-induced damage threshold of silicon in millisecond, nanosecond, and picosecond regimes.*Journal of Applied Physics*, *108*(3), 033103-033103.

17. Grigoropoulos, C. P. (2009). *Transport in laser microfabrication: fundamentals and applications*. Cambridge University Press.

18. Mansuripur, M., Connell, G. A., & Goodman, J. W. (1982). Laser-induced local heating of multilayers. *Applied Optics*, *21*(6), 1106-1114.

19. Wang, B., Qin, Y., Ni, X., Shen, Z., & Lu, J. (2010). Effect of defects on long-pulse laser-induced damage of two kinds of optical thin films. *Applied Optics*, *49*(29), 5537-5544.

20. Vinci, R. P., & Vlassak, J. J. (1996). Mechanical behavior of thin films. *Annual Review of Materials Science*, *26*(1), 431-462.

21. Dini, J. W. (1997). Properties of coatings: Comparisons of electroplated, physical vapor deposited, chemical vapor deposited, and plasma sprayed coatings. *Material And Manufacturing Process*, *12*(3), 437-472.

22. Tritt, T. M. (Ed.). (2004). *Thermal conductivity: theory, properties, and applications*. Springer Science & Business Media.

23. Amundsen, T., & Olsen, T. (1965). Size dependent thermal conductivity in aluminum films. *Philosophical Magazine*, *11*(111), 561-574.

24. Ristau, D., & Ebert, J. (1986). Development of a thermographic laser calorimeter. *Applied Optics*, *25*(24), 4571-4578.

25. Lambropoulos, J. C., Jolly, M. R., Amsden, C. A., Gilman, S. E., Sinicropi, M. J., Diakomihalis, D., & Jacobs, S. D. (1989). Thermal conductivity of dielectric thin films. *Journal of applied physics*, *66*(9), 4230-4242.

26. Decker, D. L. (1990, December). Thermal properties of optical thin-film materials. In *San Dieg-DL Tentative* (pp. 244-252). International Society for Optics and Photonics.

27. Henager Jr, C. H., & Pawlewicz, W. T. (1993). Thermal conductivities of thin, sputtered optical films. *Applied Optics*, *32*(1), 91-101.

28. Wu, Z. L., Thomsen, M., Kuo, P. K., Lu, Y., Stolz, C., & Kozlowski, M. (1997). Photothermal characterization of optical thin film coatings. *Optical Engineering*, *36*(1), 251-262.

29. Burzo, M. G., Komarov, P. L., & Raad, P. E. (2003). Thermal transport properties of gold-covered thin-film silicon dioxide. *Components and Packaging Technologies, IEEE Transactions on*, *26*(1), 80-88.

30. Yamane, T., Nagai, N., Katayama, S. I., & Todoki, M. (2002). Measurement of thermal conductivity of silicon dioxide thin films using a 3ω method. *Journal of Applied Physics*, *91*(12), 9772-9776.

31. Kim, D. J., Kim, D. S., Cho, S., Kim, S. W., Lee, S. H., & Kim, J. C. (2004). Measurement of thermal conductivity of TiO2 thin films using 3ω method. *International Journal of Thermophysics*, *25*(1), 281-289.

32. Chien, H. C., Yao, D. J., Huang, M. J., & Chang, T. Y. (2008). Thermal conductivity measurement and interface thermal resistance estimation using SiO2 thin film. *Review of Scientific Instruments*, *79*(5), 054902-054902.

33. Baklanov, M., Maex, K., & Green, M. (Eds.). (2007). *Dielectric films for advanced microelectronics* (Vol. 12). John Wiley & Sons.

34. Torchio, P., Gatto, A., Alvisi, M., Albrand, G., Kaiser, N., & Amra, C. (2002). High-reflectivity HfO_2-SiO_2 ultraviolet mirrors. *Applied Optics*, *41*(16), 3256-3261.

35. Commandré, M., & Pelletier, E. (1990). Measurements of absorption losses in TiO2 films by a collinear photothermal deflection technique. *Applied Optics*, *29*(28), 4276-4283.

36. Khoshman, J. M., & Kordesch, M. E. (2006). Optical properties of a-HfO_2 thin films. *Surface and Coatings Technology*, *201*(6), 3530-3535.

37. Stenzel, O., Wilbrandt, S., Kaiser, N., Vinnichenko, M., Munnik, F., Kolitsch, A., ... Grössl, M. (2009). The correlation between mechanical stress, thermal shift and refractive index in HfO_2, Nb_2O_5, Ta_2O_5 and SiO_2 layers and its relation to the layer porosity. *Thin Solid Films*, *517*(21), 6058-6068.

38. Cevro, M., & Carter, G. (1995). Ion-beam and dual-ion-beam sputter deposition of tantalum oxide films. *Optical Engineering*, *34*(2), 596-606.

39. Ghodsi, F. E., Tepehan, F. Z., & Tepehan, G. G. (1997). Optical properties of Ta_2O_5 thin films deposited using the spin coating process. *Thin Solid Films*, *295*(1), 11-15.

40. Thielsch, R., Gatto, A., Heber, J., & Kaiser, N. (2002). A comparative study of the UV optical and structural properties of SiO_2, Al_2O_3, and HfO_2 single layers deposited by reactive evaporation, ion-assisted deposition and plasma ion-assisted deposition. *Thin Solid Films*, *410*(1), 86-93.

41. Ai, W., & Xiong, S. (2011, October). Characterization of hafnia thin films made with different deposition technologies. In *XLIII Annual Symposium on*

Optical Materials for High Power Lasers (pp. 81900J-81900J). International Society for Optics and Photonics.

42. Fan, Z., Wu, Z., & Tang, X. (1993, March). Laser-induced damage in optical coatings. In *Optical Systems Design'92* (pp. 459-468). International Society for Optics and Photonics.

43. Zhao, Q., & Fan, Z. (1996, May). Improving the laser resistance of Al mirror and Si window by depositing dielectric protection layers. In *Laser-Induced Damage in Optical Materials: 1995* (pp. 569-574). International Society for Optics and Photonics.

44. Papernov, S., & Schmid, A. W. (1997, May). Heat transfer from localized absorbing defects to the host coating material in HfO_2/SiO_2 multilayer systems. In *Laser-Induced Damage in Optical Materials: 1996* (pp. 283-291). International Society for Optics and Photonics.

45. Zhao, Q., Wu, Z., Thomsen, M., Han, Y., & Fan, Z. (1998, April). Interfacial effects on the transient temperature rise of multilayer coatings induced by a short-pulse laser irradiation. In *Laser-Induced Damage in Optical Materials: 1997* (pp. 491-498). International Society for Optics and Photonics.

46. Hu, H., Fan, Z., & Luo, F. (2001). Laser-Induced Damage of a 1064-nm ZnS/MgF_2 Narrow-Band Interference Filter. *Applied Optics*, *40*(12), 1950-1956.

47. Liu, G., Zhou, M., Hu, G., Liu, X., Jin, Y., He, H., & Fan, Z. (2010). Calculation of temperature fields with a film-substrate interfacial layer model to discuss the layer-pair number effects on the damage thresholds of LaF_3/MgF_2 high reflectors at 355nm. *Applied Surface Science*, *256*(13), 4206-4210.

48. Wang, B., Zhang, H., Qin, Y., Wang, X., Ni, X., Shen, Z., & Lu, J. (2011). Temperature field analysis of single layer TiO_2 film components induced by long-pulse and short-pulse lasers. *Applied Optics*, *50*(20), 3435-3441.

49. Gallais, L., & Commandré, M. (2005). Photothermal deflection in multilayer coatings: modeling and experiment. *Applied Optics*, *44*(25), 5230-5238.

50. Li, S. H., He, H. B., Ling, X. L., Tao, C. X., Zhao, Y. A., & Fan, Z. X. (2009). Temperature field analysis of single-layer TiO_2 films. *Applied Optics*, *48*(28), 5380-5385.

51. Shan, Y. G., He, H. B., Wang, Y., Li, X., Li, D. W., & Zhao, Y. A. (2011). Electrical field enhancement and laser damage growth in high-reflective coatings at 1064nm. *Optics Communications*, *284*(2), 625-629.

52. Chiang, D., Tseng, S. F., Hsiao, W. T., & Hsiao, C. N. (2013). Temperature profile of the multilayer structure irradiated by pulsed laser. *Applied Physics A*, *110*(3), 571-578.

53. Ling, X., Wang, G., Zhao, Y., Liu, X., & Shao, J. (2013). Laser-induced damage of the optical coatings due to organic contamination in vacuum. *Applied Surface Science*, *270*, 346-351.

54. Tang, X., Fan, Z., & Wang, Z. (1994). Surface inclusion adhesion of optical coatings. *Optical Engineering*, *33*(10), 3406-3410.

55. Fan, Z., Zhao, Q., & Wu, Z. (1997, May). Temperature field design of optical thin film coatings. In *Laser-Induced Damage in Optical Materials: 1996* (pp. 362-370). International Society for Optics and Photonics.

56. ANSYS FLUENT 12.0 UDF Manual, ANSYS Inc., 2011.

57. Apfel, J. H. (1977). Optical coating design with reduced electric field intensity. *Applied Optics*, *16*(7), 1880-1885.

58. Gill, D. H., Newnam, B. E., & McLeod, J. (1978). Use of non-quarterwave designs to increase the damage resistance of reflectors at 532 and 1064 Nanometers. In *NBS Ninth Symposium on Materials for High Power Lasers, Boulder, Colo.(Oct. 1977)*.

59. Arnon, O., & Baumeister, P. (1980). Electric field distribution and the reduction of laser damage in multilayers. *Applied Optics*, *19*(11), 1853-1855.

60. Demichelis, F., Mezzetti-Minetti, E., Tallone, L., & Tresso, E. (1984). Optimization of optical parameters and electric field distribution in multilayers. *Applied Optics*, *23*(1), 165-171.

61. Goodson, K. E., Flik, M. I., Su, L. T., & Antoniadis, D. A. (1993). Annealing-temperature dependence of the thermal conductivity of LPCVD silicon-dioxide layers. *Electron Device Letters*, *14*(10), 490-492.

62. Lee, S. M., & Cahill, D. G. (1997). Heat transport in thin dielectric films. *Journal of Applied Physics*, *81*(6), 2590-2595.

63. Ocak, M., Sert, C., & Okutucu, T. Ö. (2013, November). Investigation of non-quarter wave design on multilayer optical thin film coatings from a heat transfer point of view. In *SPIE Laser Damage* (pp. 888506-888506). International Society for Optics and Photonics.

64. Stenzel, O., Wilbrandt, S., Kaiser, N., Vinnichenko, M., Munnik, F., Kolitsch, A., ... Grössl, M. (2009). The correlation between mechanical stress, thermal shift and refractive index in HfO_2, Nb_2O_5, Ta_2O_5 and SiO_2 layers and its relation to the layer porosity. *Thin Solid Films*, *517*(21), 6058-6068.

65. Mei-Qiong, Z., Dong-Ping, Z., Tian-Ya, T., Hong-Bo, H., Jian-Da, S., & Zheng-Xiu, F. (2005). Optical, structural and laser-induced damage threshold properties of HfO2 thin films prepared by electron beam evaporation. *Chinese Physics Letters*, *22*(5), 1246.

66. Fadel, M., Omer, O. A., & Basily, R. R. (1998). A study of some optical properties of hafnium dioxide (HfO_2) thin films and their applications. *Applied Physics A*, *66*(3), 335-343.

67. Haque, S. M., Sagdeo, P. R., Balaji, S., Sridhar, K., Kumar, S., Bhattacharyya, D., ... Sahoo, N. K. (2013). Effect of substrate bias and oxygen partial pressure on properties of RF magnetron sputtered HfO_2 thin films. *Journal of Vacuum Science & Technology B*, *32*(3), 03D104.

68. Miller, M. G., Chow, R., & Loomis, G. E. (1994, July). Electrostatic reduction of particulates for laser resistant hafnia coatings. In *Laser-Induced Damage in Optical Materials*: 1993 (pp. 426-432). International Society for Optics and Photonics.

69. Oliver, J. B., Papernov, S., Schmid, A. W., & Lambropoulos, J. C. (2008, October). Optimization of laser-damage resistance of evaporated hafnia films at 351nm. In Boulder Damage Symposium XL Annual Symposium on *Optical Materials for High Power Lasers* (pp. 71320J-71320J). International Society for Optics and Photonics.

70. Stolz, C. J., Sheehan, L. M., Von Gunten, M. K., Bevis, R. P., & Smith, D. J. (1999, September). Advantages of evaporation of hafnium in a reactive environment for manufacture of high-damage-threshold multilayer coatings by electron-beam deposition. In *Optical Systems Design and Production* (pp. 318-324). International Society for Optics and Photonics

71. Zhang, D., Fan, S., Zhao, Y., Gao, W., Shao, J., Fan, R., & Fan, Z. (2005). High laser-induced damage threshold HfO_2 films prepared by ion-assisted electron beam evaporation. *Applied Surface Science*, *243*(1), 232-237.

72. Stenzel, O., Wilbrandt, S., Yulin, S., Kaiser, N., Held, M., Tünnermann, A., ... & Kaiser, U. (2011). Plasma ion assisted deposition of hafnium dioxide using argon and xenon as process gases. *Optical Materials Express*, *1*(2), 278-292.

73. Blanchin, M. G., Canut, B., Lambert, Y., Teodorescu, V. S., Barau, A., & Zaharescu, M. (2008). Structure and dielectric properties of HfO_2 films prepared by a sol–gel route. *Journal of Sol-Gel Science and Technology, 47*(2), 165-172.

74. Ocak, M., Sert, C., & Okutucu-ÖZYURT, T. (2015, December). A novel highly reflective multilayer optical coating design with modified layer thicknesses. Manuscript in preparation.

75. Chien, H. C., Yao, D. J., Huang, M. J., & Chang, T. Y. (2008). Thermal conductivity measurement and interface thermal resistance estimation using SiO_2 thin film. *Review of Scientific Instruments*, *79*(5), 054902-054902.

76. Dai, G., Chen, Y., Lu, J., Shen, Z., & Ni, X. (2009). Analysis of laser induced thermal mechanical relationship of HfO2/SiO2 high reflective optical thin film at 1064 nm. *Chinese Optics Letters*, *7*(7), 601-604.

77. Panzer, M. A., Shandalov, M., Rowlette, J., Oshima, Y., Chen, Y. W., McIntyre, P. C., & Goodson, K. E. (2009). Thermal properties of ultrathin hafnium oxide gate dielectric films. *Electron Device Letters, IEEE*, *30*(12), 1269-1271.

78. Stolz, C. J., & Runkel, J. (2013, November). Brewster angle thin film polarizing beamsplitter laser damage competition:“S” polarization. In *SPIE Laser Damage* (pp. 888509-888509). International Society for Optics and Photonics.

79. Xu, C., Dong, H., Ma, J., Jin, Y., Shao, J., & Fan, Z. (2008). Influences of SiO_2 protective layers and annealing on the laser-induced damage threshold of Ta_2O_5 films. *Chinese Optics Letters*, *6*(3), 228-230.

80. Carniglia, C. K., Apfel, J. H., Allen, T. H., Tuttle, T. A., Lowdermilk, W. H., Milam, D., & Rainer, F. (1980). Recent Damage Results on Silica Titania Reflectors at 1 micron. *Laser-Induced Damage in Optical Materials: 1979*, *568*, 377-390.

81. Hart, T. T., Lichtenstein, T. L., Carniglia, C. K., & Rainer, F. (1982). Effects of undercoats and overcoats on damage thresholds of 248 nm coatings (No. UCRL-86711; CONF-811117-3). *Lawrence Livermore National Lab.;* Optical Coating Lab., Inc., Santa Rosa, CA (USA).

82. Carniglia, C. K., Hart, T. T., & Staggs, M. C. (1986). Effect of overcoats on 355-nm reflectors. In *Laser Induced Damage in Optical Materials: 1984*. ASTM International.

83. Stolz, C. J., & Taylor, J. R. (1993, June). Damage threshold study of ion-beam-sputtered coatings for a visible high-repetition laser at LLNL. In *Optical Materials for High Power Lasers* (pp. 182-191). International Society for Optics and Photonics.

84. Walton, C. C., Genin, F. Y., Chow, R., Kozlowski, M. R., Loomis, G. E., & Pierce, E. L. (1996, May). Effect of silica overlayers on laser damage of HfO_2-SiO_2 56 degrees incidence high reflectors. In *Laser-Induced Damage in Optical Materials: 1995* (pp. 550-559). International Society for Optics and Photonics.

85. Stolz, C. J., Genin, F. Y., & Pistor, T. V. (2004, June). Electric-field enhancement by nodular defects in multilayer coatings irradiated at normal and 45 incidence. In*XXXV Annual Symposium on Optical Materials for High Power Lasers: Boulder Damage Symposium* (pp. 41-49). International Society for Optics and Photonics.

86. Liu, H., Xiong, S., & Zhang, Y. (2006, August). High-power DPL thin films prepared by ion beam sputtering. In Proceedings of Optical Engineering (Vol. 6286, p. 628605). International Society for Optical Engineering; 1999.

87. Zhan, M., He, H., Zhao, Y., Tian, G., Shao, J., & Fan, Z. (2006). Overcoat dependence of laser-induced damage threshold of 355nm HR coatings. *Applied Surface Science*, *252*(6), 2126-2130.

88. Yuan, L., Zhao, Y. N., Wang, C. J., He, H. B., Fan, Z. X., & Shao, J. D. (2007). Effect of SiO2 protective layer on the femtosecond laser-induced damage of HfO_2/SiO_2 multilayer high-reflective coatings. *Applied Surface Science*, *253*(7), 3450-3454.

89. Xu, C., Dong, H., Ma, J., Jin, Y., Shao, J., & Fan, Z. (2008). Influences of SiO_2 protective layers and annealing on the laser-induced damage threshold of Ta_2O_5 films. *Chinese Optics Letters*, *6*(3), 228-230.

90. Cho, B., Danielewicz, E., & Rudisill, J. E. (2010, October). Laser induced damage threshold of 266 AR coatings with different coating designs. In *Laser Damage Symposium XLII: Annual Symposium on Optical Materials for High Power Lasers* (pp. 78420B-78420B). International Society for Optics and Photonics.

91. Stolz, C. J., Genin, F. Y., Reitter, T. A., Molau, N. E., Bevis, R. P., Von Gunten, M. K., & Anzellotti, J. F. (1997, May). Effect of SiO_2 overcoat thickness on laser damage morphology of HfO2/SiO2 Brewster's angle polarizers at 1064 nm. In *Laser-Induced Damage in Optical Materials: 1996* (pp. 265-272). International Society for Optics and Photonics.

92. Meng, Z. Y., Huang, S. L., Liu, Z., Zeng, C. H., & Bu, Y. K. (2012). Design and fabrication of a novel high damage threshold $HfO_2/TiO_2/SiO_2$ multilayer laser mirror. *Optoelectronics Letters*, *8*, 190-192.

93. Patel, D., Schiltz, D., Langton, P. F., Emmert, L., Acquaroli, L. N., Baumgarten, C., ... Menoni, C. S. (2013, November). Improvements in the laser damage behavior of Ta_2O_5/SiO_2 interference coatings by modification of the top layer design. In *SPIE Laser Damage* (pp. 888522-888522). International Society for Optics and Photonics.

94. Genin, F. Y., Stolz, C. J., & Kozlowski, M. R. (1997, May). Growth of laser-induced damage during repetitive illumination of HfO_2/SiO_2 multilayer mirror and polarizer coatings. In *Laser-Induced Damage in Optical Materials: 1996* (pp. 273-282). International Society for Optics and Photonics.

95. Hu, H., Fan, Z., & Luo, F. (2001). Laser-Induced Damage of a 1064-nm ZnS/MgF_2 Narrow-Band Interference Filter. *Applied Optics*, *40*(12), 1950-1956.

96. Stolz, C. J., & Runkel, J. (2013, November). Brewster angle thin film polarizing beamsplitter laser damage competition:"S" polarization. In *SPIE Laser Damage* (pp. 888509-888509). International Society for Optics and Photonics.

97. ISO 11254-1, "Lasers and laser-related equipment - Determination of laser-induced damage threshold of optical surfaces - Part 2 : 1- on -1 test", 2000.

98. ISO 11254-21, "Lasers and laser-related equipment - Determination of laser-induced damage threshold of optical surfaces - Part 2 : S- on -1 test", 2001.

99. Electron beam physical vapor deposition. (2014, May 7). In Wikipedia, Retrieved from http://en.wikipedia.org/w/index.php?title=Electron_beam_physical_vapor_deposition&oldid=607538474. [Last accessed on January 2016].

100. Electron beam evaporation. (2015, April). Retrived from http://www.lesker.com/newweb/ped/techniques.cfm#Electron. [Last accessed on January 2016].

101. Matl, K., (2008). Optical coating systems and processes complete solution for the production of high end optical coatings, [Power Point slides]: Leybold Optics GMBH.

102. Tench, R. J., Chow, R., & Kozlowski, M. R. (1994). Characterization of defect geometries in multilayer optical coatings. *Journal of Vacuum Science & Technology A*, *12*(5), 2808-2813

103. Genin, F. Y., & Stolz, C. J. (1996, November). Morphologies of laser-induced damage in hafnia-silica multilayer mirror and polarizer coatings. In Third International Workshop on *Laser Beam and Optics Characterization* (pp. 439-448). International Society for Optics and Photonics.

104. Ristau, D., Jupé, M., & Starke, K. (2009). Laser damage thresholds of optical coatings. *Thin Solid Films*, *518*(5), 1607-1613.

105. Cheng, X., Zhang, J., Ding, T., Wei, Z., Li, H., & Wang, Z. (2013). The effect of an electric field on the thermomechanical damage of nodular defects in dielectric multilayer coatings irradiated by nanosecond laser pulses. *Light: Science & Applications*, *2*(6), e80.

106. Brett, M. J., Tait, R. N., Dew, S. K., Kamasz, S., Labun, A. H., & Smy, T. (1992). Nodular defect growth in thin films. *Journal of Materials Science: Materials in Electronics*, *3*(1), 64-70.

107. Wang, Z., Bao, G., Jiao, H., Ma, B., Zhang, J., Ding, T., & Cheng, X. (2013). Interfacial damage in a Ta_2O_5/SiO_2 double cavity filter irradiated by 1064 nm nanosecond laser pulses. *Optics Express*, *21*(25), 30623-30632.

108. Dijon, J., Ravel, G., & Andre, B. (1999, April). Thermomechanical model of mirror laser damage at 1.06 µm: II. Flat bottom pits formation. In *Laser-Induced Damage in Optical Materials*: 1998 (pp. 398-407). International Society for Optics and Photonics.

109. Zhao, Y., Gao, W., Shao, J., & Fan, Z. (2004). Roles of absorbing defects and structural defects in multilayer under single-shot and multi-shot laser radiation. *Applied Surface Science, 227*(1), 275-281.

110. Hu, J., Zhang, W., Ma, P., & Xu, Q. (2006, February). Laser-induced damage of transmissive optics at 1064 nm. In *2nd international Symposium on Advanced Optical Manufacturing and Testing Technologies* (pp. 61492H-61492H). International Society for Optics and Photonics.

111. Liu, Z., Luo, J., Zheng, Y., Ma, P., Zhang, Z., Wei, Y., & Chen, S. (2014). Damage morphology change condition and thermal accumulation effect on high-reflection coatings at 1064nm. *Optics Express*, *22*(9), 10151-10164.

112. Nikon Corporation. (2005). Eclipse industrial microscopes LV150 D [Data sheet]. Retrieved from http://www.coherent.com.au/content/media/Nikon/LV150,%20LV150A,%20LV100D.pdf. [Last accessed on January 2016]

113. Differential interference contrast microscopy. (2015, March 13). In Wikipedia, The Free Encyclopedia. Retrieved from https://en.wikipedia.org/w/index.php?title=Differential_interference_contrast_microscopy&oldid=651151413. [Last accessed on January 2016].

114. Zygo Corporation. (2014). NewView^{TM} 7100 specifications [Data sheet]. Retrieved from http://action.zygo.com/acton/attachment/4246/f-002d/1/-/-/-/-/NewView_7300_Specs.pdf. [Last accessed on January 2016].

115. White light interferometry. (2015, July 13). In Wikipedia, The Free Encyclopedia. Retrieved from https://en.wikipedia.org/w/index.php?title=White_light_interferometry&oldid=671309117. [Last accessed on January 2016].

116. Apfel, J. H. (1976). Electric fields in multilayers at oblique incidence. *Applied Optics*, *15*(10), 2339-2343

117. Hansen, W. N. (1968). Electric fields produced by the propagation of plane coherent electromagnetic radiation in a stratified medium. *JOSA*, *58*(3), 380-388.

APPENDIX A

COMPUTATION OF THE SQUARE OF THE NORMALIZED EFI VARIATION

Square of the normalized EFI variation term is an important parameter for the computation of heat source term (Eqn. (1.9)) as mentioned in previous chapters. This parameter was calculated in chapter 3.1 and chapter 3.2 with using commercial softwares MacLeod and Excel. MacLeod was used to obtain EFI variation and Excel was used to convert EFI variation in to normalized squared form. In this section an alternative computer code is composed in MATLAB in order to calculate square of the normalized EFI variation. Then this code is used in chapter 3.3-chapter 3.5. Characteristic matrix method, used for square of the normalized EFI computation in MATLAB, is illustrated in the following pages.

The composed code shortens computational processes for users and it has some additional features such as

- calculation of NQWD layer thicknesses
- calculation of relative amount of laser absorption of coating layers
- calculation of total reflectance and transmittance of coating stack
- calculation of the coordinates of the EFI peak points

manipulation of the layer thicknesses for desired optimization constraints

A.1 Theoretical Details For The Calculation Of Square Of The Normalized EFI Variation

When a light beam is directed onto a layered structure it results in absorption due to the interaction of the electric and magnetic fields with the layered solid structure [116]. Absorption of light in stratified multilayer films were well studied in the literature since the pioneering study of Hansen [117] was published in 1968. Researchers noted that in a stratified stack composed of absorbing and/or nonabsorbing layers, the absorption of light (electromagnetic energy) at any position is directly proportional to the EFI at that position [57]. In addition the mean-square EFI for which relatively simple relationships exist was seen as important rather than the field itself.

Characteristic matrix method is one of the methods for calculation of square of the normalized EFI variation through a stratified multilayer stack. In this method square of the normalized EFI variation is emphasized as [59];

$$E_n^2(z) = \frac{|E(z)|^2}{|E_0^+|^2} \tag{A.1}$$

As seen in Eqn (A.1)., the denominator ($|E_0^+|^2$) is the squared of the electric field in the incident wave. This part can be calculated by following a few steps as described below.

The first step is to calculate characteristic matrix $\mathrm{M}_i$for i^{th} layer in the stratified N layer multilayer stack.

$$\mathrm{M}_i = \begin{bmatrix} \cos(\beta_i) & \mathrm{j}\,\varrho_i^{-1}\sin(\beta_i) \\ \mathrm{j}\,\varrho_i\sin(\beta_i) & \cos(\beta_i) \end{bmatrix} \tag{A.2}$$

In Eqn. (A.2) the β_i term is the optical phase thickness and can be calculated as shown in Eqn. (A.3).

$$\beta_i = 2\pi\lambda^{-1}\cos(\emptyset_i)n_i d_i \tag{A.3}$$

Where λ is the wavelength of the incident wave, n_i is the refractive index, $\emptyset_i$is the angle of incident and d_i is the physical thickness of the i^{th} layer. ϱ_i term in Eqn. (A.3) is the effective refractive index. For transverse electric (TE) polarized flux at non normal incident,

$$\varrho_i = n_i \cos(\emptyset_i) \tag{A.4}$$

and for transverse magnetic polarized flux at non normal incident,

$$\varrho_i = n_i \sec(\emptyset_i) \tag{A.5}$$

further, if the angle of incidence is zero,

$$\varrho_i = n_i \tag{A.6}$$

for both TM and TE polarized fluxes.

The second step is the calculation of the matrix product for N layer stratified multilayer stack

$$M = \prod_{i=1}^{N} \mathrm{M}_i = \begin{bmatrix} M_{11} & j\, M_{12} \\ j\, M_{21} & M_{22} \end{bmatrix} \tag{A.7}$$

In the last step electric field in the incident wave calculated for normal incidence and the transverse electrical polarization.

$$|E_0^+|^2 = \frac{1}{4}\left\{\left(M_{11} + M_{22}\frac{\varrho_s}{\varrho_0}\right)^2 + \left(\frac{M_{21}}{\varrho_0} + M_{12}\varrho_s\right)^2\right\} \tag{A.8}$$

Calculation procedure of the numerator is similar to the denominator part but it varies through z direction as given in Eqn. (A.1). First of all, the phase of retardation term $\beta_i$will be calculated as given Eqn. (A.9).

$$\beta_i(Z) = 2\pi\lambda^{-1}\cos(\emptyset_i) n_i \left(Z - \sum_{p=0}^{i-1} d_p\right) \tag{A.9}$$

In Eqn. (A.9), Z indicates the distance from the outer surface of the first layer to an arbitrary depth inside the multilayer stack. In the next step characteristic matrix, Eqn. (A.7), will be multiply with the inverse matrix ($M'(Z)$) Eqn. (A.10), in order to obtain equality which is given in Eqn. (A.11).

$$M'(Z) = \begin{bmatrix} \cos\big(\beta_i(Z)\big) & -j\, \varrho_\mathrm{i}^{-1} \sin\big(\beta_i(Z)\big) \\ -j\, \varrho_\mathrm{i} \sin\big(\beta_i(Z)\big) & \cos\big(\beta_i(Z)\big) \end{bmatrix} = \begin{bmatrix} M'_{11} & j\, M'_{12} \\ j\, M'_{21} & M'_{22} \end{bmatrix} \tag{A.10}$$

$$M''(Z) = M'(Z) \times M(Z) = \begin{bmatrix} M''_{11} & j\,M''_{12} \\ j\,M''_{21} & M''_{22} \end{bmatrix} \tag{A.11}$$

The double primed matrix, Eqn. (A.11), gives us the characteristic matrix of the stack beneath a thin surface layer of thickness Z. The final step is the computation of squared electric field at any arbitrary Z distance with using the Eqn. (A.12) for normal incidence and for the transverse polarized flux.

$$|E(Z)|^2 = [(M''_{11})^2 + (\varrho_s\, M''_{12})^2] \tag{A.12}$$